INFORMATION TO USERS

This manuscript has been reproduced from the microfilm master. UMI films the text directly from the original or copy submitted. Thus, some thesis and dissertation copies are in typewriter face, while others may be from any type of computer printer.

The quality of this reproduction is dependent upon the quality of the copy submitted. Broken or indistinct print, colored or poor quality illustrations and photographs, print bleedthrough, substandard margins, and improper alignment can adversely affect reproduction.

In the unlikely event that the author did not send UMI a complete manuscript and there are missing pages, these will be noted. Also, if unauthorized copyright material had to be removed, a note will indicate the deletion.

Oversize materials (e.g., maps, drawings, charts) are reproduced by sectioning the original, beginning at the upper left-hand corner and continuing from left to right in equal sections with small overlaps. Each original is also photographed in one exposure and is included in reduced form at the back of the book.

Photographs included in the original manuscript have been reproduced xerographically in this copy. Higher quality 6" x 9" black and white photographic prints are available for any photographs or illustrations appearing in this copy for an additional charge. Contact UMI directly to order.

UMI®

Bell & Howell Information and Learning
300 North Zeeb Road, Ann Arbor, MI 48106-1346 USA
800-521-0600

Development of a Synthetic Enzyme for Detection and Quantitation of Thiols

Suzanne Katherine Schreyer

A Thesis

in

The Department

of

Chemistry and Biochemistry

Presented in Partial Fulfilment of the Requirements
for the Degree of Master of Science at
Concordia University
Montreal, Quebec, Canada

June 1997

National Library of Canada
Acquisitions and Bibliographic Services
395 Wellington Street
Ottawa ON K1A 0N4
Canada

Bibliothèque nationale du Canada
Acquisitions et services bibliographiques
395, rue Wellington
Ottawa ON K1A 0N4
Canada

Your file Votre référence

Our file Notre référence

0-612-40196-0

Canada

Abstract

Development of a Synthetic Enzyme for the Detection and Quantitation of Thiols

Suzanne Katherine Schreyer

A voltammetric survey of quinone and ferricinium derivatives showed that several are useful for electrocatalytic thiol oxidation. Those showing the highest rates are the quinone form of dihydroxybenzylamine and the dimethylaminomethylferricinium ion, which oxidize glutathione at rates of 18 $M^{-1}s^{-1}$ and 111 $M^{-1}s^{-1}$ at pH 7.0.

Synthesis of artificial enzymes by coupling these catalysts with the primary or secondary monotosylate of β-cyclodextrin yielded unique species based on RP-HPLC, and UV-Visible spectroscopy. After isolation by RP-HPLC, synzymes were examined for thiol oxidation under pseudo-first order conditions, and thiol oxidation rates were determined. Only the secondary ferrocene-β-cyclodextrin product gave enhanced thiol oxidation rates in comparision with free dimethylaminomethylferricinium. Further tests on this species showed it was a better catalyst for cysteine than for glutathione oxidation as oxidation rates for the cysteine were 1470 $M^{-1}s^{-1}$ as compared to 260 $M^{-1}s^{-1}$ for the glutathione. Enhanced thiol oxidation rates were also observed at pH 8.0 (k_{obs} = 4123 $M^{-1}s^{-1}$) for the secondary ferrocene-β-cyclodextrin with cysteine, as compared to pH 7.0.

Acknowledgments

I would like to thank my supervisor, Dr. Susan Mikkelsen, for her advice and help in the past two years. As well, I would like to thank the members of my committee, Dr. O.S. Tee, and Dr. M. Lawrence for their input, and for taking the time to evaluate this thesis.

I would also like to thank Craig Fenwick, George Tsaprailis, and Angelo Filoso for all the mass spectrometry work in the past two years.

I would like to thank my parents, Drs. Jarka and Val Srajer, for their continued support throughout so many years of school, and for their encouragement to strive academically.

Finally, I would like to thank Joe Albanese, and all the guys (Ally, Tom, Mandy, Charlie and Spike) for providing much needed comic relief and cheer throughout this thesis.

Table of Contents

List of Tables ..... **vii**

List of Figures ..... **viii**

1.0 Introduction **1**
- 1.1 Enzymatic catalysis 1
- 1.2 Synthetic enzymes 2
  - 1.2.1 Survey of different synzymes 2
  - 1.2.2 Cyclodextrin-based synzymes 11
- 1.3 Cyclodextrin modified electrodes 26
- 1.4 Objectives of our research 29
- References 31

2.0 Experimental **34**
- 2.1 Materials 34
  - 2.1.1 Free substrates and free catalysts 34
  - 2.1.2 Synthesis of derivatized CDs 35
  - 2.1.3 Chemicals used in kinetic analysis and characterization 35
- 2.2 Instrumentation 36
- 2.3 Methods 37
  - 2.3.1 Synthetic procedures 37
    - 2.3.1.1 Preparation of a primary Tosyl-β-CD 37
    - 2.3.1.2 Synthesis of the secondary tosyl-β-CD 38
    - 2.3.1.3 Synthesis of quinone-β-cyclodextrin 39
    - 2.3.1.4 Synthesis of ferrocene-β-CD 41
  - 2.3.2 Purification of Cyclodextrin Derivatives 43
    - 2.3.2.1 Purification of the DHBA-CD Products 43
    - 2.3.2.2 Purification of ferrocene CD derivatives 44
  - 2.3.3. Characterization of products 45
  - 2.3.4 Electrochemical methods 46
  - References 51

3.0 Results and Discussion **52**
- 3.1 Electrocatalytic Measurements of Rates of Thiol Oxidation ... 52
  - 3.1.1 Quinone Derivatives 52
  - 3.1.2 Ferricinium Derivatives 59
- 3.2 Isolation and Characterization of Cyclodextrin Derivatives. 65
  - 3.2.1 UV-Visible Spectrophotometry 65
    - 3.2.1.1 DHBA and DHBA Products 65
    - 3.2.1.2 Ferrocene and Ferrocene Products 68

3.2.2 Carbohydrate Assay..... 71
3.2.3 Mass Spectrometric Analysis..... 73
3.3 Catalytic properties of CD derivatives to thiol oxidation.... 83
3.3.1 DHBA-β-CD derivatives and thiol oxidation..... 83
3.3.2 Ferrocene derivatives..... 84
3.4 Behavior of Secondary Ferrocene-β-Cyclodextrin Derivative as a Synthetic Enzyme..... 89

4.0 Conclusions and Suggestions for Future Research..... 93

Appendix A Experimental results used for determining rate constants for free systems..... 95

Appendix B Experimental results for free ferrocene-based systems..... 117

Appendix C Experimental data used to calculate rates for synzymes..... 123

Appendix D pH effect on oxidation of cysteine by ferrocenes..... 129

Appendix E Product inhibition study..... 131

Appendix F Raw Data for Calibration Plots..... 133

List of Tables

Table 1.1	Pseudo-First order rate constants for the deacetylation of p-NPA in the presence of catalysts and cyclohexanol inhibitor.....	15
Table 1.2	Electron transfer rate constants measured from time-resolved fluorescence spectroscopy for 6.0μM Porphyrin-CD and Quinones.....	19
Table 1.3	Comparision of rate constants for oxidation of thiols by riboflavin and flavin substituted Cds.....	23
Table 1.4	Effect of the ferrocene-CD mediator on oxidation of alcohols to aldehydes	24
Table 3.1	Raw Data for DHBA/GSH at pH 3.8.....	56
Table 3.2	Effect of pH on GSH oxidation rates by DHBA in the presence and absence of 10 mM β-CD.....	58
Table 3.3	Observed rates for GSH oxidation by various quinone derivatives.....	59
Table 3.4	Observed GSH oxidation rates for ferricinium derivatives.....	61
Table 3.5	Raw Data for GSH oxidation by FCO in 0.1 M phosphate buffer at pH 7.0	63
Table 3.6	Comparison of UV-Vis and Carbohydrate Assay Results for the Concentration of 2°- Fc-β-CD.....	72
Table 3.7	Observed thiol oxidation rates with functionalized DHBA-β-CDs.....	83
Table 3.8	Rate constants for thiol oxidation by ferricinium derivative.....	84
Table 3.9	Cysteine oxidation by 2-Fc-β-CD in 0.10 M phosphate buffer, pH 8.0.....	88
Table 3.10	Thiol oxidation rates in the presence and absence of disulfide products, obtained by dilution experiments. Initial concentrations were 0.50 mM catalyst, 5.5 mM glutathione, 4.8 mM cysteine, 2.4 mM GSSG,and 0.17 mM cystine.....	91

List of Figures

Figure 1.1	An octopus azaparacylcophane is the cationic host for the hydrophobic vit. B_{12}	7
Figure 1.2	A single compartment bilayer membrane composed of a synthetic peptide lipid, with vit. B_{12} incorporated into cavity	8
Figure 1.3	Calix[6]arene derivative with hydrophobic cavity formed by Y-groups on bottom of image	9
Figure 1.4	Structure of the p-tert-butylcalix[5]arene trisferrocenoyl ester molecule	10
Figure 1.5	Structures and dimensions of the three common cyclodextrins	13
Figure 1.6	Breslow's enzyme - the first artificial enzyme named in literature	14
Figure 1.7	Lipoxygenase mimic	18
Figure 1.8	A lipophilic β-CD with a ferrocene attached as an effective electron transfer mediator for the oxidation of alcohols	25
Figure 3.1	Quinone catalytic groups studied	53
Figure 3.2	Structures of thiol substrates	53
Figure 3.3(a)	Reversible quinone redox wave. 0.63 mM DHBA in 0.1 M acetate buffer at pH 3.8. on GCE	54
Figure 3.3(b)	Catalytic wave for 5.8 mM GSH oxidation with 0.63 mM DHBA/10 mM β-CD in 0.1 M acetate buffer at pH 3.8 on GCE	54
Figure 3.4	Plot of varying concentration of GSH and DHBA with and without free β-CD in 0.1 M acetate buffer at pH 3.8. Thiol oxidation current was measured at 600 mV using GCE as working; Ag/AgCl as reference and Nichrom as auxilliary electrode. Scan rate was 2 mV/sec	57
Figure 3.5	Ferrocene derivatives tested for catalytic effect on thiol oxidation.	60
Figure 3.6	Plot of voltammetric experimental data of FCO as electrocatalyst for GSH oxidation in the presence and absence of 10 mM β-CD	

Scan at 2 mV/sec, current measured at 700 mV. GCE as working, Ag/AgCl as reference electrodes..... 64

Figure 3.7 DHBA standard (7.27×10^{-5} M) in pH 7.0 phosphate buffer..... 66

Figure 3.8(a) Primary DHBA-β-CD in pH 7.0 phosphate buffer..... 67

Figure 3.8(b) Secondary DHBA-β-CD in pH 7.0 phosphate buffer..... 67

Figure 3.9 FMAM (0.042 mM) in pH 7.0 phosphate buffer..... 69

Figure 3.10(a) Primary Fc-β-CD product in pH 7.0 phosphate buffer..... 70

Figure 3.10(b) Secondary Fc-β-CD product in pH 7.0 phosphate buffer..... 70

Figure 3.11 β-CD standard curve generated from a carbohydrate assay of β-CD, measured at 490 nm. using water as a blank..... 71

Figure 3.12 ES-MS of β-CD in pH 4.0 sodium acetate buffer, in positive ion mode..... 76

Figure 3.13 ES-MS of primary tosylated β-CD, after purification by RP-HPLC. Spectrum shown is derived, to correct for Na..... 76

Figure 3.14 ES-MS of secondary Ts-β-CD, after correcting for Na..... 77

Figure 3.15 ES-MS of primary DHBA-β-CD product in pH 4.0 sodium acetate buffer. Peaks correspond to sodium adducts..... 78

Figure 3.16 ES-MS of secondary DHBA-β-CD product in pH 4.0 sodium acetate buffer. Peaks correspond to sodium adducts..... 79

Figure 3.17 ES-MS of primary Fc-β-CD product in pH 4.0 sodium acetate buffer. Peaks correspond to sodium adducts..... 80

Figure 3.18 ES-MS of secondary Fc-β-CD product in pH 4.0 sodium acetate buffer. Peaks correspond to sodium adducts. 81

Figure 3.19 ES-MS of hydroxypropyl β-CD in pH 4.0 sodium acetate buffer. Peaks correspond to sodium adducts..... 82

Figure 3.20(a) Linear voltammetry scan (2 mV/sec) of 0.30 mM 2-Fc-β-CD in deaerated 0.10 M phosphate buffer, pH 7.0.

GCE working; Ag/AgCl reference electrodes used..... 86

Figure 3.20(b) Linear voltammetry scan (2 mV/sec) of 0.30 mM 2-Fc-β-CD and 8.2 mM cysteine in pH 7 phosphate buffer. GCE working; Ag/AgCl reference electrodes used..... 86

Figure 3.21 Plot of electrocatalytic current at 400 mV against concentration according to eq. 5. Conditions identical to those in Fig.3.20. First six points used to determine cysteine oxidation rate by linear regression..... 87

Figure 3.22 Plot of 0.80 mM 2-Fc-β-CD as electrocatalyst for varying GSH concentration. GCE as working, Ag/AgCl as reference electrodes..... 89

Figure 3.23 Plot of 0.80 mM 2-Fc-β-CD as electrocatalyst for varying concentration of GSH. Carbon paste working, Ag/AgCl as reference electrodes..... 90

Figure 3.24 Plot of 0.80 mM 2-Fc-β-CD and varying concentration of cysteine. GCE as working, Ag/AgCl as reference electrodes..... 90

Chapter 1

Introduction

1.1 Enzymatic Catalysis

Native enzymes function by bringing together in a particular geometric arrangement a substrate and a catalytic site[1]. This orientation effect aligns the substrate at a favorable angle to the catalytic group, and binding groups near the catalytic site will stabilize the reactive intermediate. A particular enzyme will generally be selective for a particular substrate. This selectivity also increases the effectiveness of the reaction.

The active site of the enzyme consists of the catalytic region, where bonds are broken or formed, as well as the substrate binding region which determines the selectivity of the enzyme for the substrate. Active sites often provide a hydrophobic environment where the substrate molecule and catalytic reaction groups are oriented favorably to each other so as to favor the formation of a transition state[2]. Rates of catalysis tend to correlate favorably with substrate avidity as well as with substrate desolvation. Consequently, optimum rate accelerations are achieved when the substrate molecules are well desolvated and tightly bound to the active site[3]. Moreover, since catalysis occurs in an aqueous environment the hydrophobic active site must be housed within a milieu capable of interacting with water. This is often achieved by hydrophilic moieties present at or near the surface of the enzyme molecule within which the active site is buried[3].

Upon binding of the substrate and catalytic group at the binding site, an enhancement in the rate of reaction occurs due to the lower energy content of the intermediate complex; the activation energy to form the transition state is much lower in the enzymatic reaction,

since the transition state is stabilized. In the enzymatic reaction the enzyme and substrate combine so as to stabilize the intermediate formed, hence lowering the energy content, and decreasing the activation energy.

1.2 Synzymes

In designing effective artificial enzymes it is important to combine selective substrate binding with a catalytic group in order to generate enhanced catalytic rates in an aqueous environment. The artificial enzymes created usually consist of either macrocyclic compounds or molecular assemblies, which are capable of providing selective substrate binding and catalysis similar to native enzymes, but with the advantages of stability and sterilizability. Native enzymes, while more selective to their substrates, tend to denature at the temperatures and conditions required for sterilization and tend to be less stable over long periods.

1.2.1 Survey of different synzymes

An artificial enzyme based on a synthetic polymer chain of partially quaternerized poly(ethylenimine) in which 10% of the residues were primary amines (PEIQ-NH_2) was developed by Klotz[4], and used in a potentiometric pCO_2 sensor by Ho et al.[5] The reaction catalyzed is the decarboxylation of oxalacetate as per:

$$HOOCC(=O)CH_2CO_2^- + H^+ \rightarrow HOOCC(=O)CH_3 + CO_2 \qquad (1)$$

The native enzyme, oxalacetate decarboxylase (EC 4.1.1.3), when compared to the synzyme PEIQ-NH_2 for its utility in a biosensor, had a number of disadvantages. Mainly, the native enzyme had an operating lifetime of only one week compared to over 6 months for the synzyme. As well, no co-factors were required for the synzyme, and the pH optimum of the

artificial enzyme was in the range desirable for operation to detect CO_2.

Further examples of artificial enzymes are illustrated by synzymes developed to catalyze isomerization reactions as occur with the coenzyme B_{12}-dependent enzymes. In these synzymes, Vitamin B_{12} derivatives (Cob(II)7C_3esters) were incorporated into different hydrophobic environments to simulate vitamin B_{12} enzyme functions of intramolecular 1,2-migrations which are usually catalyzed by methylmalonyl-CoA mutase. Methylmalonyl-CoA mutase catalyzes the reaction shown in equation 2, below:

$$\begin{matrix} -C-C- \\ X\ H \end{matrix} \xrightleftharpoons{Co\text{-}A} \begin{matrix} -C-C- \\ H\ X \end{matrix} \qquad (2)$$

where X can be either a halide or a methyl group.

One host was an octopus azaparacyclophane ($APC[C_2Lys(C_5N^-)2C_{14}]_4$) which encased the Vitamin B_{12} derivative in a cationic cavity in a 1:1 ratio[6], as shown in Figure 1.1

The alkylation reaction with alkyl bromides (equation 3) was then followed by electronic spectroscopy following the absorbance decay at 392 nm which corresponds to the Co^I species, and a rate enhancement was found due to a combination of desolvation of the included species, and formation of a ternary complex in the cavity. Comparison was made to the system when no cyclophane was present, where it was found that the rate of alkylation was negligible, indicating the role that the cyclophane plays as an artificial enzyme in simulating Vit. B_{12} functions.

In a similar series of reactions, the ability of the cyclophane-vitamin B_{12} coenzyme to catalyze ring-expansion reaction and simulate the glutamate mutase reaction was studied.[7]

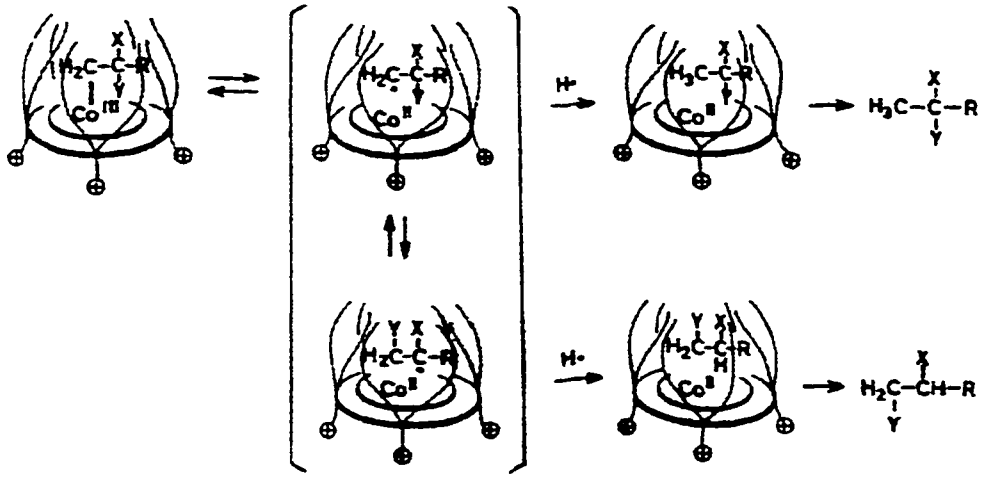

(3)

The native enzyme catalyzes the ring opening reaction shown in equation 4:

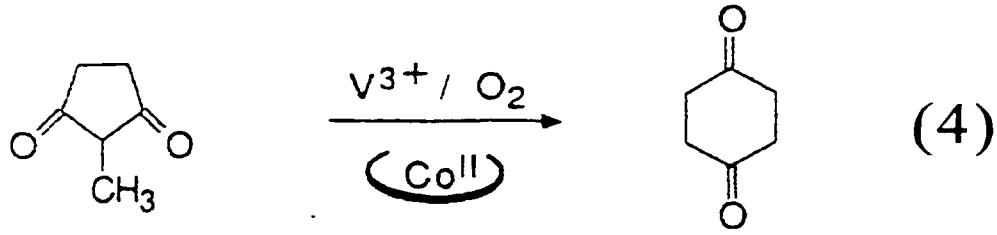

(4)

With the synzyme, ring expansion was found to be favored when the cyclophane was present indicating the formation of an energetically favorable ternary complex within the hydrophobic cavity. This is believed to be a similar mechanism to that occurring with the native enzyme-vitamin B_{12} system.

Further work simulating the vitamin B_{12} coenzyme system was done by Murakami[8] et al. when they incorporated the vitamin B_{12} coenzyme, as the $Cob7C_3$ester, into the hydrophobic pocket of a single compartment bilayer member which was composed of the synthetic peptide lipid $N^{-}C_5Ala2C_{16}$ as shown in Figure 1.2. The rate of 1,2-migration of alkyl ligands in the vesicle was compared to the rate of migration of alkyl ligands in methanol and

benzene, and the yield of the desired migration product was found to be 63%, as compared to a yield of 10% when no vesicles were present. Upon comparison of the products obtained, the predominant product of 63% was also the predominant product formed in glutamate mutase sytems. Therefore, it was concluded that the formation of the stabilized ternary complex simulated the complex formed in native enzyme-vitamin B_{12} coenzyme systems.

Another example of an artificially catalyzed system involves a calix(6)arene synzyme as shown in Figure 1.3. The calixarene catalyzes the addition of dichlorocarbenes onto a limonene to selectively produce a mono-adduct[9], as shown in equation 5.

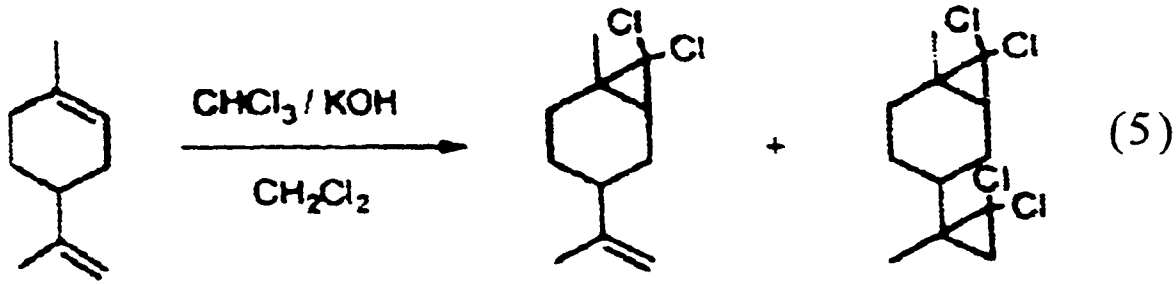

(5)

A comparison was then made to a system which contains no calixarene, where the di-adduct is the predominant product. The reaction kinetics were followed by collecting the extract and analyzing the products by IR, GC-MS and NMR. Although this system is not compared to a native enzyme system, it does illustrate the use of a host to selectively generate a species that would not otherwise be produced. Nomura's group were also able to show Michaelis-Menten type kinetics for the system, indicating that the reaction occurs within the cavity of the calixarene, and that there is stabilization of the intermediates by virtue of the reaction occurring inside the cavity.

Further work on calixarenes has also showed that a modified calix(5)arene acts as a

redox-active host molecule which can sense neutral guest molecules. A p-tert-butylcalix(5)arene tris ferrocenyl ester (Figure 1.4) was synthesized[10] as a receptor for a guest molecule.

Addition of a neutral species, either DMF, DMSO, or ethanol from 1.6 to 16.7 %(v/v) caused shifts in the redox couples of the ferrocene moieties indicating the possible addition of the species into the cavity. For example, with increasing amounts of DMF, the oxidation of the ferrocene groups at 350 mV and 450 mV, merged into a single three electron oxidation wave. Therefore, there is assumed to be an association between the ferrocene moiety and the added neutral polar guest species, which is manifested as a decrease in the separation of the redox potentials of the ferrocene groups, as the guests interpose themselves between the redox-active groups, and shield the mutual electrostatic influences of the ferrocenes.

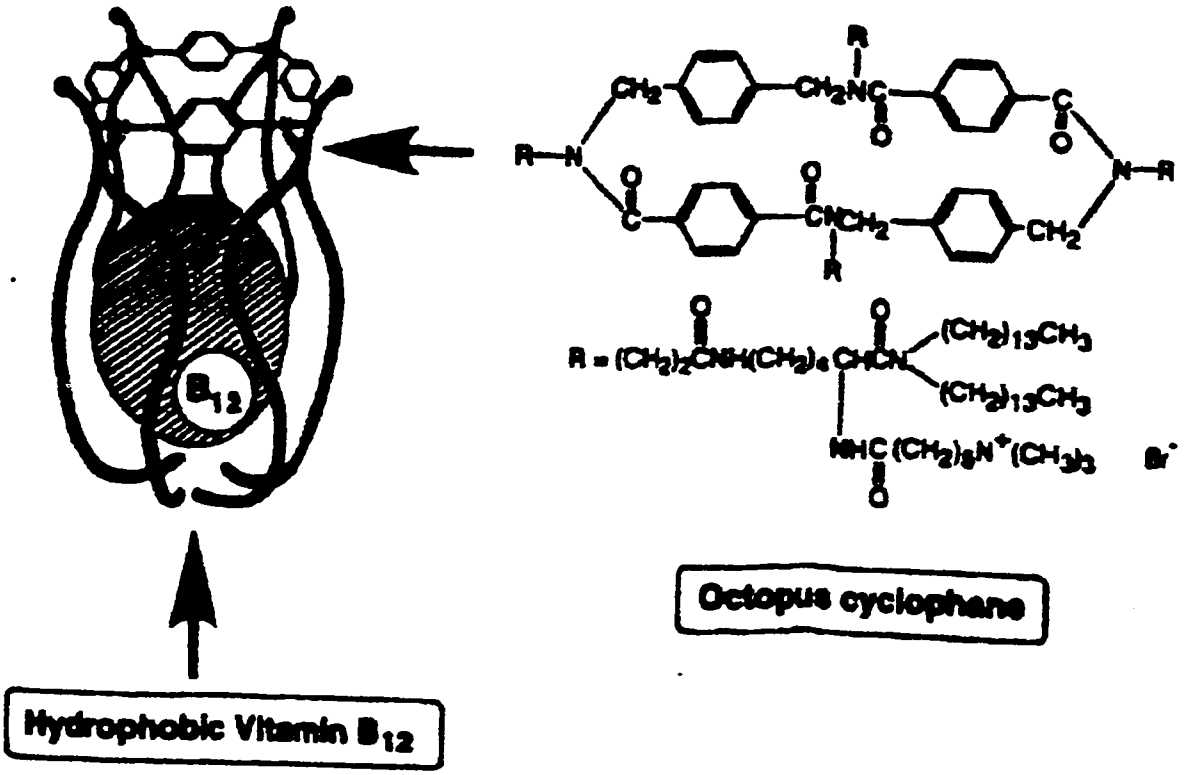

Figure 1.1 - An octopus azaparacylcophane is the cationic host for the hydrophobic vit. B_{12}.

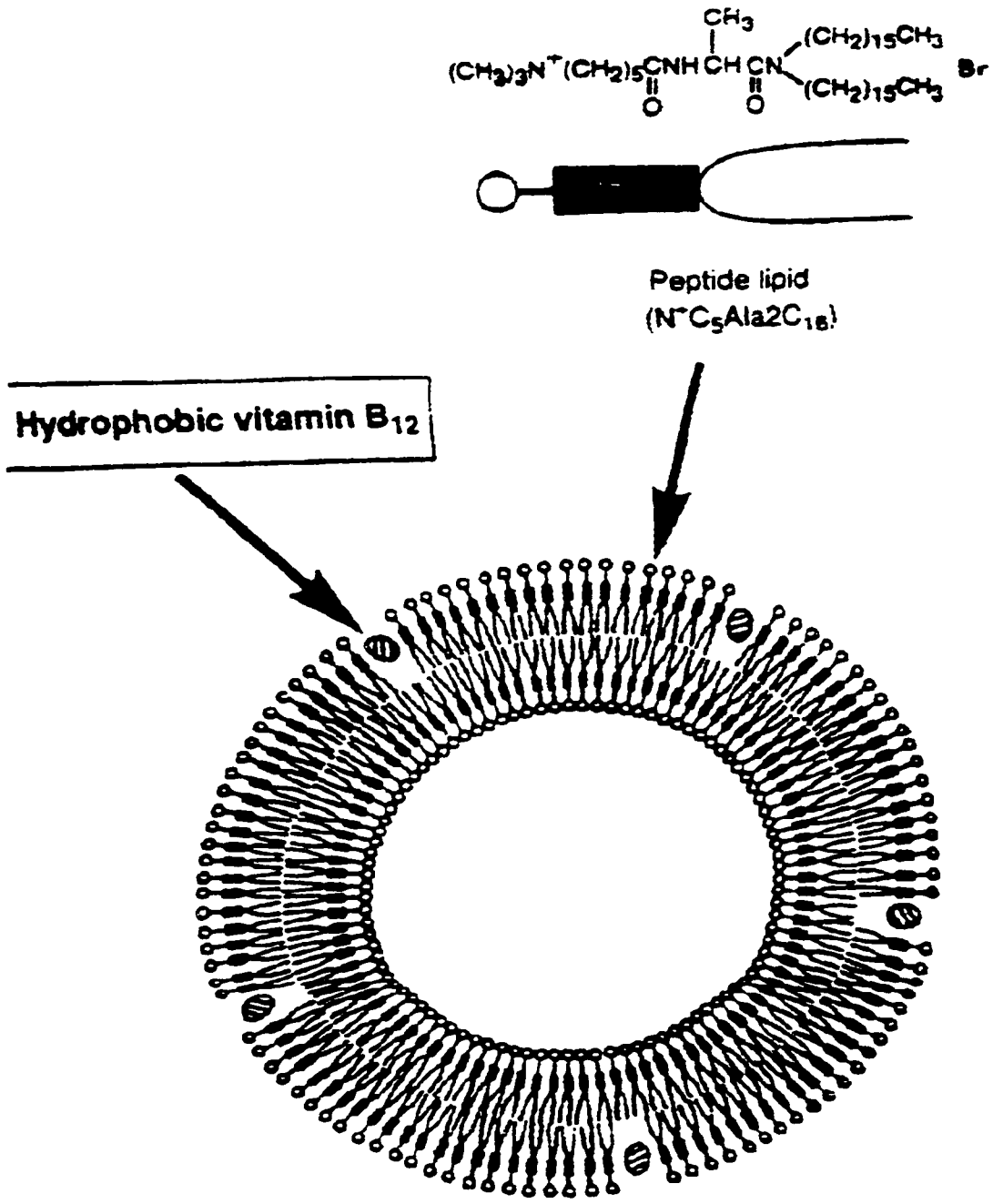

Figure 1.2 - A single compartment bilayer membrane composed of a synthetic peptide lipid, with vit. B_{12} incorporated into cavity.

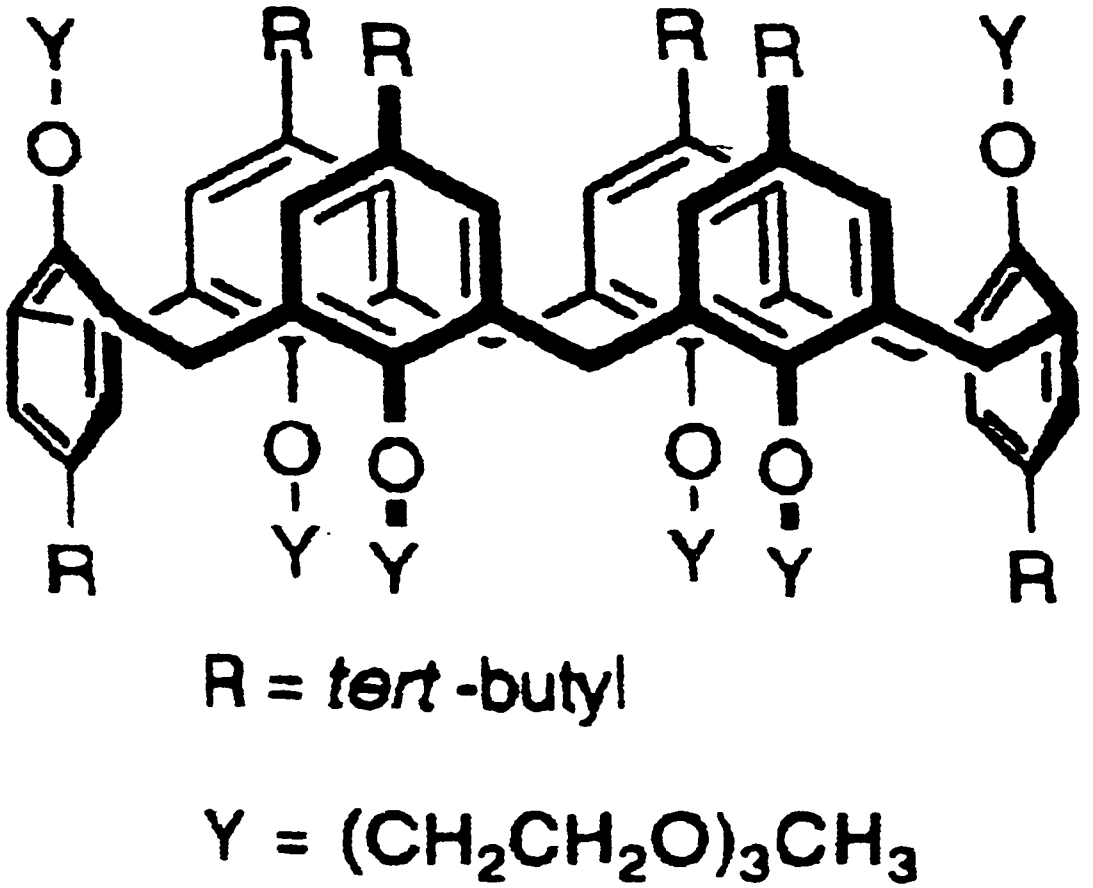

Figure 1.3 - Calix[6]arene derivative with hydrophobic cavity formed by Y-groups on bottom of image.

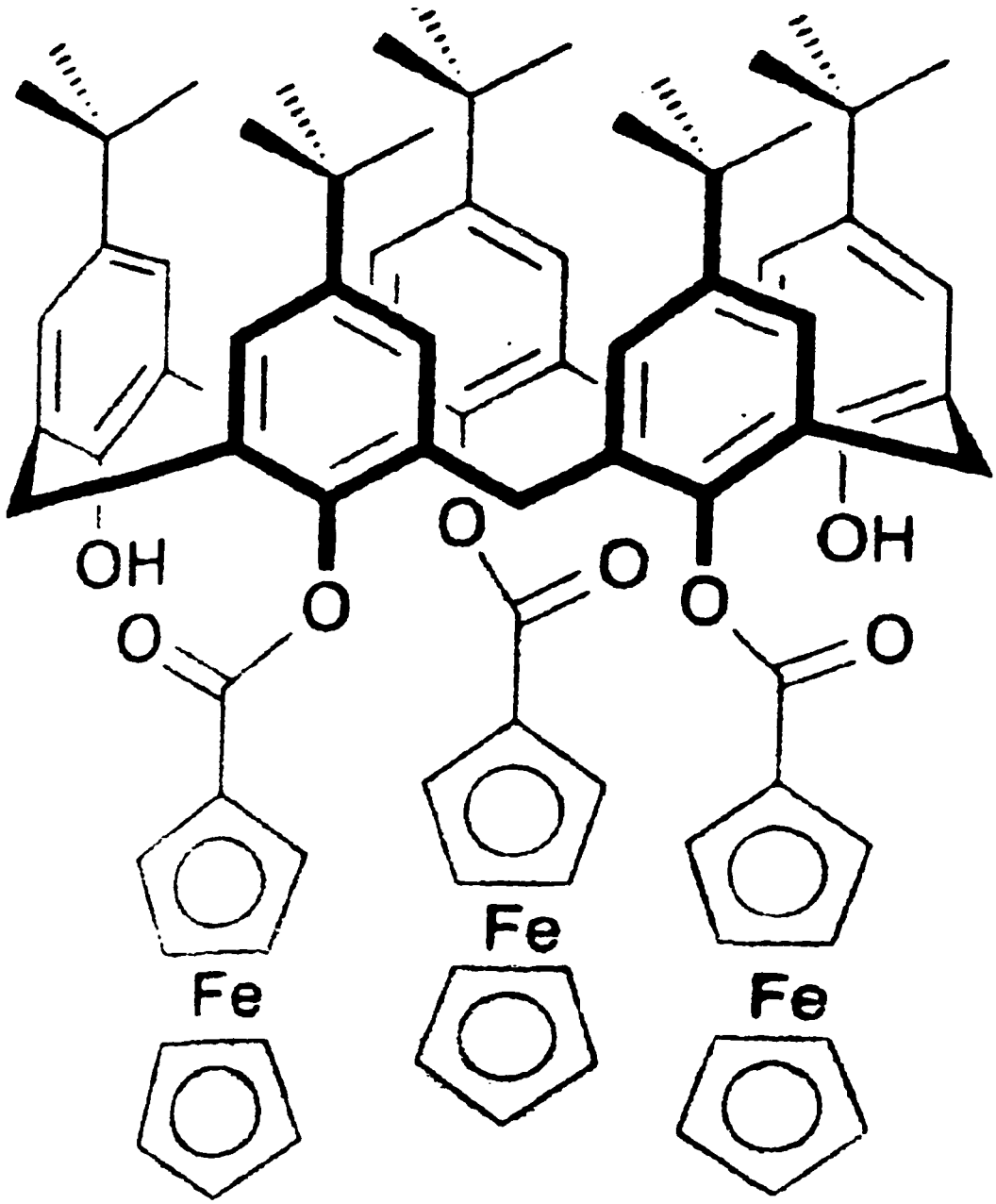

Figure 1.4 - Structure of the p-tert-butylcalix[5]arene trisferrocenoyl ester molecule.

1.2.2 Cyclodextrin-based synzymes

Cyclodextrins are water-soluble cyclic oligomers of glucopyranose units which contain a hydrophobic cavity capable of including various hydrophobic guest molecules[11] The hydrophobic cavity will then mimic the hydrophobic pockets of native enzymes, and provide an active site for substrate and catalytic site binding and reaction. The most common cyclodextrins in use are shown in Figure 1.5.

The cyclodextrin used in the research involved in this thesis is the β-cyclodextrin (β-CD) which contains a cavity of 0.78 nm, sufficiently wide to include the substrates we will be working with. The other two common cyclodextrins, the α- and γ-cyclodextrin are shown for comparison, but were not used in our synthesis, mainly due to the smaller size of the α-CD cavity and the higher cost of the γ-CD, as compared to β-CD.

Cyclodextrins (CD) are ideal molecules for the creation of artificial enzymes due to their deep hydrophobic cavities which can facilitate reaction of an attached catalytic group with an included substrate, and their solubilities in aqueous environments. The ability of cyclodextrins to function as the binding site in artificial enzymes after replacement of one or more hydroxyl groups, either on the primary or the secondary side of the cavity, with a functional catalytic group has been well-documented[3,12]. The hydrophobic cavity is amenable to the formation of inclusion complexes with hydrophobic guest species, and either through proximity effects or because the cavity can also accommodate a catalytic group, increased catalytic rates have been observed for a variety of reactions, many of which involve ester cleavage.

Studies on how cyclodextrins stabilize the transition states of complexes, and thus

facilitate formation of a product with enhanced reaction rates have been extensively studied by several groups. Breslow[13] has documented several cases where transition state stabilization gave enhanced reaction. This group was the first to coin the term "artificial enzyme" to describe a species with a cyclodextrin binding group and a copper ion catalytic group (see Figure 1.6) which was an effective hydrolytic catalyst for substrates which bind in the cavity but would not normally bind well to metal ions, such as p-nitrophenyl acetate (p-NPA).

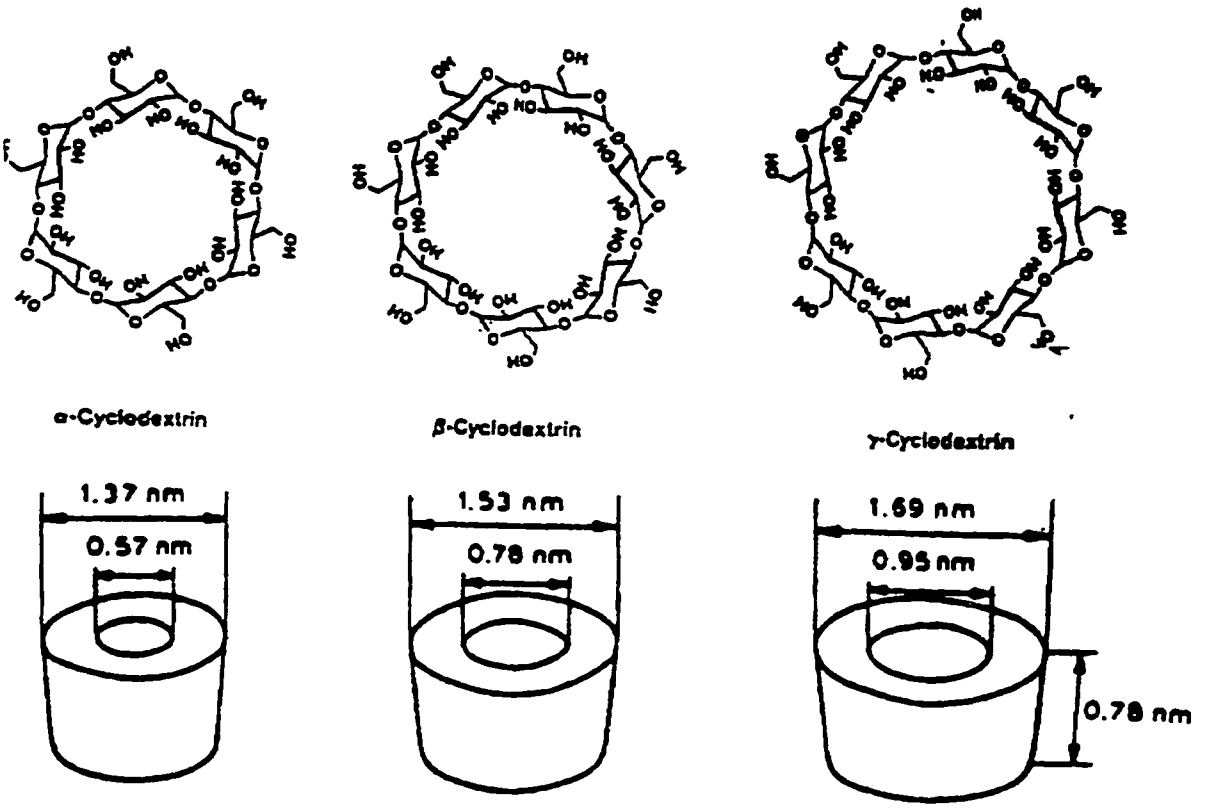

Figure 1.5 - Structures and dimensions of the three common cyclodextrins.

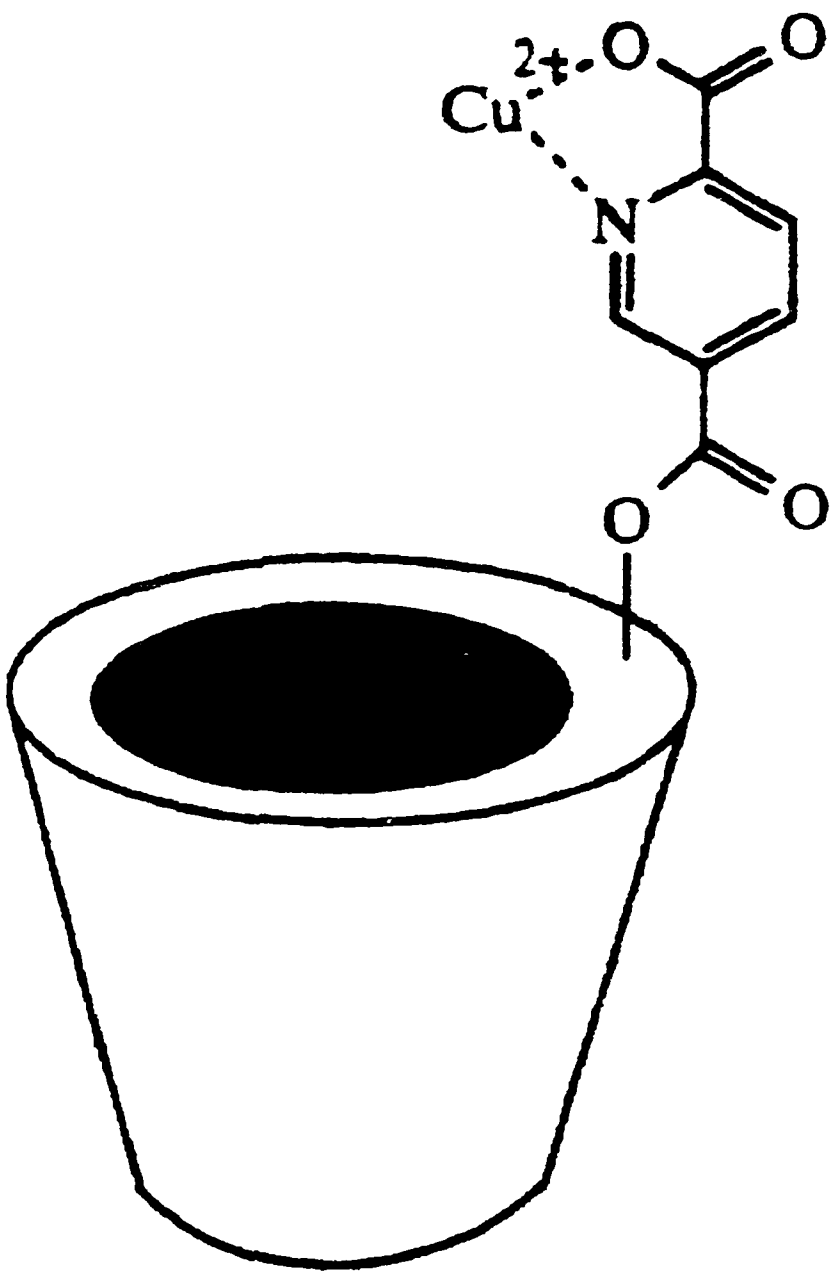

Figure 1.6 - Breslow's enzyme - the first artificial enzyme named in literature.

These substrates bind in the hydrophobic cavity in a favorable orientation to the catalytic group, and this facilitates the formation of hydrolysis products. The accelerations in rate were found to be due to geometric control, giving a large selectivity which, when combined with an effective catalytic group, such as the copper or a nickel ion, gives selective acceleration. This was substantiated by experimental results which showed that the synzyme with a nickel - pyridine-2,5-dicarboxylic acid (Ni-PCA) functional group was approximately four times more reactive to p-NPA than an equivalent amount of the free Ni-PCA (no CD present) as shown in Table 1.1. Consistent with the interpretation that there is binding in the CD cavity, and consequent reaction, are the results obtained when an inhibitor, cyclohexanol, was added. Cyclohexanol will bind to the CD cavity, and prevent the p-NPA from binding. The hydrolysis reaction was competitively inhibited when the synzyme was present, but the inhibitor had no effect on the hydrolysis reaction between free Ni-PCA and p-NPA.

Table 1.1 - Pseudo-First order rate constants for the deacetylation of p-NPA in the presence of catalysts and cyclohexanol inhibitor.

Substrate	Catalyst, mM	Cyclohexanol inhibitor, M	k_{obs}, min^{-1}
p-NPA	----------		7.1×10^{-5}
p-NPA	PCA-Ni (5.01)		2.60×10^{-2}
p-NPA	CD-PCA-Ni (5.01)		9.91×10^{-2}
p-NPA	CD-PCA-Ni (5.01)	0.134	4.78×10^{-2}
p-NPA	PCA-Ni (5.01)	0.134	2.61×10^{-2}

A more detailed study of the stabilization of the transition state of a substrate-CD

complex which results in increased rates for hydrolysis, as well as other types of organic reactions was studied by Tee[14], where mechanistic explanations were given for the stability of the transition state in various processes ie. decarboxylation, bromination, cleavage, and hydrolysis. In these cases, size of the substrate, and orientation play a significant role in rate accelerations. The mechanistic study is based on the Kurz method to develop transition state equilibrium constants, and hence determine the relative energies of catalyzed and uncatalyzed transition states. From this it is possible to determine the strength of binding of the catalyst and the transition state species.

Various studies on the catalysis of reactions have also focused on the use of cyclodextrins to solubilize species and hence increase their reaction rates in aqueous solutions.[15] For example, Luong et al. solubilized 100 mM dimethylferrocene in an aqueous solution of hydroxypropylβ-CD, and used this complex as an effective mediator for the enzyme catalyzed oxidation of glucose, hypoxanthine, and lactate. They were able to detect 3-10 μM of the substrates, with the ferrocene included HP-β-CD as the electrocatalyst. However, the main reason that reaction rates are enhanced for the substrates in these cases is due to the ability of the cyclodextrin to solubilize the catalyst. Hence, it is more valid to focus on examples which involve the attachment of a catalytic site onto a cyclodextrin for the formation of an artificial enzyme, as shown in the following examples.

The lipoxygenase mimic developed by Kuroda, Sera and Ogoshi[16] has a porphyrin ring sandwiched between two beta-cyclodextrins (β-CD), as shown in Figure 1.7. Like its native counterpart, it shows regio- and stereoselective oxidation of fatty acids, by preferentially attacking the 12 and 13 position of linoleic acid double bonds to give hydroperoxidation

products (see equation 6).

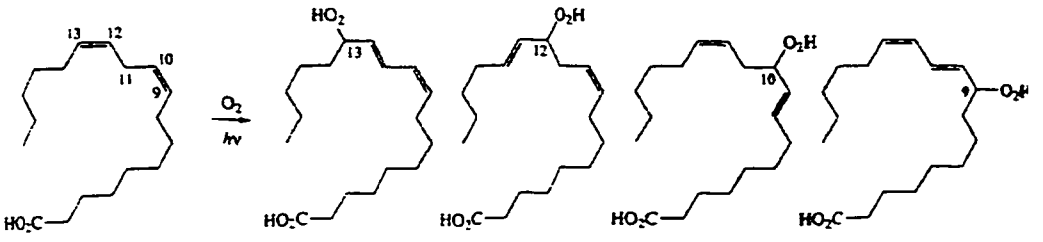

(6)

The authors suggest that this selectivity is due to the simultaneous accommodation of linoleic acid and singlet oxygen in the hydrophobic cavity of the β-CD. As well, the binding site regulates the attacking face of the alkene to the oxygen as demonstrated by a predominance of the L-chiral form of the resulting product. Hence, there is selectivity in the synzyme as to position of attack, and catalysis is accomplished by binding the substrate in a hydrophobic cavity where the catalytic functionality has access to it. Both of these properties are analogous to native enzymes.

Porphyrin β-CD sandwich species also have applications in the mimicking of natural photoreduction centers.[17] In this study free quinones and the porphyrin β-CD sandwich were employed as electron acceptors and donors, respectively, and experimental results indicated that certain quinones (anthraquinone, and naphthaquinone) will bind in the β-CD cavity, quench fluorescence from the porphyrin, and result in effective photoinduced electron transfer within the complex. The electron transfer rates for quinones tested are shown in Table 1.2.

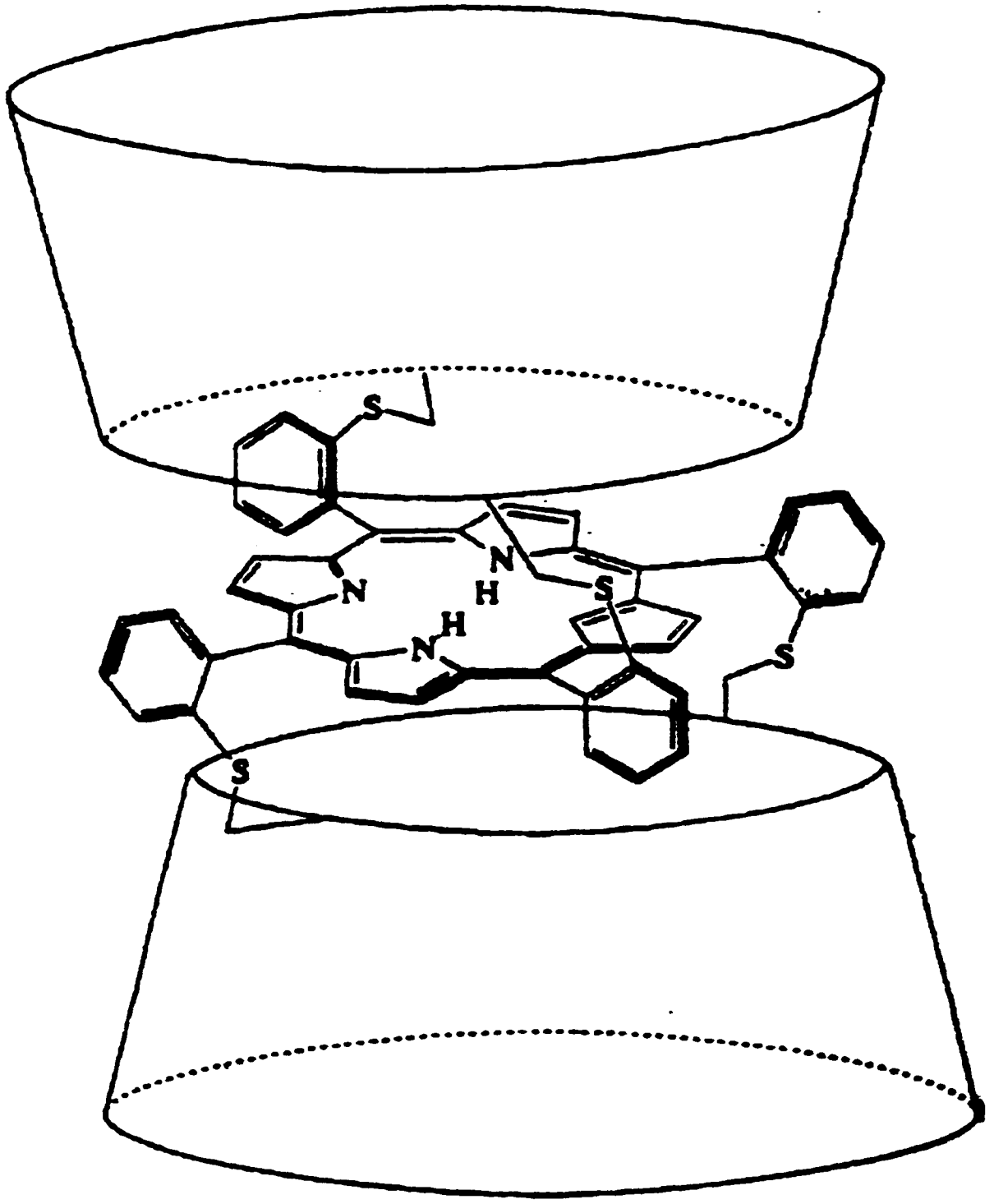

Figure 1.7 - Lipoxygenase mimic

Table 1.2 - Electron transfer rate constants measured from time-resolved fluorescence spectroscopy for 6.0μM Porphyrin-CD and Quinones

Quinone	k_{ET}, s^{-1}
none	
naphthoquinone (NQ)	2×10^9
anthraquinone-2-sulfonate (AQ)	1×10^9
adamantane quinone derivative (AdQ)	1×10^9

It is postulated that the quinone approached the porphyrin from the out-of-plane direction, inserted into the CD cavity which resulted in fluorescence quenching of the porphyrin system, as measured by the decrease in fluorescence intensity at 654 nm. Electron transfer rates between the porpyrin and the quinone occurred at a rate given in the previous table, and this electron transfer was observed using time-resolved fluorescence spectroscopy over a concentration range of the quinone between 0 to 3 mM. Without any quinone present, the fluorescent decay profile of the porphyrin-CD had a lifetime of 3.2 ns. The decay profile became biphasic (two lifetimes obtained) when quinones were added. Electron transfer rates were measured from the difference between the two lifetimes, where the first lifetime measure (τ_1) was found to be, within experimental error, the intact lifetime of the porphyrin-CD. This biomimetic process would be of interest in the study of electron transfer reactions as binding sites and reaction sites are not covalently attached, therefore different sites could be made, and investigated as to their effect on the electron transfer rates, which could then be applied as models to natural photosynthetic systems.

Another biomimetic study involved the preparation of a tetrameric iron-sulfur complex

$[Fe_4S_4(SR)_4]^{-2}$, where R is β-CD, in order to study iron-promoted redox processes.[18] This early work involved the preparation of the model compound to study the natural process of iron-sulfur protein active sites, and X-ray analysis and electronic absorption studies indicated a structural and electronic resemblance between the natural compound and the synthetic complex. Due to the similarity in structure, redox potential studies were performed on this complex in order to understand what is occurring in the natural system. The one electron reduction potentials of the models became less negative, and approached the redox potentials of the native systems as the ligand structure (R-groups) contain electron withdrawing groups, and if the reaction is in an aqueous medium. It is postulated that the hydroxyl groups in the CD ligands substantially increase the ease of reduction of the iron sulfide core, and the solvation sphere surrounding the metal cluster enhances the proximity between cluster and substrate.

Another group prepared an oxodiperoxomolybdenum complex ($MoO(O_2)_2L$), where L is β-CD, to investigate the oxidation of thioanisole by hydrogen peroxide.[19] Due to the proximity of the hydrophobic and chiral CD cavity, and the molybdenum catalyst, enantioselective reactions occurred with a predominance of the R-(+)phenylmethyl sulfoxide product. Without the CD no optical activity was observed in the product mixture. Based on these results, the authors suggest a mode of interaction between the catalytic group attached to the CD, where the guest is included in the cavity and the molybdenum catalytic site caps the CD cavity.

Further examples of metalloenzymes[20] are reported where cyclodextrins are functionalized with polyamines and then capped by various ions (Cu^{2+}, Zn^{2+}, Mg^{2+}). With

these species, hydrophobic substrates bind to the CD more strongly than when no metal ion is present. These metalloenzymes were used as models to study the metal-substrate binding interactions of specific hydrophobic anions. A model was proposed for the binding which the authors termed *double recognition*, in that it involved simultaneous binding of the substrate to the metal ion and to the CD, in a cooperative approach involving two mutually independent selective recognition sites. This recognition provides a stepwise approach similar to that in biological recognition which also involves multiple recognition interactions.

A cyclodextrin-based redox enzyme was prepared as a model for natural flavin redox enzymes, and its mechanism was studied under varying pH and metal ion requirements.[21] It was determined that the metal ions behave as electron mediators between the substrate, Meldola Blue (8-dimethylamino-2,3-benzophenoxazine), and the enzyme (β-CD derivatized with residues of 7,8-dimethylalloxazine; the prosthetic group of natural flavin adenine dinucleotide (FAD) enzymes). The two step reduction of the Meldola Blue was followed and found to increase when the metal ions (Fe^{3-} , Mn^{2-}, or Mg^{2-}) are present as electron mediators. As well, in the presence of the CD-derivatives, the overall acceleration of the reduction was between 3-5 over that of a system with no CD present, just the riboflavin moiety.

Another example of a CD-based synzyme involves a flavin catalytic group attached to β-CD, but used to oxidize thiols[22,23]. The flavin group was attached to either the primary or the secondary side of the β-CD, and thiol oxidation rates were compared between the two derivatized CD's and with only the flavin group present. The reaction between the flavin and the thiol involves the addition of the thiol onto the flavin, subsequent bond cleavage of the

thiol to form a disulfide, and regeneration of the flavin as shown in equations 7-8.

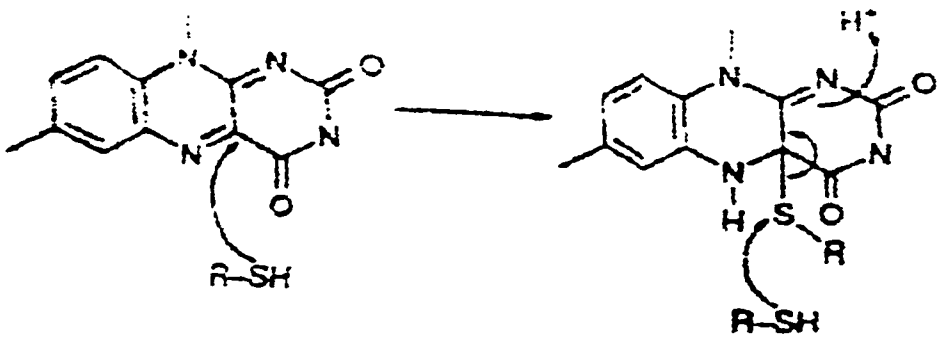

(7)

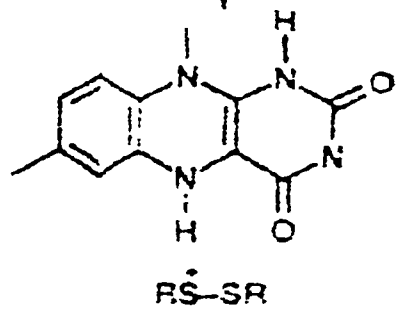

(8)

It was determined that the thiol included in the CD cavity, bringing it close to the flavin catalytic site- the double bond in the flavin as shown in equation 7. This conformation and binding were responsible for the enhanced rate observed when the secondary side derivatized CD is present, due to a combination of the proximity effect and the enhanced stability of the complex. Results with the three catalysts are shown in Table 1.3 for comparision.

Table 1.3 - Comparision of rate constants for oxidation of thiols by riboflavin and flavin substituted CDs.

Flavin	Substrate	k_{cat}/K_D, $M^{-1}s^{-1}$	k_2, $x10^{-2}$, $M^{-1}s^{-1}$	$(k_{cat}/K_D)/k_2$
Cl-phenylmethane thiol	2-FlCD	0.412		21
Cl-phenylmethane thiol	6-FlCD		11.8	
Cl-phenylmethane thiol	Rfl		1.93	
Phenylmethane thiol	2-FlCD	0.587		53
Phenylmethane thiol	RFl		1.11	

k_{cat} is the thiol oxidation rate by the flavin-CD;

K_D is the dissociation constant of the flavin-CD and the thiol, and;

k_2 is the uncatalyzed reaction rate of the flavin and the thiol, either because the flavin is not including in the CD cavity, or because it exists as the free flavin group (no CD present).

It was determined that the primary side substituted flavin-β-CD did not give an increased rate due to the conformation of the thiol in this system being away from the CD cavity. The primary flavin-β-CD's therefore gave similar kinetics to those observed when only riboflavin is present in solution. Favorable orientation between thiol and flavin occurs only with the secondary flavin-β-CD, where rate enhancement over that of riboflavin alone

was 53 times when the flavin was phenylmethane thiol.

A different redox study involved the preparation of a lipophilic β-CD with a ferrocene moiety covalently attached (shown in Figure 1.8), which could oxidize alcohols onto their corresponding aldehydes both efficiently and selectively.[24]

The ferrocene-CD complex is a strong oxidant and an effective electron transfer mediator, which successfully catalyzed the oxidation of benzyl alcohol and 1-naphthalene methanol to their corresponding aldehydes in acetonitrile. Without the presence of the β-CD little oxidation was noted, and scant yield of the aldehyde was reported as shown in Table 1. 4.

Table 1.4 - Effect of the ferrocene-CD mediator on oxidation of alcohols to aldehydes

Mediator (mM)	Alcohol (mM)	Aldehyde yield, %
Methyl ferrocenecarboxylate(11.8)	Benzyl alcohol (381)	0.07
Fc-β-CD (11.2)	Benzyl alcohol (337)	36.8
Methyl ferrocenecarboxylate(11.8)	1-napthalene methanol (341)	6.05
Fc-β-CD (11.1)	1-napthalene methanol (338)	96.0

The authors postulate that the inclusion of the ferrocene into the CD cavity initially occurs. As the ferrocene is electrochemically oxidized to the ferricinium form, it is excluded from the cavity, and the alcohol substrate is included, resulting in close proximity between the ferricinium cation on the CD and the alcohol. As the distance between the two species is now

short, effective electron transfer can occur, and oxidation of the alcohol to the aldehyde occurs. Thus the ferrocene/ferricinium system acts as an effective electron transfer mediator for the electrocatalytic conversion of the alcohols to the aldehydes.

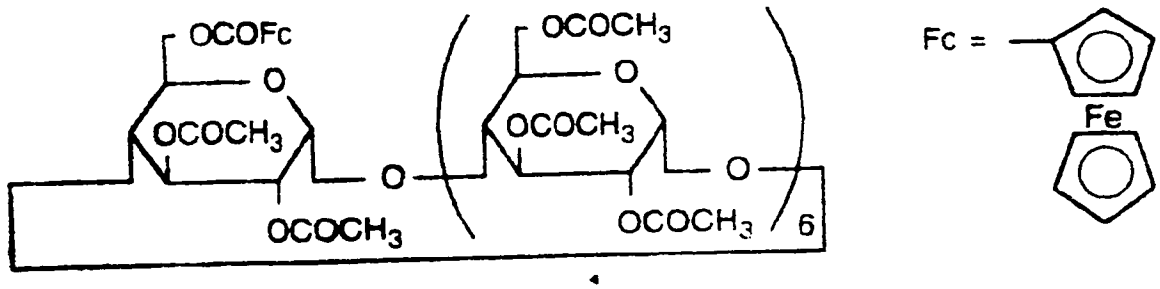

Figure 1.8 - A lipophilic β-CD with a ferrocene attached as an effective electron transfer mediator for the oxidation of alcohols.

1.3 Cyclodextrin modified electrodes

The first studies of cyclodextrins on electrode surfaces involved the measurement of CD on a dropping mercury electrode by alternating current polarography to determine the adsorption/desorption equilibrium on the surface.[25] The study of adsorption of CDs on mercury surfaces continued through the 1980's, and a model for the adsorption was suggested by Jaworski et al[26]. In short, monolayer coverage can be found at a level of CD concentration (10^{-4} to 10^{-5}M) and after rapid equilibration (14 seconds), adsorption was found to fit the Langmuir isotherm. One interesting result of this study was the different orientations that the different CDs took upon adsorption. Based on surface tension and differential capacity measurements, it is believed that the smaller α-CD will orient itself parallel to the mercury surface, while β-CD tends to orient itself perpendicular to the surface. This effect is concentration dependant, as when the number of molecules at the surface increase, the α-CDs will re-orient themselves perpendicular to the surface.

The results of these studies were applied to CD adsorption onto gold and silver electrodes. For gold electrodes, adsorption also followed a Langmuir isotherm, with monolayer coverage of CD occurring at the millimolar level.[27] As with the mercury electrodes, orientation differed based on the type of CD, with β-CD having a perpendicular orientation. For silver electrodes, similar adsorption results were obtained[28], with results fitting a Langmuir isotherm. However, maximum adsorption could not be determined from differential capacity measurements, therefore the researchers were unable to determine the orientation of CD on the silver surface. In this study, the authors postulate a parallel orientation for β-CD both for silver and gold electrodes, which is in contrast to the earlier

study.[29]

Chemisorption of cyclodextrin species onto electrode surfaces has attracted a lot of attention due to the possible use of these systems in sensors, especially in the design of ion channel sensors. These are ordered assemblies of polyamine-CD derivatives which are composed of $6^A,6^B,6^C,6^D,6^E,6^F,6^G$ -heptadeoxy-$6^A,6^B,6^C,6^D,6^E,6^F,6^G$ -hetakis(dodecylamino)-β-cyclodextrin ($(6\text{-}C_{12}H_{25}NH)_7$-β-CD) deposited on a glassy carbon electrode surface (GCE) by the Langmuir-Blodgett method[29]. Complexation of the CDs with anionic or cationic guests caused a corresponding change in the ion permeability of the membrane as measured using marker ions (ferricyanide) by cyclic voltammetry. Reduced permeability was observed in the presence of the anionic guests, phthalates, maleate and fumarate, which when present caused a decrease in currents due to the ferricyanide couple. It was proposed that this could act as a model for the on/off switch of an ion channel sensor. More recent work has involved the development of an alkyl derivative of β-CD acting as a receptor site for uncharged guest species, and as a channel entrance for marker species, which in this study was p-quinone.[30] The quinones could readily pass through the CD cavity when no guests were included to give a reductive peak on a cyclic voltammetry scan. When the guest was added (a variety of alcohols and other organic species were tested), the channels were blocked to quinone transport, and a decrease in quinone reduction peaks was observed. Further studies to increase the selectivity and sensitivity of the system were done to generate more efficient signal amplification, where it was determined that the main factor controlling the permeability of the quinones through the channels is due to the steric bulkiness of the marker as contrasted with hydrophobicity requirements when monolayers of simple alkanes rather than CD's are

rather than CD's are used.[31]

Other studies which attempt to develop a chemical sensor with chemical amplification for analyte species involve the derivitization of β-CD hydroxyl groups to thiols, and subsequent attachment to gold electrodes. One group[32] derivatized all seven of the primary side groups to thiols and chemisorbed the thiolated β-CD onto a gold electrode to form six to seven Au-thiolate bonds, with a maximum surface coverage of 64-75%. The reason for the poor surface coverage was thought to be due to the large cross-sectional area of the thiolated CD and the poor lateral interactions upon chemisorption. To seal off pinholes and other defects, pentanethiol was added as a sealing agent, which decreased the measured electrode-solution capacitance. To assess the quality of the layer, electroactive species such as the ferricyanide couple or ruthenide couple were added and their voltammetric currents were measured. It was determined that there was effective coverage of the surface as the there was hindrance of the electrode process for the marker ions. It should be noted that the pentanethiol treatment may be expected to block CD cavities as well as blocking pinholes and other monolayer defects.

Improved packing density for thiolated β-CD species was found when only one of the primary hydroxyls was thiolated[33]. This species was then chemisorbed onto a gold electrode with increased packing density, and a surface coverage of 99.6%. The β-CD was functionalized with mercaptopropionic acid on the primary side, then subsequently reacted to form the disulfide. The thiolate linkage to a gold electrode gave a flexible, chemisorbed CD layer which provided a close barrier to ferricyanide reduction, by orienting to prevent the marker ion from penetrating to the electrode surface.

The researchers also incorporated an anion, 2-(p-toluidinyl)naphthalene-6-sulfonic acid (TNS), into the CD cavity in order to measure the ability of the chemisorbed CD layer to distinguish specific interaction with guest molecules. Since TNS readily forms an inclusion complex with CD (K_D = 2500 M^{-1}), and carries a negative charge, it will form a charge barrier for electroactive anions which will increase the charge transfer resistance. There was a large increase in the charge transfer resistance observed after addition of 2,6-TNS, but not in the presence of 1-anilinonaphthalene-2-sulfonic acid (1,2-ANS), a species which does not bind to CD. Based on this result, it is possible to monitor guest inclusion in the CD cavity, allowing for differentiation between specific and non-specific interaction.

Finally, in a interesting twist on the attachment of derivatized CDs onto electrode surfaces, a group has attached β-CD-tetradecabenzoate or acetate to piezoelectric ST-cut quartz through a bifunctional bis(1,6-trichlorosilylhexane)derivatized oxide surface by a linkage through the siloxane groups.[34] This was proposed as a model sensor for the detection of volatile organic compounds (VOC). The sensors response would be unique for each type of VOC detected, as each VOC gave a characteristic frequency shift.

1.4 Objectives of our research

The work described in this thesis involves the development and characterization of a thiol selective, CD-based artificial enzyme. To develop the synzyme, various quinone and ferrocene derivatives were tested in the presence and absence of β-CD for their ability to catalyze cysteine and glutathione oxidation. Upon determination of the catalysts which showed the greatest effects on thiol oxidation rates, these catalysts were attached to the primary and secondary side of β-CD. Further catalytic studies were done to establish if the

point of attachment, and the type of derivatized β-CD have an effect on thiol oxidation rates. To quantify the catalytic effect, cyclic voltammetry was used to measure the electrocatalytic oxidation currents for the thiols over different concentrations, and from this, observed pseudo-first order rate constants for thiol oxidation were determined. Comparisons were made between the rates for free catalysts only, free catalysts with free β-CD, and systems containing the functionalized β-CD species.

Further work was then done to characterize the β-CD species through the use of carbohydrate assays, electrospray mass spectrometry (ES-MS), and UV-Visible absorbance studies. Once characterized, further kinetic studies were done to obtain calibration plots with various electrodes, and attempts to determine binding constants of the thiols and their disulfides in the β-CD cavity were done by fluorescence displacement studies.

The ultimate goal of this research is to determine which derivatized β-CD-complex gives the highest rate constant for thiol oxidation, and apply this system to a sensor for the detection and quantitation of thiols in biological systems. The interest in developing a sensor for thiol detection is due to the implied stability of these synthetic enzyme-based sensors to pH, temperature fluctuations, and various solvent systems which cause native enzymes to denature, and due to the sterilizability of these sensors which will make them useful in biotechnology applications.

References

1. R.W. McGilvery, and G.Goldstein, "Biochemistry, A Functional Approach", 2nd ed., W.B. Saunders Co., New York, 1979. pp. 253

2. R.W. McGilvery, and G.Goldstein, "Biochemistry, A Functional Approach", 2nd ed., W.B. Saunders Co., New York, 1979. pp. 255-256

3. Y. Murakami, J. Kikuchi, Y. Hisaeda, and O. Hayashida. *Chem Rev.*, **1996**, *96*, pp. 721-758.

4. I.M. Klotz. *Ann. N.Y. Acad. Sci.* **1984**, *434*, 302-320.

5. M.Y.K. Ho, and G.A. Rechnitz. *Anal. Chem.* **1987**, *59*, 536-537.

6. Y. Murakami, Y. Hisaeda, J. Kikuchi, T. Ohno, M. Suzuki, Y. Matsuda, and T. Matsuura. *J. Chem. Soc. Perkin Trans. II* **1988**, 1237-1246.

7. Y. Murakami, Y. Hisaeda, and T. Ohno. *J. Coord. Chem.* **1990**, *21*, 13-22.

8. Y. Murakami, Y. Hisaeda, and T. Ohno. *J. Chem. Soc. Perkin Trans. 2* **1991**, 409-416.

9. E. Nomura, H. Taniguchi, and Y. Otsuji. *Bull. Chem. Soc. Jpn.* **1994**, *67*, 792-799.

10. P.D.Beer, Z. Chen, M.G.B. Drew, and P.A. Gale. *J. Chem. Soc., Chem. Commun.* **1995**, 1851-1852.

11. M.L. Bender, and M. Komiyama. "Cyclodextrin Chemistry", Springer-Verlag, New York, 1978. pp. 2-12

12. M. Komiyama, and H. Shigekawa. Cyclodextrins as Enzyme Models in "Comprehensive Supramolecular Chemistry," Vol.3, Elsevier Science, Oxford, 1996. pp.401-422

13. R. Breslow. *Acc. Chem. Res.* **1995**, *28*, 146-153.

14. O.S. Tee Stabilization of Transition States by Cyclodextrins and other Catalysts in "Advances in Physical Organic Chemistry",Vol. 29, Academic Press,1994. pp. 1-85

15. J.H.T. Luong, R.S. Brown, K.B. Male, M.V. Cattaneo, and S. Zhao. *Tibtech*, **Nov. 1995**, *13*, 457-463.

16. Y. Kuroda, T. Sera, and H. Ogoshi. *J. Am. Chem. Soc.* **1991**, *113*, 2793-2794.

17. Y. Kuroda, M. Ito, T. Sera, and H. Ogoshi. *J. Am. Chem. Soc.* **1993**, *115*, 7003-7004.

18. B. Siegel. *J. inorg. mucl. Chem.* **1979**, *41*, 609-610.

19. M. Bonchio, T. Carofiglio, F. Di Furia, and R. Fornasier. *J. Org. Chem.* **1995**, *60*, 5986-5988.

20. I. Tabushi, N. Shimizu, T. Sugimoto, M. Shiozuka, and K. Yamamura. *J. Am. Chem. Soc.* **1977**, *99*, 7100-7103.

21. M. Marzona, and C. Roda. β-Cyclodextrin-(7,8-Dimethylalloxazine) Derivatives as Artificial Oxido-Reductase Agents in "Proceedings of the Fifth Int. Symposium on Cyclodextrins". Torino, Italy, Kluwer Academic Publ., 1990. pp. 687-690.

22. H. Ye, W. Tong, and V.T. D'Souza. *J. Chem. Soc. Perkin Trans. 2* **1992**, 2071-2075.

23. D. Rong, H. Ye, T.R. Boehlow, and V.T. D'Souza. *J. Org. Chem.* **1992**, *57*, 163-167.

24. I. Suzuki, Q. Chen, Y. Kashiwagi, T. Osa, and A. Ueno. *Chem. Lett.* **1993**, 1719-1722.

25. J. Szejtli. Inclusion of Gold Molecules, Selectivity and Molecular Recognition by Cyclodextrins in "Comprehensive Supramolecular Chemistry Vol. 3". Elsevier Science, Oxford, 1996. pp. 201

26. R.K. Jaworski, M. Golędzinowski, and Z. Galus. *J. Electroanal. Chem.* **1988**, *252*, 425-440.

27. G. Jarzabek. *J. Electroanal. Chem.* **1990**, *294*, 253-265.

28. M. Brzostowska-Smolska, M. Milkowska, and J. Taraszewska. *Polish J. Chem.* **1995**, *69*, 132-140.

29. S. Nagase, M. Kataoka, R. Naganawa, R. Komatsu, K. Odashima, and Y. Umezawa. *Anal. Chem.* **1990**, *62*, 1252-1259.

30. K. Odashima, M. Kotato, M. Sugawara, and Y. Umezawa. *Anal. Chem.* **1993**, *65*, 927-936.

31. K. Odashima, and K. Koga. Cyclophanes and Related Hosts for Recognition and Discrimination of Nonpolar Structures at Membrane Surfaces in "Comprehensive Supramolecular Chemistry Vol. 3". Elsevier Science, Oxford, 1996. pp. 185-189

32. M. Rojas, R. Koniger, J.F. Stoddart, and A.E. Kaifer. *J. Am. Chem. Soc.* **1995**, *117*, 336-343.

33. C. Henke, C. Steinem, A. Janshoff, G. Steffan, H. Luftmann, M. Sieber, and H-J. Galla. *Anal. Chem.* **1996**, *68*, 3158-3165.

34. L.W. Moore, K.N. Springer, J-X. Shi, X. Yang, B.I. Swanson, and DeQ. Li. *Adv. Mater.* **1995**, *7*(8), 729-731.

Chapter 2

Experimental

2.1 Materials

2.1.1 Free substrates and free catalysts

For initial screening of quinones for catalytic activity; 1,2-naphthoquinone-4-sulfonic acid, sodium salt (Lot 1-6086, 95%) was purchased from Baker. All other quinones; hydroquinone (Lot AX03328PW, 99⁻%), 1,4-benzoquinone (Lot 06012DG, 98%), 3,4-dihydroxybenzylamine hydrobromide (Lot 12330PZ, 98%), and Trolox (Lot 02525LZ, 97%) were purchased from Aldrich. Screening of free ferrocene groups was done using ferrocene carboxaldehyde (Lot CY13519MX, 98%) and dimethylaminomethyl ferrocene (Lot 02117AZ, 98%), both purchased from Aldrich. Other reagents used were ferrocene (Lot 174D, practical grade) purchased from Eastman, potassium ferricyanide (98.9%) from Fisher, and ferricinium hexafluorophosphate (Lot 10523HN, 98%) purchased from Aldrich.

The thiol substrates, reduced glutathione (Lot 12103KN, 98-100%), and L-cysteine hydrochloride hydrate (Lot 12203PW, 98%) were purchased from Aldrich. The thiol products, oxidized glutathione (Lot 102H8050, 98%) and L-cystine dihydrochloride (Lot 45H00541, 99⁻%) were both purchased from Sigma.

The cyclodextrins used were β-cyclodextrin hydrate (Lot 08025JG) purchased from Aldrich, and hydroxypropyl β-cyclodextrin (Wacker) obtained from Dr. Tee's laboratory.

Electrochemical tests were run in either a 0.1 M acetate buffer made from ACS reagent grade anhydrous sodium acetate (Lot 31H014616) from Sigma, and ACS reagent grade glacial acetic acid from Baker; or 0.1 M phosphate buffer made from reagent grade

sodium phosphate, monobasic (Lot 720005) from Fisher, and sodium phosphate, dibasic (Lot 82H0283) purchased from Sigma.

2.1.2 Synthesis of derivatized CDs

For initial tosylation of the β-CD, ACS reagent grade p-toluenesulfonyl chloride (Tosyl chloride, Lot 04920CY) , and a 67% dispersion of sodium hydride in mineral oil (Lot 03421LF) from Aldrich were used. Solvents were either ACS reagent grade N,N-dimethylformamide (Lot 01025AV) from Aldrich or ACS reagent grade dimethylsulfoxide (Lot G41625) from Baker, which were dried over 4A molecular sieves (Lot 06216KW) from Aldrich.

Work-up of the tosylated β-CD involved addition of ethylene diamine (Lot 79F0799, 99.5%) from Sigma, ACS reagent grade anhydrous pyridine (Lot 00901MX) from Aldrich, sodium cyanoborohydride (Lot 25895607, 90%) and 4-(2-hydroxyethyl)1-piperazineethanesulfonic acid (HEPES) (Lot 06819MX, 99%) from Aldrich.

2.1.3 Chemicals used in kinetic analysis and characterization

The carbohydrate assay used D-(+) glucose (Lot 83H0957) from Sigma, analytical grade sulfuric acid from Baker, and ACS reagent grade phenol (Lot 740538) from Fisher. Fluorescence inhibition studies used 8-anilino-1-naphthalene-sulfonic acid(ANS) (Lot PZ02115LZ, 95%) from Aldrich. All polishing of electrodes was done using a suspension of 1.0 micron alumina (Lot 406321008) purchased from Buehler. HPLC mobile phase was water and HPLC grade acetonitrile (Lot H25809) from Baker or optima grade acetonitrile (Lot 961398) from Fisher. Other solvents used were ACS certified butanol (Lot 8801766) from Fisher; ethanol, acetone, and methanol purchased from Chemical stores (technical

grade), and; HPLC grade iso-propanol (Lot 3032KLMM) from Mallinckrodt. ACS assured hydrochloric acid from BDH, and ACS reagent grade sodium hydroxide pellets from ACP Chemicals were also used at various times.

All solutions were made using distilled, deionized water from a Barnstead Nanopure ion-exchange system.

2.2 Instrumentation

For chromatography work, a Waters 510 HPLC pump was used; the detector was a Waters 410 Differential Refractometer and the column used was a Phenomenex Sephadex RP-C_{18} column (column grade is ODP-50 4D; column size is 4.6 mm ID * 150 ml). Peak plotting was done by a GW-BASIC 3.2 program (version 2.1), HPLC.bas on a 386 computer.

For determining molar absorptivity and comparing samples, and for the carbohydrate assay, a Varian Cary 1 double-beam UV-Visible Spectrophotometer was used with Cary 13 analysis software.

All electrochemical experiments were done using a BAS 100A Potentiostat. All tests were done under nitrogen degassing and a nitrogen blanket (Prodair High Purity Grade). Working electrodes were glassy carbon (GCE); gold or carbon paste electrodes, all from BAS. The reference electrode was silver/silver chloride electrode. The auxiliary electrode was a Nichrome wire obtained from technical services.

All mass spectral analyses were done using a Finnegan MAT SSQ 700 electrospray mass spectrometer.

2.3 Methods

2.3.1 Synthetic procedures

In order to attach the catalytic groups, quinone or ferrocene derivatives, onto β-CD, a preliminary synthesis step was required, whereby either the primary face or the secondary side of the β-CD was tosylated. Toluenesulfonyl chloride (Tosyl-Cl) is an efficient leaving group, and so can be readily substituted in subsequent reactions with a nucleophilic catalytic group.

2.3.1.1 Preparation of a primary Tosyl-β-CD

Primary tosylation proceeds by a one step mechanism[1], in a basic solvent such as pyridine or an aqueous sodium hydroxide. The tosyl chloride adds on to the primary hydroxyl to form the primary substituted β-CD (1'-β-CD).

To prepare the primary tosylated β-CD, 1.79 mmol of β-CD and an excess of tosyl-Cl (43.1 mmol) was dissolved in 200 ml of DMF and left stirring at room temperature for 2 days. About 30 ml of water was then added to the yellow solution, giving an exothermic reaction. A sample taken from the reaction flask had acetone added to it, but no precipitate formed. The remaining solution was vacuum distilled to remove excess solvent, to give a thick, yellow

liquid.

2.3.1.2 Synthesis of the secondary tosyl-β-CD[2]

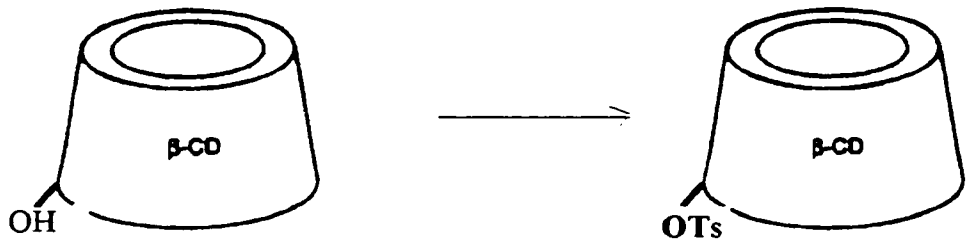

The tosylation of the secondary side of the β-CD is a two step reaction[3]. A strong base, sodium hydride, is required to abstract a proton from the secondary alcohol. During this step it is important to have anhydrous conditions otherwise solvolysis of the system will occur and starting products are regenerated, therefore the reaction is done in dry DMF or DMSO. These solvents have been previously dried over molecular sieves (4A) for 24 hours. Once the proton is abstracted the solvent stabilizes the ionic nature of the transition state as the tosyl group adds on.

The experimental procedure involved first, drying the DMF over the molecular sieves for 8 hours, decanting the liquid into a second flask with fresh molecular sieves and leaving the mixture to dry for a further 12 hours. Meanwhile, β-CD was dried in a 110° C oven, overnight, then stored in a desiccator. For the secondary tosylation reaction, 2.23 mmoles of β-CD was dissolved in 70 ml of dry DMF, then 5.57 mmoles of sodium hydride suspension was added, with stirring. The reaction flask was closed with a drying tube to prevent water from entering, and left stirring overnight at room temperature. A second reaction flask contained 2.27 mmoles of tosyl-Cl in 10 ml of dry DMF. This was also left stirring overnight, at room temperature. Then it was quickly added to the CD mixture, closed with the drying

tube, and left stirring, at room temperature, for 5 days. At this point, the reaction was stopped by the addition of 60 ml of water, added 1 drop at a time since the reaction is exothermic when water is added. Once the water is added, the entire solution was poured into 1 L of acetone, and left in the fridge for 2 hours to precipitate out a white powder. The powder was filtered using vacuum filtration, and stored in the desiccator.

2.3.1.3 Synthesis of hydroquinone-β-cyclodextrin

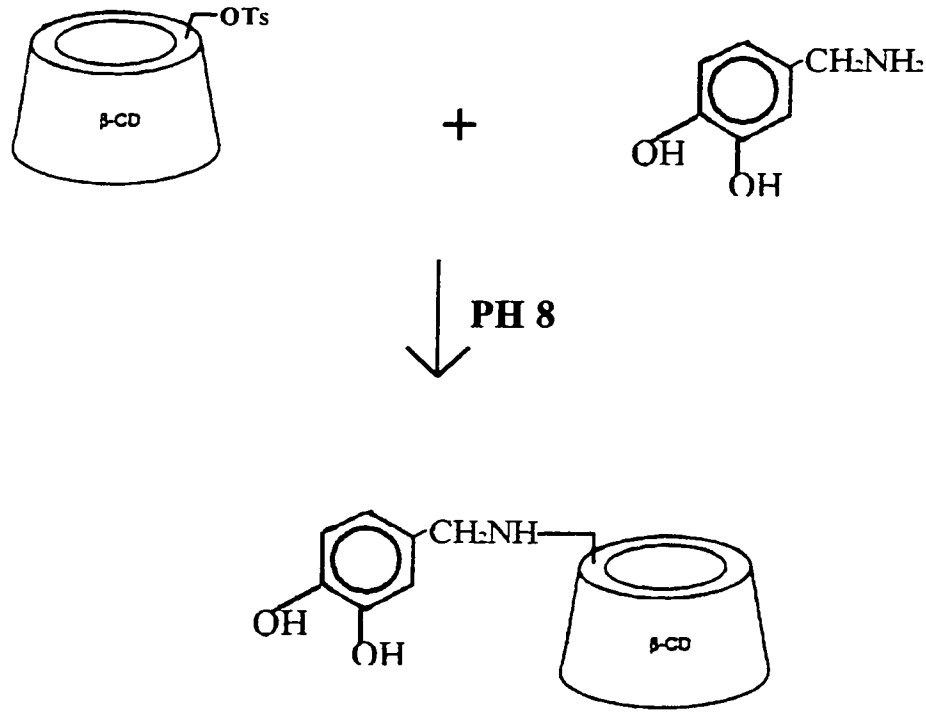

For reaction with the primary tosylated β-CD, it was assumed, based on β-CD as the limiting reagent, and assuming 30% yield of primary product, that 1.5 mmol of the primary product was present. A five-fold excess of the DHBA was added (7.5 mmol) to the solution,

and the flask is left stirring for 2 days at room temperature. About 2 ml of 5 M NaOH was added to raise the pH to 8.5. After 2 days the resulting brown solution is poured into 500 ml of acetone, to give a white precipitate, which was collected by vacuum filtration and stored in the desiccator.

Using the secondary tosylate β-CD, a five-fold molar excess (2.19 mmol) of dihydroxybenzylamine (DHBA) was added, in 15 ml of water, with pH adjusted to pH 8 using 4 drops of 5 M sodium hydroxide solution. The resulting brown solution was left stirring for 4 days at room temperature, at which time, 500 mL of acetone was added to precipitate out any unreacted cyclodextrin species. The brown precipitate was collected by vacuum filtration, washed with acetone, and left to dry in the desiccator. The filtrate was vacuum distilled to remove excess acetone and solvent to a deep orange color. This product solution was stored at 4°C.

2.3.1.4 Synthesis of ferrocene-β-CD

To prepare the substituted ferrocene-β-CD, it was necessary to first prepare the ferrocene compound. This reaction[4] involves the reduction of a Schiff base which has been formed from ferrocene carboxaldehyde and ethylenediamine in a HEPES buffer. The Schiff base intermediate is reduced to a secondary amine by the sodium cyanoborohydride to finally form the methylated derivative of the ferrocene.

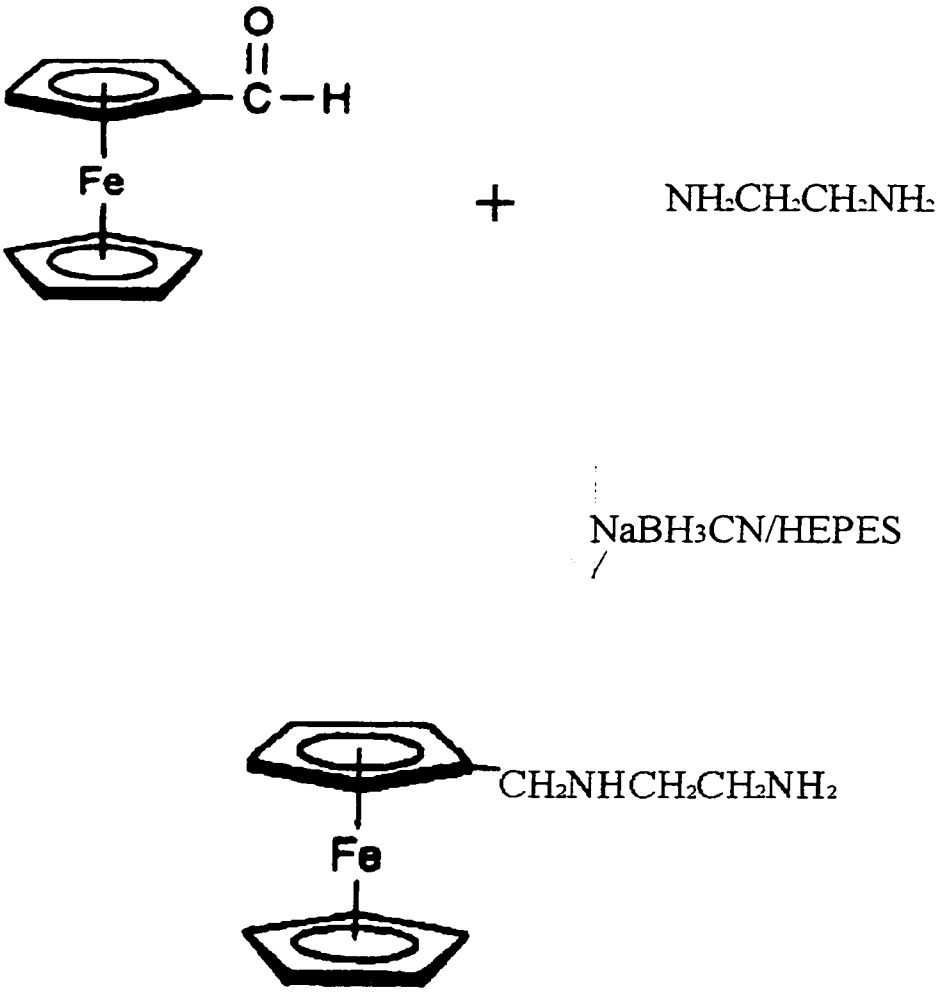

To prepare the primary or secondary substituted ferrocene-CD derivative, 10.10 mM FCO, 9.90 mM ethylene diamine, and 100.40 mM cyanoborohydride were added to of 100 mMHEPES buffer(pH 7.5), and left stirring at room temperature overnight. The solution, a bright orange, was then filtered to remove any undissolved FCO, and based on ethylene diamine as the limiting reagent, a 1:1 mole ratio of the primary or secondary tosylated β-CD (9.85 mM of tosylated β-CD) was added. The reaction was left stirring for 5 days at room temperature, then stored in the fridge.

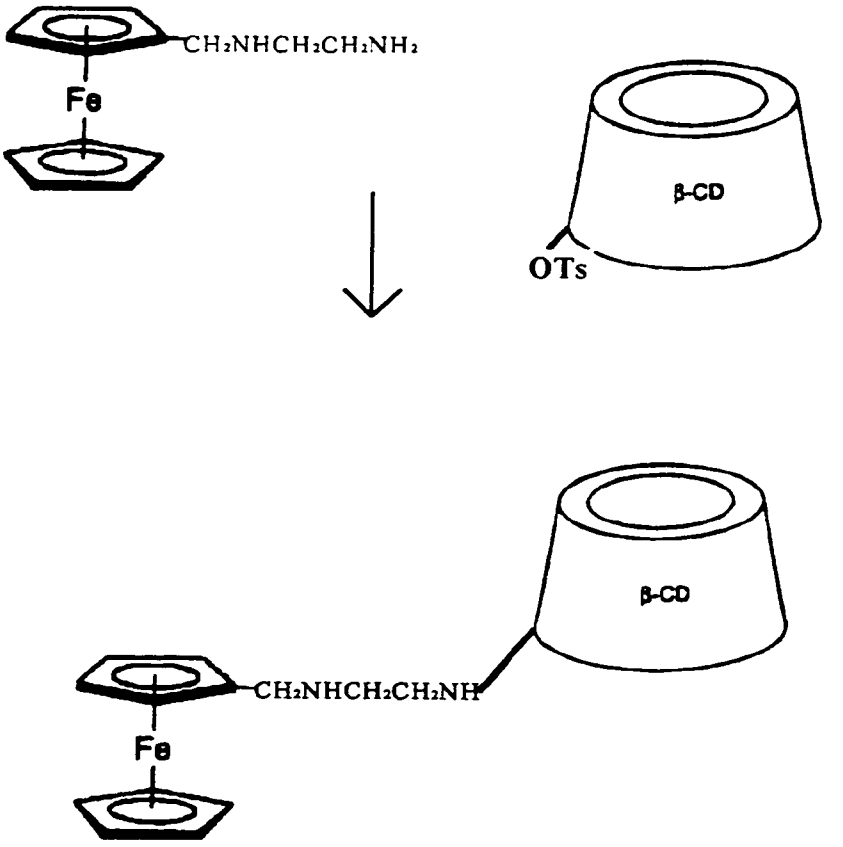

2.3.2 Purification of Cyclodextrin Derivatives

To purify and collect the products from the derivatization reactions, reversed phase HPLC (RP-HPLC) was used.

2.3.2.1 Purification of the DHBA-CD Products

In order to identify which peaks on the chromatogram belong to unreacted starting materials, and which belong to the desired product, the starting materials were injected into the column (0.3 mL each injection) in separate runs in order to determine the time of elution of each starting material. Then, separately, the derivatized species were also run on the column, and unique peaks identified, as shown in the table below. Separation was done using as mobile phase 10:90 acetonitrile:water, on the C_{18}- RP column, at a flowrate of 1 mL/min under 1800 psi column pressure, using a refractive index detector.

Chromatogram due to:	Retention time of peaks, min.:
β-cyclodextrin	2.3
Tosyl chloride	2.5
DHBA	1.9, 2.4
1-Ts-β-CD	2.1, 2.3, 13.6
2-Ts-β-CD	2.1, 2.3, 12.1
1-DHBA-β-CD	1.9, 2.5, **3.7**
2-DHBA-β-CD	1.9, 2.3, **5.5**, 12.0

In all cases, the void volume was at 1.9 - 2.5 minutes. The peaks collected from each run are highlighted in bold.

2.3.2.2 Purification of ferrocene cyclodextrin derivatives

Again, starting materials were injected separately to generate chromatograms of the individual starting materials. Then, in separate runs, the derivatized ferrocene-CD species were injected, and unique peaks were identified, which did not belong to the chromatograms of the starting compounds. The RP-HPLC conditions were the same as the previous section. The table below summarizes the retention times of the peaks due to each species from their unique chromatograms.

Chromatogram due to:	Retention time of peaks, min.:
β-CD	2.3
Tosyl-Cl	2.3
ferrocene carboxaldehyde	2.3, 7.9
Ethylene diamine	2.3
Ferrocene -ethylene diamine product	2.3, 19.5
1-Fc-β-CD	2.1, 2.8, **5.5**
2-Fc-β-CD	2.3, **5.9**, 7.9, **9.8**, 19.5

The void volume was at 2.1- 2.3 minutes. Fractions collected are highlighted in bold. Since there were two unique peaks for the secondary ferrocene product, both were collected, and differential pulse voltammetric scans of the two fractions, as compared to ferrocene carboxaldehyde indicated no redox activity for the sample collected at 5.9 minutes. Therefore this fraction was not collected in subsequent runs.

Once the unique peaks corresponding to the possible functionalized products were identified, an extensive collection procedure was begun. It should be noted that for purposes

of collection of the secondary ferrocene product, the mobile phase ratio was adjusted to 5:95 acetonitrile:water, in order to improve resolution. Once sufficient volume (80 - 100 ml) was collected, the samples were concentrated under vacuum (Büchi 461 Rotovapor), using a nitrogen-cooled vacuum pump. From each 80 to 100 mL sample we were able to obtain about 20 mL of a colored solution.

2.3.3. Characterization of products

In order to characterize the products, the first step after collecting and concentrating the products was to obtain UV-Visible spectra. Comparison of the product spectra was made with either an aqueous solution of DHBA (λ_{max}=206 nm; ϵ= 1.56x10^4 M^{-1}cm^{-1}) for the quinone derivative, or aqueous dimethylaminomethyl ferrocene solution (λ_{max}= 204 nm; ϵ=2.71x10^4 M^{-1}cm^{-1}) for the ferrocene-CD derivative. All solutions were diluted in 0.1 M phosphate buffer at pH 7.0, and this was used as the reference blank.

Further characterization of the products obtained was also done using electrospray mass spectrometry. Both the DHBA-β-CD and the Fc-β-CD purified products were examined using mass spectroscopy, with comparisons made to a β-CD mass spectra. The results of these experiments will be presented in the next chapter.

For the 2-Fc-β-CD, further characterization included a carbohydrate assay in an attempt to clarify the substitution and to show that cyclodextrin was present. This assay involved the development of calibration curves using glucose standards and β-CD standards. The unknown was tested, and results compared to the standard calibration curves obtained from the digest of the glucose, and β-CD. In this carbohydrate assay[5], β-CDs are hydrolyzed to glucose units, and with the presence of concentrated sulfuric acid, glucose is dehydrated

to furanal. This reaction was done in an ice bath to prevent excess heating and degradation of the species which gave false readings. Upon formation of the intermediate, phenol is added to produce a bright yellow product, whose absorbance could be read at 492 nm.

The exact procedure[6] for the carbohydrate assay involved the preparation of a 0.278 mM solution of glucose in distilled water, and 4.45×10^{-5} M β-CD in distilled water. A series of dilutions are pipetted into vials, making up to 2 ml with water, resulting in 10 vials containing glucose dilutions, 10 vials with varying β-CD dilutions and 4 vials without any added carbohydrates as blanks. The vials are placed in an ice bath, and 5 ml of concentrated sulfuric acid is added to each vial. Once the vials are cool, 500 μL of an 80% phenol solution (80% (w/w) phenol/water) are pipetted in. The vials are capped and stored overnight at room temperature. The ferrocene-β-CD product is also pipetted into vials, and a series of dilutions are made. The other reagents are added in the same manner as for the glucose or the β-CD. Absorbance was measured at 492 nm using plastic cuvettes, both with water as the blank, and the carbohydrate-free vials as the blank.

2.3.4 Electrochemical methods

To determine the observed rate constants for the oxidation of the thiols by the different catalytic groups, the oxidation current from voltammetric scans was found. The mechanism involved in generating our catalytic waves is termed the ECE mechanism[7], where E denotes the electrochemical reaction, and C is the chemical reaction. This mechanism involves the electrochemical generation of a species, which then reacts with another species in solution, regenerating the starting material for the electrochemical reaction. The sequence of events is thus:

E: $R \rightleftharpoons O + ne$ (1)

C: $O + Y \rightarrow R + Z$ (2)

E: $R \rightarrow O + ne$ (3)

In terms of the reactions followed in our experiments, the sequence of events would involve the generation of the catalytic group (quinone or ferricinium) at the electrode followed by the subsequent chemical reaction with the substrate (thiol, either cysteine or glutathione) in solution, to regenerate the hydroquinone or ferrocene.

The voltammetric scan is begun at a potential that is negative of the catalyst's formal reduction potential, and is scanned linearly in a positive direction. At some potential it is sufficiently positive as to cause oxidation of our catalytic species. This oxidation causes the anodic current to increases as the surface concentration of the reduced form decreases. Then, in solution, the oxidized catalyst reacts with the thiol, producing thiyl radical, RS·, which then yields the disulfide by dimerization, and the catalytic group is subsequently re-oxidized at the electrode to continue the redox cycling. Unless otherwise noted, scans were generally performed from at least 400 mV negative of the formal potential to 400 mV positive of this value, at a scan rate of 2 mV/s. All experiments must be done under nitrogen, to avoid interference from molecular oxygen.

In order to determine the observed catalytic rates, a pseudo first order reaction was assumed, and a 10-fold excess of the thiol substrate was used. The rates were measured by generating a series of voltammograms of differing absolute concentrations while maintaining a 10:1 concentration ratio of thiol substrate to catalyst, and measuring the observed oxidation current. If no thiol is present, a normal cyclic voltammogram of the catalytic group shows the

reversible nature of the redox reaction. However, once the substrate is present, and catalysis and redox cycling proceed, a catalytic wave is generated.

A series of voltammetric scans was performed at varying concentration of substrate and catalytic group. Electrocatalytic currents were measured at a fixed potential for each catalyst from the voltammograms. These currents are related to the observed thiol oxidation rate by the following equation:[8]

$$i_{\infty} = nFA[C](Dk[S])^{1/2} \qquad (4)$$

where n is the number of electrons; F is Faraday's constant (96,487 C/mol); A is the area of the electrode (0.0707 cm^2); D is the diffusion coefficient for the catalytic species; C and S refer to the concentration of the catalyst and thiol substrate, respectively; i is the limiting oxidation current in μA, which is measured on the voltammetric scan, and; k is the observed thiol oxidation rate in $M^{-1}s^{-1}$ which is to be determined.

In order to determine the observed catalytic rate, equation (4) was rearranged to the form:

$$i = m[C][S]^{1/2} \qquad (5)$$

where a plot of i against $[C][S]^{1/2}$ is used to obtain a slope:

$$m = \text{slope} = nFA(Dk)^{1/2} \qquad (6).$$

The observed thiol oxidation rate for the free systems is then calculated as:

$$k = 725.8\ (\text{slope})^2 \text{ for a two electron system} \qquad (7a)$$

$$k = 3358\ (\text{slope})^2 \text{ for a one electron system} \qquad (7b)$$

Or, for the complexed deriviatized systems, the relevant equations are:

$$k = 1773\ (\text{slope})^2 \text{ for a two electron system} \qquad (8a)$$

$$k = 8202(\text{slope})^2 \text{ for a one electron system} \qquad (8b)$$

where the diffusion coefficients used for the calculation are:

D(free quinones) = 7.4×10^{-6} cm^2/sec [9]

D(free ferrocenes) = 6.4×10^{-6} cm^2/sec [10]

D(complexed quinones) = 3.0×10^{-6} cm^2/sec, and

D(complexed ferrocenes) = 2.6×10^{-6} cm^2/sec.

The complexed diffusion coefficients were calculated based on a ratio of complexed to free diffusion coefficient[9] of 0.41 ($=D_c/D_f$).

In all experiments, acetate (pH < 5) or phosphate (pH 7-8) buffers were used at a concentration of 0.1 M. Blank voltammograms were run of the quinone by itself, the thiol, and the ferrocene alone. All solutions were de-aerated with nitrogen for 15 minutes before the scan, and a nitrogen blanket was maintained during the run. Diffusion control is necessary, so no stirring was allowed during the run.

As well, to generate the calibration plots of the Fc-β-CD synzyme, the concentration of the synzyme was held constant, while the concentration of cysteine or glutathione was varied. Again all tests were performed in phosphate buffer at a constant pH of 7. For these experiments comparison of the effects of electrodes was also done, as the scans were run using glassy carbon (GCE), gold, and a carbon paste electrodes. The GCE was polished between runs for 10 minutes on 1.0 micron alumina polishing pad, then sonicated for 5

minutes in distilled, deionized water. The other electrodes were washed with distilled, deionized water between runs, and carefully blotted with a Kimwipe only.

References

1. R. T. Morrison, and R.N. Boyd. "Organic Chemistry", 3rd ed., Allyn and Bacon, Inc., Boston, 1973. pp. 466-474.

2. D. Rong, and V.D'Souza. *Tetrahedron Lett.* **1990**, *31*, 4275-4278.

3. R. T. Morrison, and R.N. Boyd. "Organic Chemistry", 3rd ed., Allyn and Bacon, Inc., Boston, 1973. pp.458-467.

4. N. Jentoft, and D.G. Dearborn. *J. Biol. Chem.* **1979**, *254*(11), 4359-4365.

5. S.R. Mikkelsen. "Advanced Bioanalytical Chemistry", Concordia University, 1994. pp.8-9

6. M. Dubois, K.A. Gilles, J.K. Hamilton, P.A. Rebers, and F. Smith. *Anal. Chem.* **1958**, *28*, 350-353.

7. P.T. Kissinger, C.R. Preddy, R.E. Shoup, and W.R. Heineman. Fundamental Concepts of Analytical Electrochemistry in "Laboratory Techniques in Electroanalytical Chemistry", P.T. Kissinger, W.R. Heineman eds., Marcel Dekker, Inc., New York, 1984. pp. 39-43

8. A.J. Bard, and L.R. Faulkner. "Electrochemical Methods: Fundamentals and Applications", John Wiley & Sons, New York, 1980. pp. 457-459

9. Ralph N. Adams. "Electrochemistry at Solid Electrodes", Marcel Dekker, Inc., New York, 1969. pp.214-265

10. T.Matsue, D.H.Evans, T.Osa, and N.Kobayashi. *JACS.* **1985**, *107*, 3411-3417.

Chapter 3

Results and Discussion

3.1 Electrocatalytic Measurements of Rates of Thiol Oxidation.

3.1.1 Quinone Derivatives

A series of quinones shown in Figure 3.1 were examined electrochemically in order to compare rates of thiol oxidation. The thiols tested, glutathione (GSH) and cysteine (Cys) form disulfides once oxidized in a two-electron process. The structure of glutathione and cysteine are shown in Figure 3.2.

Because of the interest in using these quinones as catalytic groups in artificial enzyme, measurements were made in the presence and absence of β-cyclodextrin (β-CD). As the purpose of these initial tests was to determine the quinone derivative best suited for further work, all tests involved a comparision of glutathione (GSH) oxidation rates. The experimental data used to calculate observed thiol oxidation rates for the quinone derivatives and thiols is given in Appendix A.

An example of the voltammetric scans obtained is shown in Figures 3.3(a, b), which show the effect of added free β-CD on the oxidation of glutathione by DHBA in pH 3.8 acetate buffer.

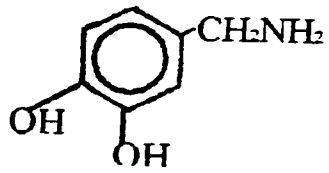

Dihydroxybenzylamine
(DHBA)

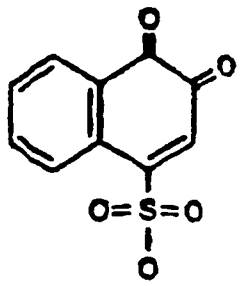

1,4-Napthoquinone
(NQ)

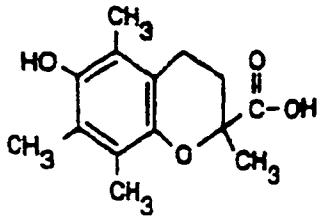

Trolox

Figure 3.1- Quinone catalytic groups studied

$H_2NCHCH_2CH_2CONHCHCONHCH_2COOH$
$COOH \qquad CH_2SH$

Glutathione (GSH)

$HSCH_2CHCOOH$
NH_2

Cysteine (Cys)

Figure 3.2 - Structures of thiol substrates.

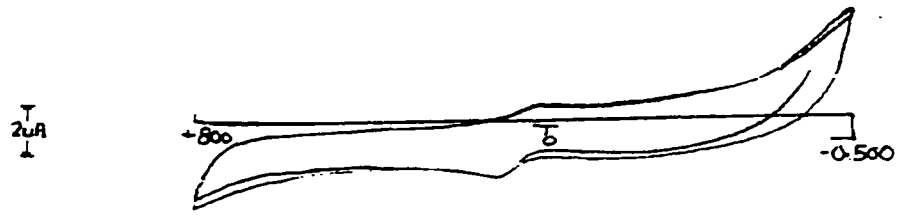

Figure 3.3(a) -Reversible quinone redox wave. 0.63 mM DHBA in 0.1 M acetate buffer at pH 3.8. on GCE.

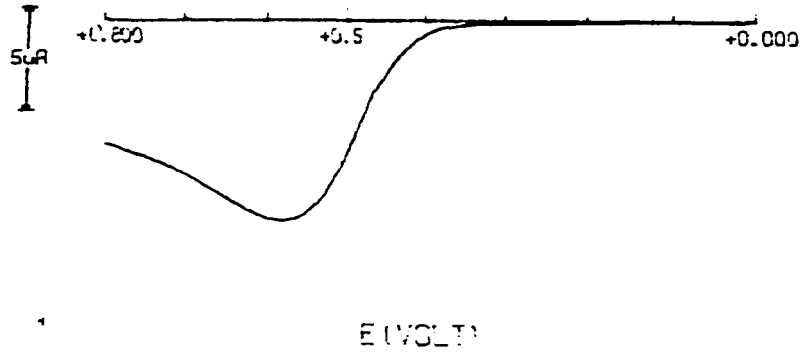

Figure 3.3(b)- Catalytic wave for 5.8 mM GSH oxidation with 0.63 mM DHBA/10 mM β-CD in 0.1 M acetate buffer at pH 3.8 on GCE.

As seen in these scans, the addition of the quinone increases the GSH oxidation current, from 0 μA with only the DHBA in solution to 9.4 μA when DHBA and free β-CD is present.

An example of the experimental results, and the subsequent plot of the data in order to determine thiol oxidation rates is given below in Table 3.1 and Figure 3.4. The table shows the relatively small change in slope observed when β-CD is added to the DHBA/GSH system. The observed thiol oxidation rates would be calculated as 25.7 and 36.7 $M^{-1}s^{-1}$, as given in Table 3.2. The data was also plotted, as shown in Figure 3.4 in order to obtain the required slope and intercept.

Table 3.1 - Raw Data for DHBA/GSH at pH 3.8

[DHBA] mM	[GSH] mM	x-axis $x10^{-5}$	i_{obs}, µA no β-CD	i_{obs}, µA 10 mM β-CD
0.6316	5.613	4.732	9.2	9.4
0.4737	4.210	3.074	7.0	6.7
0.3790	3.368	2.200	5.7	6.0
0.3158	2.806	1.673	4.8	4.8
0.2369	2.105	1.087	3.7	3.7
0.1895	1.684	0.7776	2.8	3.0
0.1579	1.403	0.5914	2.3	2.2
		intercept	1.43	1.09
		slope	1.88	2.25
		r value	0.993	0.995

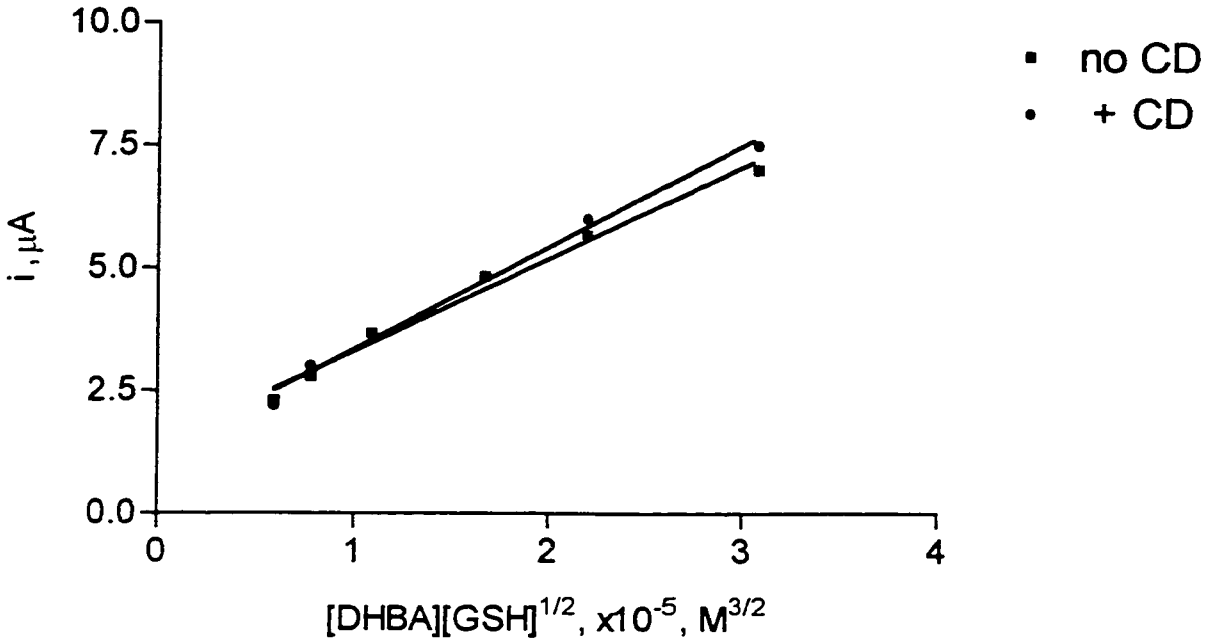

Figure 3.4 - Plot of varying concentration of GSH and DHBA as electrocatalyst, with and without free β-CD in 0.1 M acetate buffer at pH 3.8. Thiol oxidation current measured at 600 mV using GCE as working, Ag/AgCl as reference electrodes. Scan rate at 2 mV/sec.

A series of experiments was done to determine the effect of pH on GSH oxidation rates by 2-aminomethyl-1,4-benzoquinone (AMQ, the quinone form of DHBA). The results are summarized in Table 3.2.

Table 3.2 - Effect of pH on GSH oxidation rates by DHBA in the presence and absence of 10 mM β-CD

pH	k_{obs}, $M^{-1}s^{-1}$ no β-CD	k_{obs}, $M^{-1}s^{-1}$ 10 mM β-CD
2	16.3	13.4
3.6	20.7	23.0
3.7	19.8	23.3
3.8	25.7	36.7
3.9	24.0	20.7
4.0	30.5	12.6
4.2	15.0	14.0
4.6	16.6	13.0
7.0	18.3	19.0

For pH 7.0, a 0.1 M phosphate buffer was used; all other buffers were 0.1 M acetate

The results show that the largest rates were obtained in the pH 3.8 - 4.0 range, in the presence of β-CD. However, applications to sensors for bioreactors, for example, require activity at neutral pH. Therefore in comparing different quinone derivatives, pH values of 3.8 and 7.0 were used. A summary of the results for different quinones is shown in Table 3.3.

Table 3.3 - Observed rates for GSH oxidation by various quinone derivatives.

Quinone	pH	k_{obs}, $M^{-1}s^{-1}$ no β-CD	k_{obs}, $M^{-1}s^{-1}$ 10 mM β-CD
DHBA	3.8	25.7	36.7
	7.0	18.3	19.1
NQ	3.8	0.79	0.59
	7.0	0.33	0.06
BQ	3.8	4.0	4.3
	7.0	2.4	1.2
Trolox	3.8	-------	-------
	7.0	0.73	0.75

Trolox is not soluble at pH 3.8, so no data are available.

The results in Table 3.3 are consistent with the results in Table 3.2, in that GSH oxidation rates are always higher at more acidic pH, with the highest GSH oxidation rates obtained with DHBA at pH 3.8. In fact, for all these tests, only DHBA at pH 3.8 showed a rate acceleration in the presence of β-CD. With this system, the thiol substrate and the free DHBA catalyst must be simultaneously binding in the β-CD cavity. As both species interact in the β-CD cavity, an enhanced thiol oxidation rate is observed, as the catalyst and substrate are brought into close proximity to each other. All the other quinone derivatives showed either no change or a decreased rate with free β-CD.

3.1.2 Ferricinium Derivatives

Ferrocene carboxaldehyde (FCO) and dimethylaminomethylferrocene (FMAM),

(Figure 3.5), were tested as possible catalysts for thiol oxidation using GSH as the thiol in the presence and absence of 10 mM β-CD.

For comparison with the quinone results these experiments were performed at pH 3.8 and pH 7.0, using acetate buffer for the lower pH, and phosphate buffer for pH 7.0 studies.

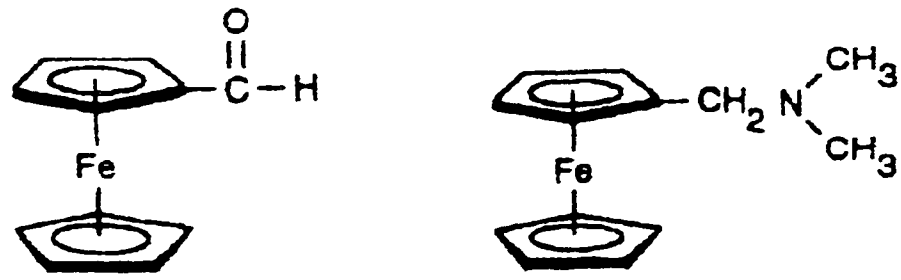

Ferrocene carboxaldehyde (FCO)

Dimethylaminomethylferrocene (FMAM)

Figure 3.5- Ferrocene derivatives tested for catalytic effect on thiol oxidation.

A summary of the results is shown in Table 3.4.

Table 3.4 - Observed GSH oxidation rates for ferricinium derivatives

Oxidant	Substrate	pH	k_{obs}, $M^{-1}s^{-1}$ no β-CD	k_{obs}, $M^{-1}s^{-1}$ 10 mM β-CD
FMAM	GSH	3.8	43	55
FMAM	GSH	7.0	96	134
FCO	GSH	3.8	2.8	7.6
FCO	GSH	7.0	2.0	21
FCN	GSH	7.0	48	38
FCN	Cys	7.0	90	38

In this table, ferricyanide (FCN) is added for comparison purposes, because it is highly negatively charged and does not bind to the cyclodextrin cavity. These results show that GSH binds β-CD, since there is a decreased rate of GSH oxidation by FCN when β-CD is present. This is analogous to the decreased rates observed for GSH oxidation by quinone derivatives in the presence of β-CD (Table 3.3).

Both ferricinium derivatives showed enhanced GSH oxidation rates in the presence of free β-CD. In these cases, the effect is much larger at pH 7.0. This effect is most obvious for the FCO/GSH system, where the ratio of rates obtained in the presence and absence of β-CD is 7.6/2.8 (2.7:1) at pH 3.8, and 21/2.0 (10:1) at pH 7.0 (see Table 3.5, and Figure 3.6 for experimental results). A compilation of data for these experiments is given in Appendix B.

Thus, it appears that the best candidate for derivatization of a cyclodextrin is a

ferrocene. For comparision, β-CD was also derivatized with DHBA. The next section concentrates on the characterization of these species. Since the ultimate goal is to use the synthetic enzyme in a biological application, all further tests of catalytic ability are performed near pH 7.0.

Table 3.5 - Raw Data for GSH oxidation by FCO in 0.1 M phosphate buffer at pH 7.0

[FCO] mM	[GSH] mM	x-axis $x10^{-5}$	i_{obs}, µA no β-CD	i_{obs}, µA 10 mM β-CD
0.580	5.515	4.337	--------	3.17
0.438	4.136	2.817	0.96	2.67
0.350	3.309	2.016	0.65	1.96
0.292	2.758	1.533	0.52	1.28
0.219	2.068	0.996	0.37	1.02
0.175	1.655	0.713	0.33	0.83
0.146	1.379	0.542	0.24	0.75
		intercept	0.11	0.20
		slope	0.26	0.86
		k_{obs}, $M^{-1}s^{-1}$	2.0	21

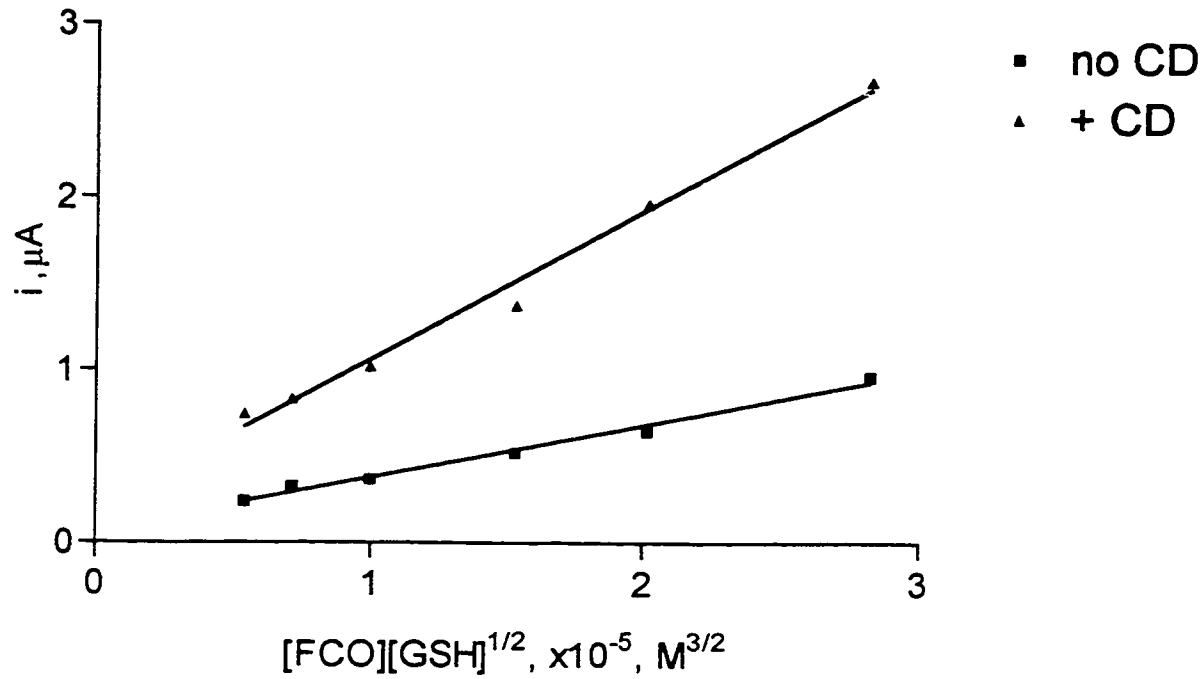

Figure 3.6 - Plot of voltammetric experimental data of FCO as electrocatalyst for GSH oxidation in the presence and absence of 10 mM β-CD. Scan at 2 mV/sec, current measured at 700 mV. GCE as working, Ag/AgCl as reference electrodes.

3.2 Isolation and Characterization of Cyclodextrin Derivatives

As mentioned in the experimental section, the primary and secondary functionalized cyclodextrins were isolated by collecting eluent fractions following RP-HPLC. After collection of the fractions of interest, they were concentrated under vacuum to yield either the DHBA-β-CD or the FC-β-CD products. This section deals with the characterization of these products.

3.2.1 UV-Visible Spectrophotometry

3.2.1.1 DHBA and DHBA Products

A DHBA standard (7.27×10^{-5} M) in pH 7.0 phosphate buffer showed two distinct peaks at wavelengths of 280 nm ($\epsilon = 2.5 \times 10^{3}$ $M^{-1}cm^{-1}$), and 205 nm ($\epsilon = 2.2 \times 10^{4}$ $M^{-1}cm^{-1}$), as shown in Figure 3.7. UV-Vis scans of the primary DHBA-β-CD and secondary DHBA-β-CD products are shown in Figure 3.8.

The 1°-DHBA-β-CD fraction collected at 3.73 minutes, then concentrated to a pink solution, while the 2°-DHBA-β-CD product was precipitated from aqueous solution by acetone to give a brown solid and a yellow filtrate. The yellow filtrate was concentrated to a bright orange solution and again purified by RP-HPLC to collect the fraction at 5.5 minutes. Again the fraction was concentrated. Each of these species had been diluted in pH 7.0 phosphate buffer.

The 1°-DHBA-β-CD product had a large peak at 204 nm ($A_{204} = 1.1$), and a small peak at 280 nm ($A_{280} = 0.14$); the 2°-DHBA-β-CD UV-Vis scan showed 2 peaks also, at 203 nm ($A_{203} = 0.33$), and at 284 nm ($A_{284} = 6.8 \times 10^{-3}$).

Based on the molar absorptivity at 205 nm from the DHBA standard, and using the

absorbances at 204 nm and 203 nm, respectively of the primary and the secondary DHBA products, the concentration of the primary product was calculated as 1.95 mM, and that of the secondary product was 2.99 mM.

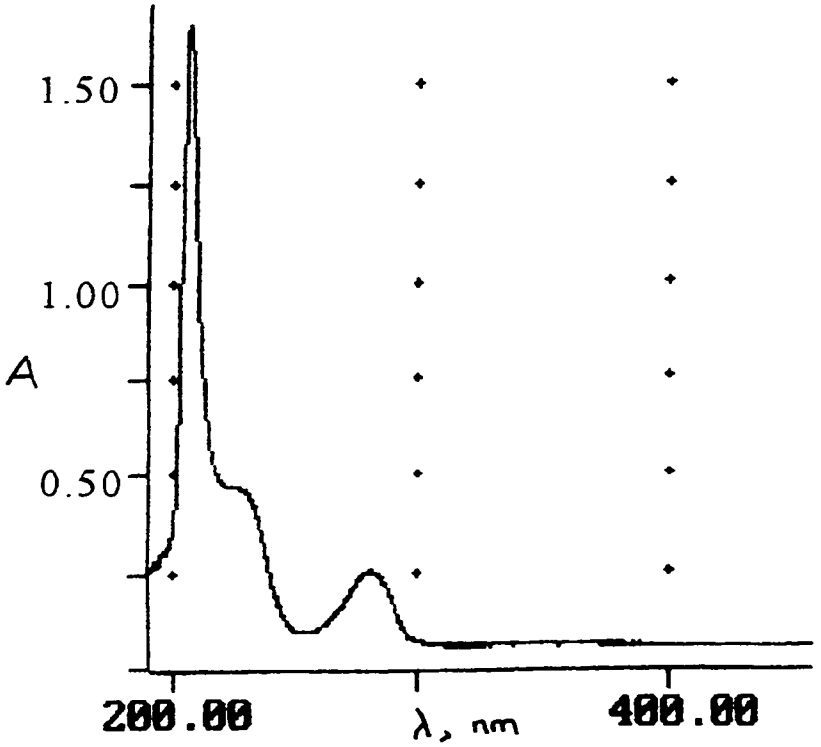

Figure 3.7 - DHBA standard (7.27×10^{-5} M) in pH 7.0 phosphate buffer.

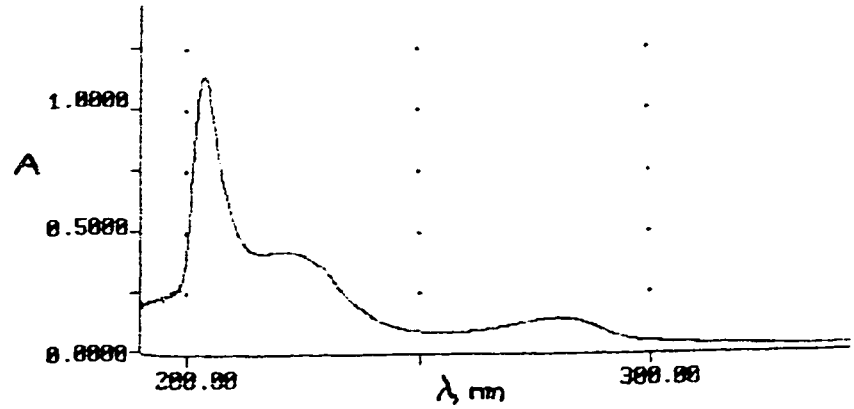

Figure 3.8(a) - Primary DHBA-β-CD in pH 7.0 phosphate buffer

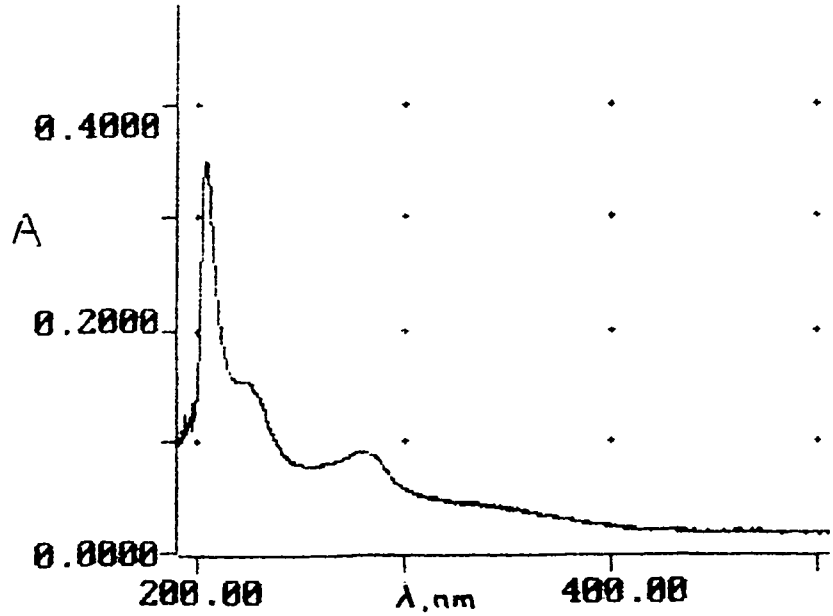

Figure 3.8(b) - Secondary DHBA-β-CD in pH 7.0 phosphate buffer

3.2.1.2 Ferrocene and Ferrocene Products

A FMAM standard (0.042 mM) in pH 7.0 phosphate buffer, shown in Figure 3.9, showed one major peak at 204 nm (ϵ =2.71 x 10^4 $M^{-1}cm^{-1}$).

The primary ferrocene β-CD product mixture was filtered, and the yellow filtrate was purified using RP-HPLC, by collecting the fraction at 11.8 minutes, which was then concentrated under vacuum. The secondary product was collected at 9.5 minutes and concentrated to a yellow solution. The results of the UV-Visible scan on the two products are shown in Figure 3.10(a,b).From the ϵ_{204} from the FMAM scan, the concentration of the primary product based on the peak at λ=203 nm (A_{203}= 0.342) was calculated to be 1.92 mM and the concentration of the secondary product based on the peak at 207 nm (A_{207} = 2.44) was 0.59 mM.

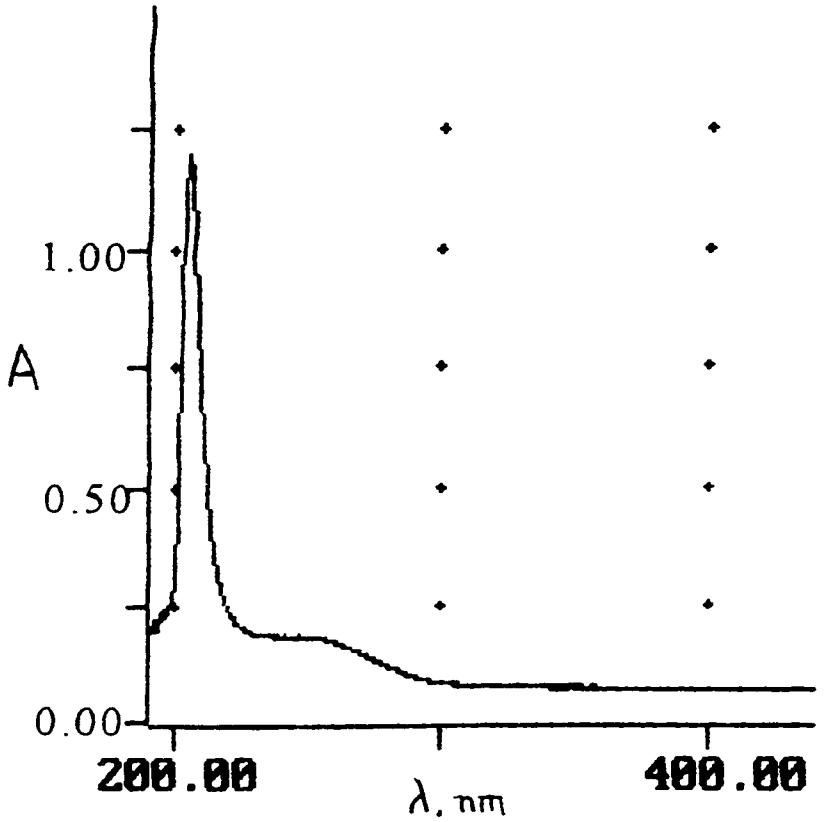

Figure 3.9 - FMAM (0.042 mM) in pH 7.0 phosphate buffer.

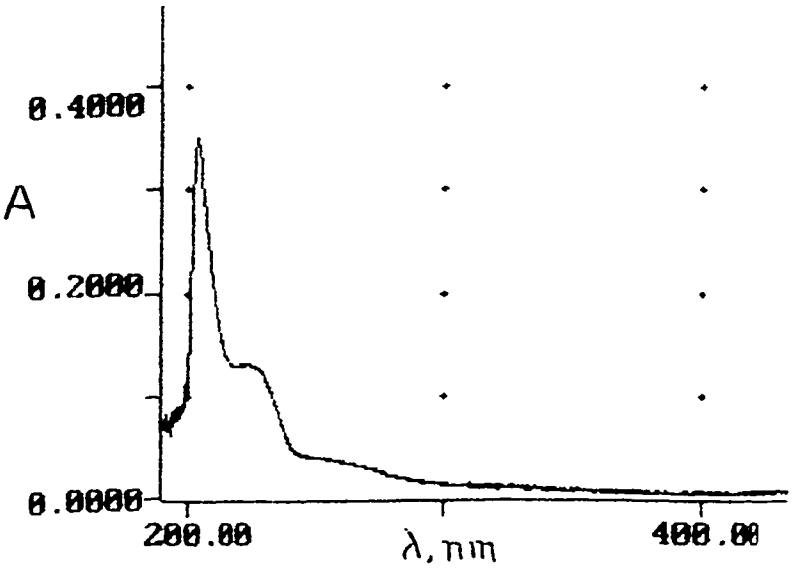

Figure 3.10(a) - Primary Fc-β-CD product in pH 7.0 phosphate buffer.

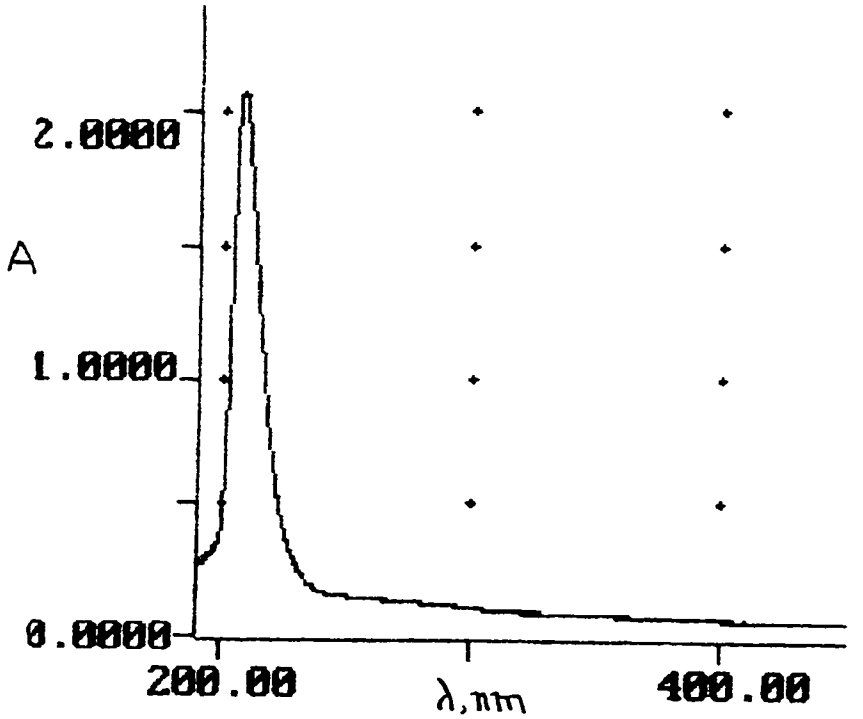

Figure 3.10(b) - Secondary Fc-β-CD product in pH 7.0 phosphate buffer

3.2.2 Carbohydrate Assay

In an effort to quantify the degree of substitution of ferrocene on the β-CD, and to determine that β-CD was present in the 2-Fc-β-CD product, a carbohydrate assay was attempted. The carbohydrate assay is based on the hydrolysis of β-CD into glucose, the conversion of six-membered glucose rings to five-membered furfurals, and subsequent conversion to a species which has an absorbance at 490 nm. Thus, the amount of glucose present in a sample can be determined by comparision to a standard curve generated using known amounts of glucose or β-CD. Since β-CD consists of 7 glucose units, a standard curve was generated of the known concentrations of β-CD, and the unknown samples were compared to the standard curve. The most linear standard plot of β-CD which was generated is shown in Figure 3.11.

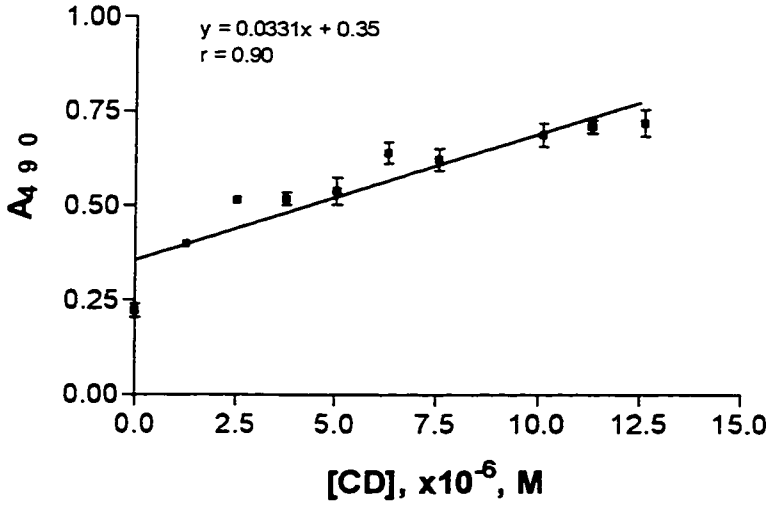

Figure 3.11 - β-CD standard curve generated from a carbohydrate assay of β-CD, measured at 490 nm. using water as a blank.

Attempts to determine stoichiometry based on the CD assay were not very successful, as not only were there problems generating a linear standard plot, the unknown product absorbance did not correlate to that of the standard curve in any statistical manner. This is shown in Table 3.6, where it can be seen there is not a match for any reasonable stoichiometry based on the results, as the unknown product known concentration does not correlate either 1:1 or 2:1 to the calculated concentration based on the standard curve.

Table 3.6 - Comparison of UV-Vis and Carbohydrate Assay Results for the Concentration of 2˙- Fc-β-CD

[Fc-β-CD] from UV-Vis, M	[Fc-β-CD] from carbohydrate assay, M
1.1×10^{-6}	0.21×10^{-6}
2.2×10^{-6}	4.4×10^{-6}
3.3×10^{-6}	5.6×10^{-6}
4.4×10^{-6}	13×10^{-6}
5.5×10^{-6}	7.1×10^{-6}

Part of the difficulty in interpreting is the large uncertainty in the assay results. For example, the blank solution consistently had a color change associated with it, even though no sugars were present in the sample. This color was also not consistent, varying between a bright orange and a yellow. The color variation also appeared in the other samples, where it was difficult to define a consistent color variation. After changing the experimental procedure by immersing the reaction vials in ice prior to hydrolysis, more consistent results were obtained, but the results were still not completely linear. It may be that the degree of

hydrolysis is inconsistent between vials, thus giving inconsistent results when phenol is added and the chromophore is formed. While commercial sugar assay kits are available, the breakdown of the cyclodextrins to the sugar unit would still be required prior to the kit assay, and if the problem arises from inconsistent and/or incomplete hydrolysis, this would still result in poor and non-linear response in our standard curves.

3.2.3 Mass Spectrometric Analysis

The first stage in the synthesis of either product was the preparation of the tosylated β-CD on either the primary or the secondary side of the β-CD. ES-MS of the tosylated products showed a mixture of the starting materials and the product peaks. Figure 3.12 shows the ES-MS of pure β-CD in 0.1 M sodium acetate buffer at pH 4.0. The peak at 1157.0 corresponds to the molecular ion peak of β-CD and sodium ion $(M + Na)^+$. Peaks at the lower (500-600 m/z) correspond to multiply charged peaks.

The MS of the primary product (see Figure 3.13) was done after separation of the primary tosylate by HPLC. Results show peaks due to β-CD (m/z = 1134); 1:1 Ts-β-CD (m/z = 1289) and; 2:1 Ts-β-CD (m/z = 1443). In this case, the MS was derived, meaning that a value of m/z = 22.998 was subtracted from the peaks in the spectra in order to subtract out the sodium from the molecular ion peak. The secondary tosylated β-CD is shown in Figure 3.14. For the secondary tosylated β-CD, the MS shown is similar to the above, but the unreacted β-CD peak at m/z = 1134 is larger as there was no initial separation of the materials. However there are clear 1:1 (m/z = 1289) and smaller 2:1 tosyl-β-CD peaks (m/z=1443).

Having confirmed the presence of the tosylated β-CD species, the next step was to

combine the Ts-β-CD with the other required starting materials to obtain the desired synthetic compound. After completion of the reactions, and isolation and purification, MS was done of the DHBA-β-CD, and of the Fc-β-CD products. However in these MS, the results are not as clear cut as for the tosylated species.

For the DHBA-β-CD products there appear to be no peaks at a m/z corresponding to the molecular ion peak. The entire spectrum has significant peaks only at the low end of approximately m/z = 600 or less. Attempts to identify if the pattern exhibited is multi-charged, and to what the peaks could correspond did not appear to be successful, as no correlation to structure and peak could be found. Part of the problem is that the peaks could correspond to multiple sodium charging and also to protonation. Therefore other means must be used to clarify the structure of the DHBA-β-CD species if any further work is to be done on this model of the synzyme.

For the Fc-β-CD products, again a series of possible multiply charged sodium and hydrogen peaks were obtained but a molecular ion peak was not. In both cases, a large peak at m/z = 403 was the predominant peak. A possible solution to this peak involves a single sodium, and four charges on a di-substituted Fc-β-CD, ie. there would be two -$^{-}NH_2CH_2CH_2^{-}NH_2$Fc arms attached onto the β-CD. However attempts to analyze the other peaks did not meet any success. Again, multiple hydrogen and sodium charging is possible. In an attempt to determine if the spectra correlate to those of other β-CD species, comparision was made with pure β-CD and hydroxypropyl-β-CD (Hp-β-CD). The β-CD showed the expected spectrum with the dominant peak at m/z = 1157 being the molecular ion peak plus sodium. The Hp-β-CD spectrum however, gave the same peak pattern as the Fc-β-

CD spectra, with dominant peaks at m/z = 403, 457, 487, and 313. Therefore, there appears to be some correlation between these systems, indicating there is a β-CD system in our products, however peak identification is not possible. As well as the possibility of multiple charging, there is also the possibility that the molecules are fragmenting in the MS, but again it is difficult to correlate the peaks obtained to some pattern of fragments and charges with sodium and/or hydrogen. It may be possible to obtain more useful spectra by MALDI-MS where the molecular ions are generated by a different mechanism.

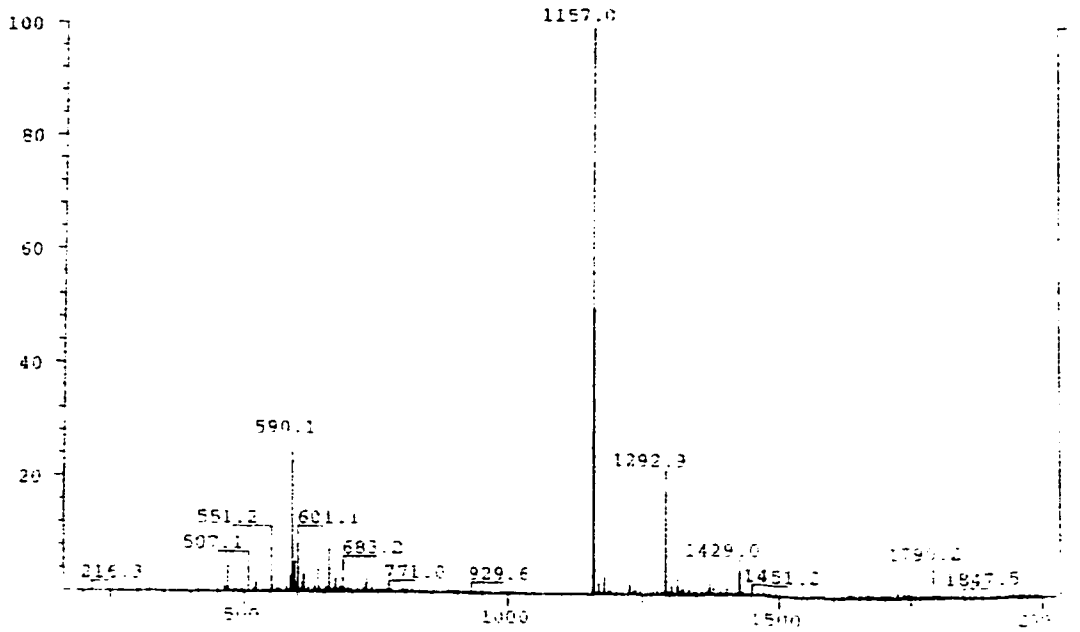

Figure 3.12 - ES-MS of β-CD in pH 4.0 sodium acetate buffer, in positive ion mode.

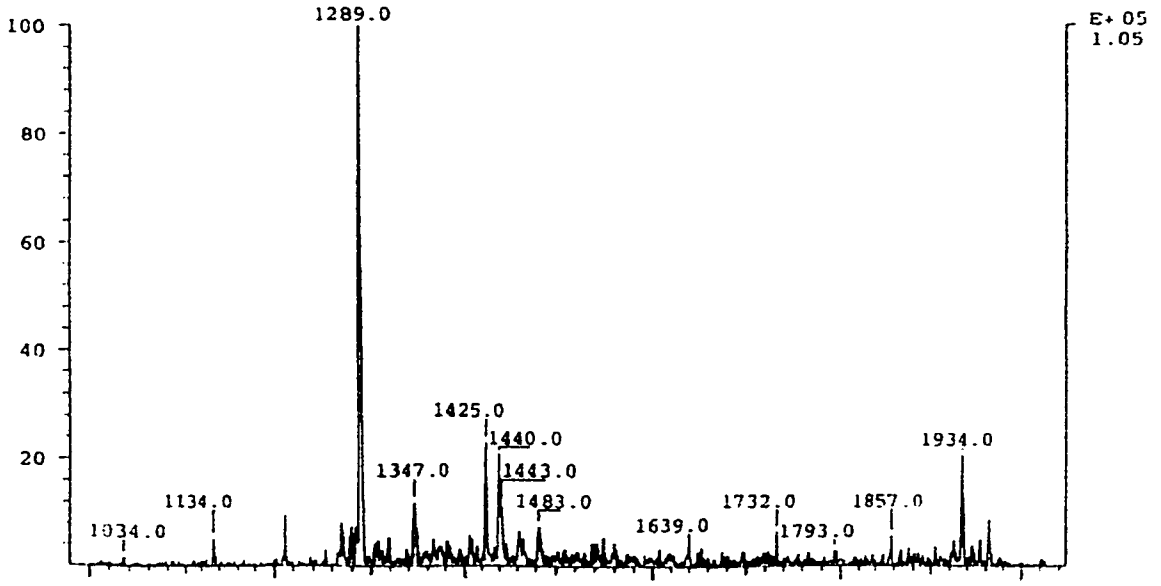

Figure 3.13- ES-MS of primary tosylated β-CD, after purification by RP-HPLC. Spectrum shown is derived, to correct for Na.

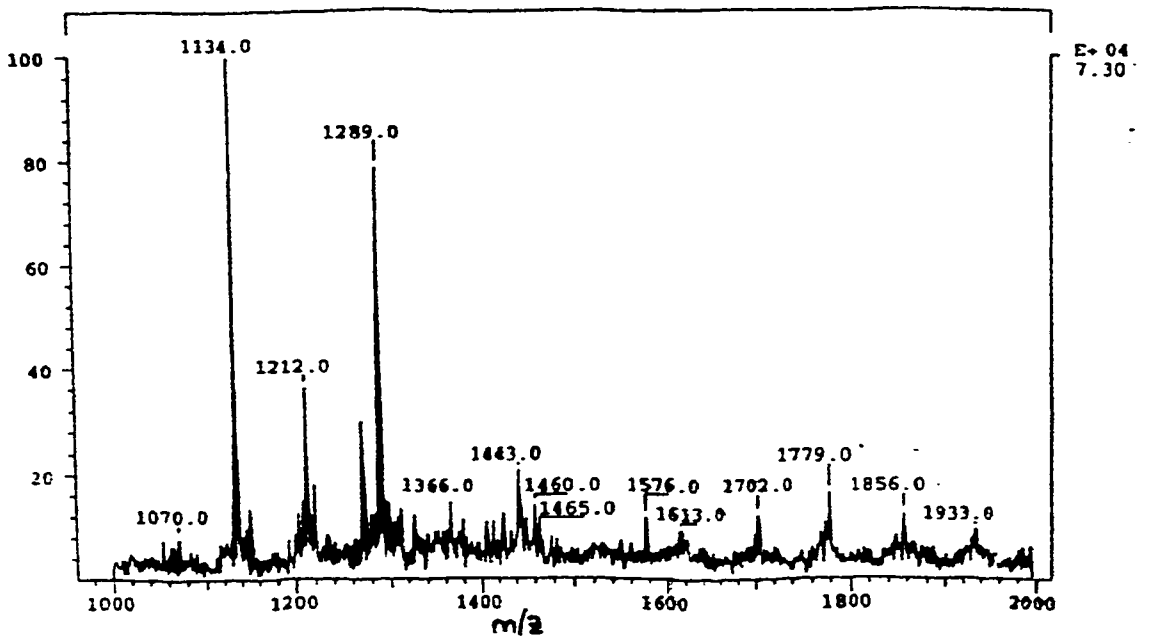

Figure 3.14- ES-MS of secondary Ts-β-CD, after correcting for Na.

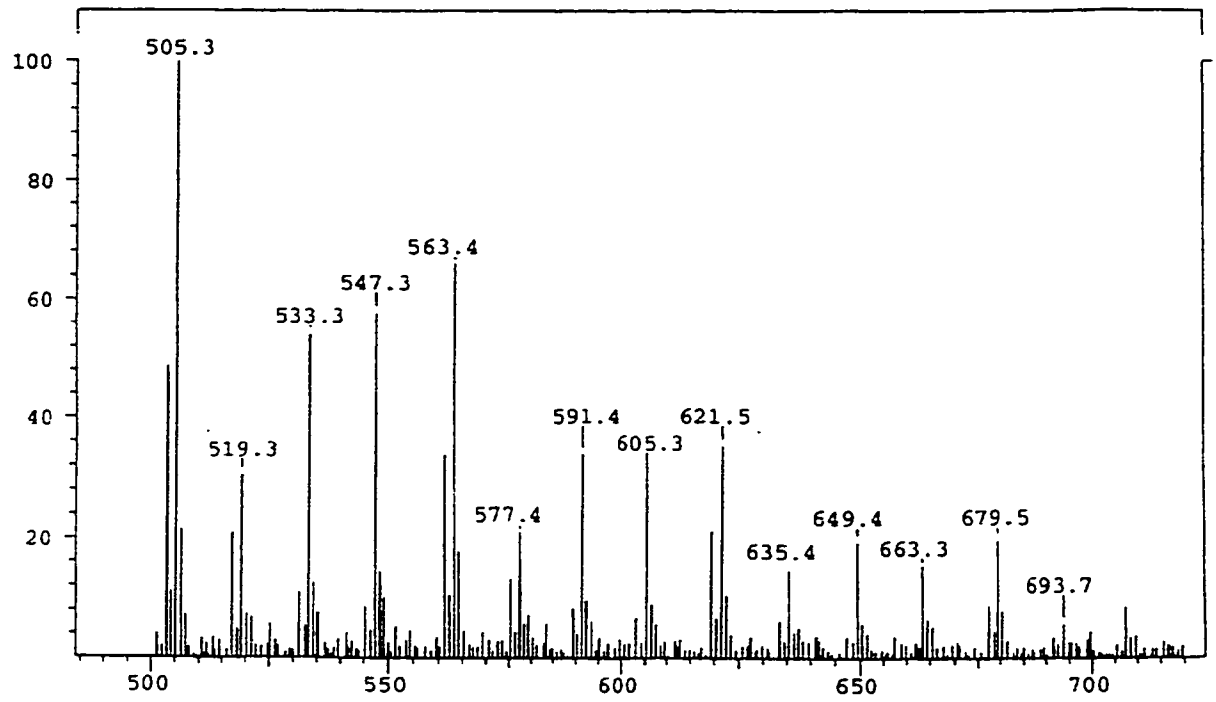

Figure 3.15 - ES-MS of primary DHBA-β-CD product in pH 4.0 sodium acetate buffer. .

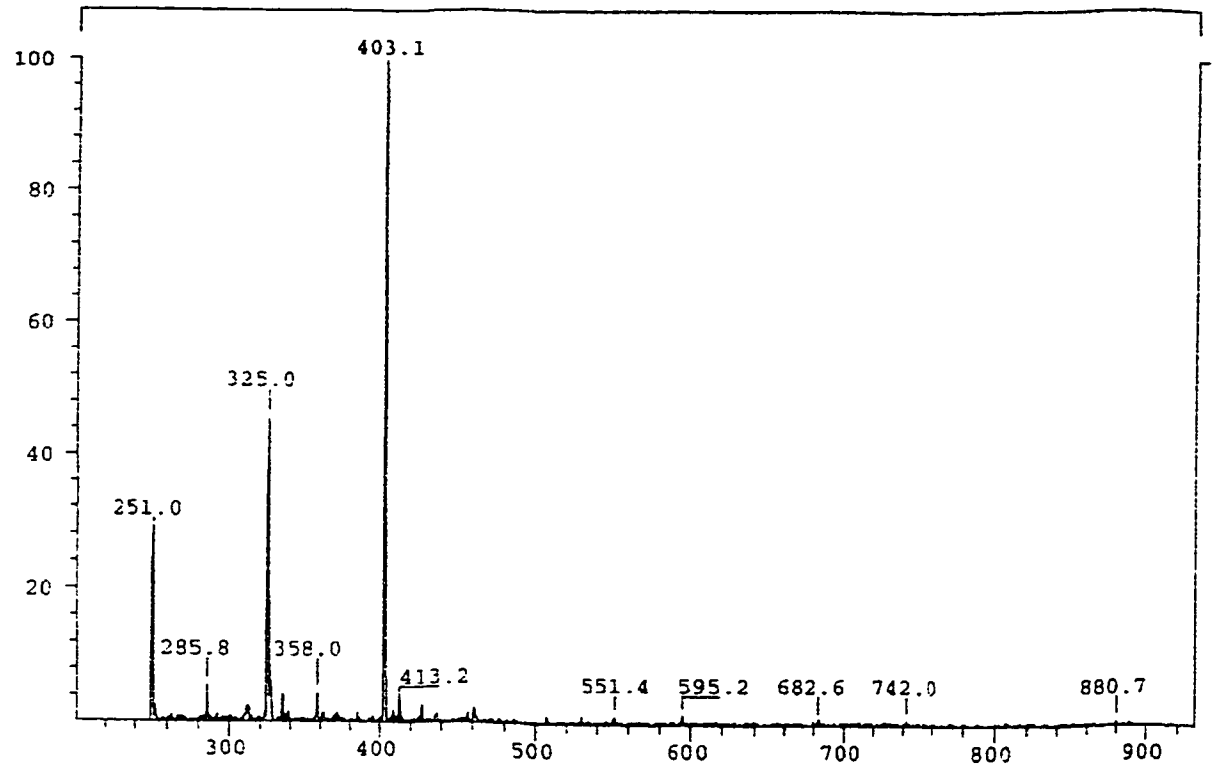

Figure 3.16 -ES-MS of secondary DHBA-β-CD product in pH 4.0 sodium acetate buffer.

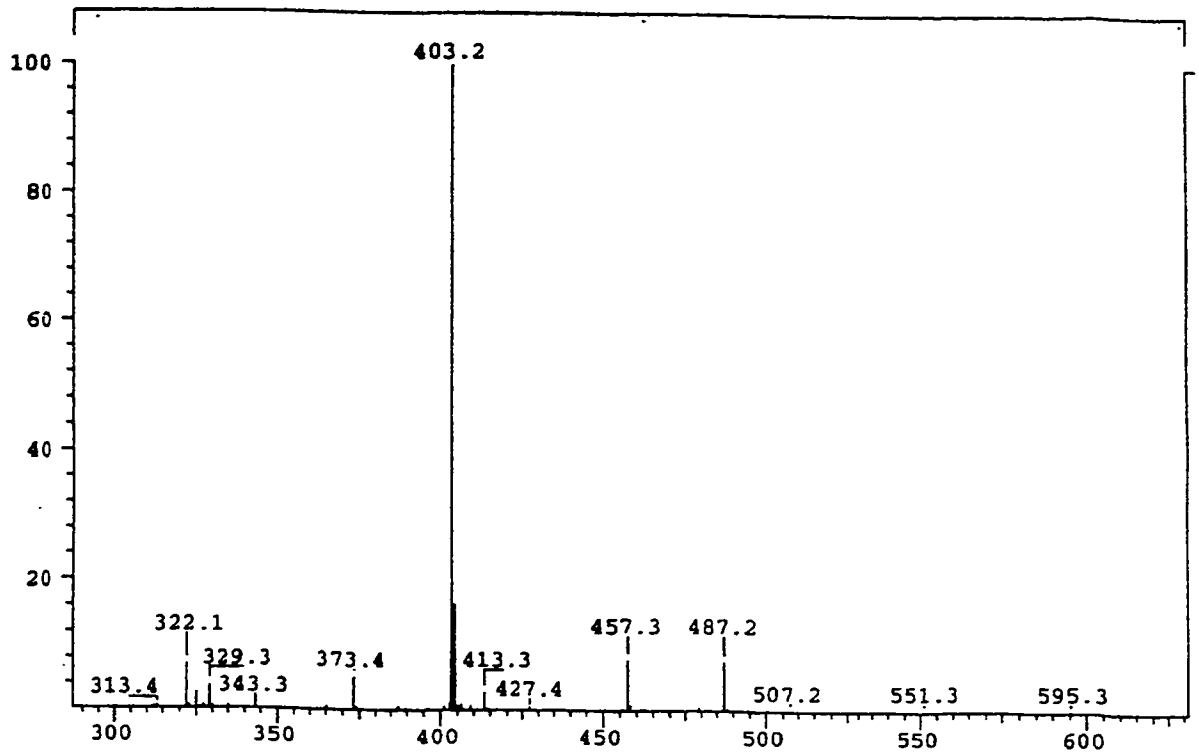

Figure 3.17- ES-MS of primary Fc-β-CD product in pH 4.0 sodium acetate buffer.

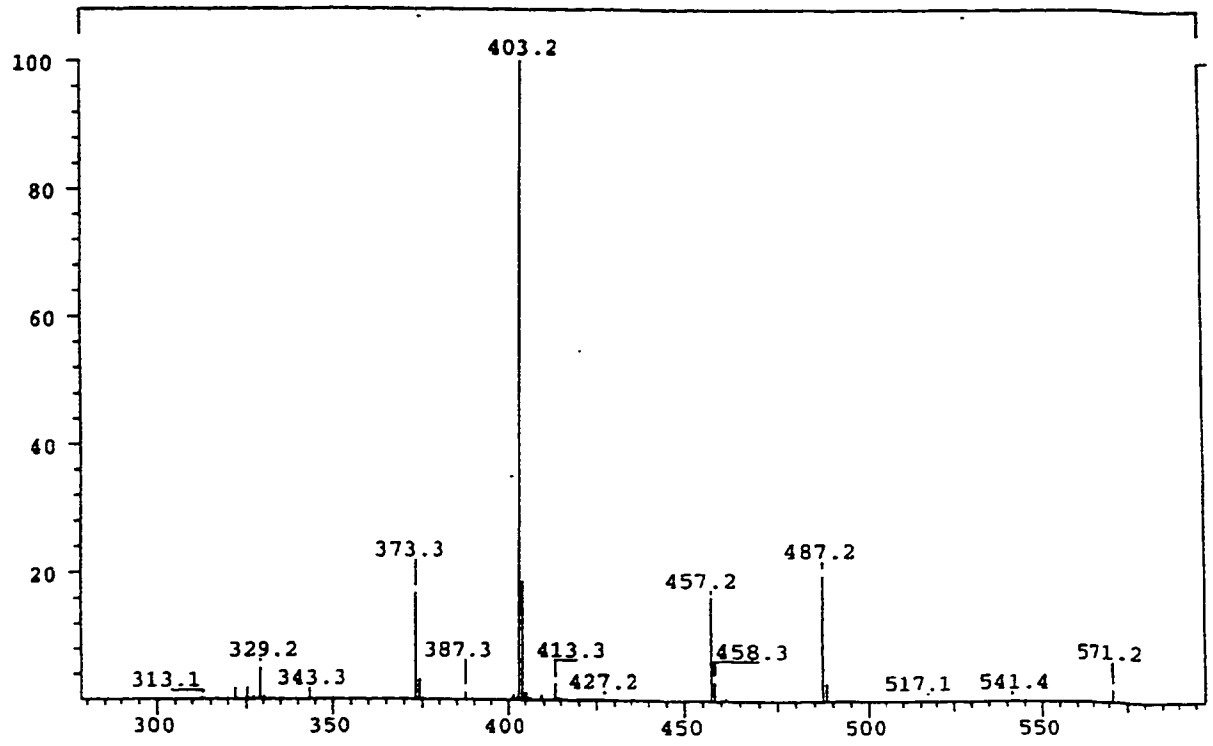

Figure 3.18 -ES-MS of secondary Fc-β-CD product in pH 4.0 sodium acetate buffer.

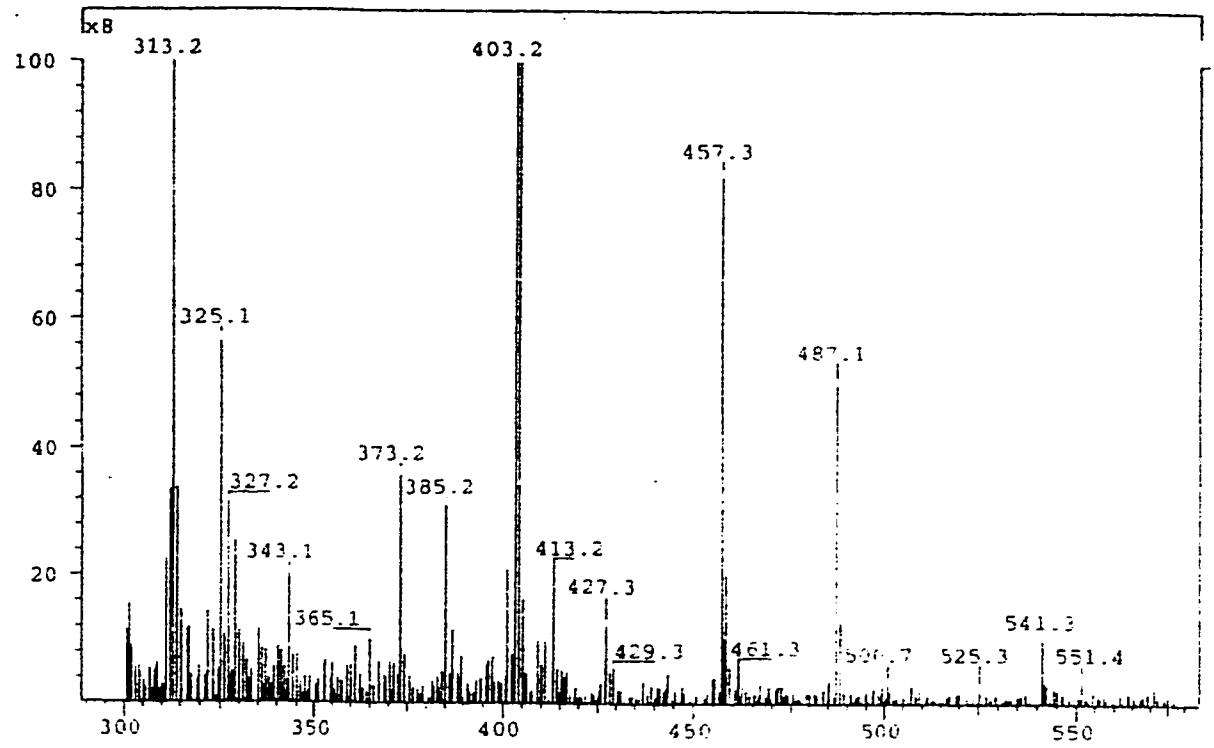

Figure 3.19 -ES-MS of hydroxypropyl β-CD in pH 4.0 sodium acetate buffer.

3.3 Catalytic properties of CD derivatives to thiol oxidation

3.3.1 DHBA-β-CD derivatives and thiol oxidation

A series of experiments were done to compare the thiol oxidation rates of the derivatized DHBA-β-CD compounds to those of the free species. After serial dilutions, a series of voltammetric scans were run to determine the electrocatalytic thiol oxidation currents. As before, the oxidation currents were plotted against the concentration of the DHBA-β-CD and the thiol which was either glutathione or cysteine. Phosphate (pH = 7.0) or acetate (pH = 3.8) buffers at 0.1 M were used to maintain the pH and act as the electrolyte. The final results are shown in Table 3.7 with free DHBA included as reference for thiol oxidation rates which should have no catalytic effect, as no β-CD is included in these two systems

Table 3.7- Observed thiol oxidation rates with functionalized DHBA-β-CDs

Catalyst	Thiol	pH	k_{obs}, $M^{-1}s^{-1}$
DHBA	GSH	3.8	26
DHBA	GSH	7.0	18
1'-DHBA-β-CD	GSH	3.8	30
1'-DHBA-β-CD	GSH	7.0	4.6
1'-DHBA-β-CD	Cys	7.0	28
2'-DHBA-β-CD	GSH	7.0	0.26
2'-DHBA-β-CD	Cys	7.0	1.1

These results show that there is no enhancement of thiol oxidation rate with either

the primary or the secondary substituted DHBA-β-CD system. There was actually a large decrease in rate, especially for the secondary substituted system, which showed a hundred-fold decrease, from 18 to 0.26 $M^{-1}s^{-1}$ at pH 7.0 (Table 3.7). There are many possible reasons for decreased catalytic activity, including accessibility and reactivity of the catalytic group towards the thiol. Further investigations of these CD derivatives were not done, due to their low reactivities, instead attention was focused on the ferrocene derivatives.

3.3.2 Ferrocene derivatives

The observed oxidation rates of cysteine and glutathione by free and CD-bound ferricinium derivatives in pH 7.0, 0.1 M phosphate buffer are shown in Table 3.8. Results obtained with ferricyanide are also shown for comparision because FCN is not expected to bind to β-CD. Raw data used to obtain these values are given in Appendix C.

Table 3.8 -Rate constants for thiol oxidation by ferricinium derivatives

Catalyst*	Thiol	k_{obs}, $M^{-1}s^{-1}$
FCO	GSH	2.2
FMAM	GSH	110
FCN	GSH	48
FCN	Cys	90
1'-Fc-β-CD	GSH	143
1'-Fc-β-CD	Cys	105
2'-Fc-β-CD	GSH	260
2'-Fc-β-CD	Cys	1470

*FCO = ferricinium carboxaldehyde
FMAM = dimethylaminomethylferricinium
FCN = ferricyanide

From these results it can be seen that the primary CD derivative is not a good catalyst for thiol oxidation, as the rates are lower than for a comparable free ferrocene (FMAM). The secondary ferrocene CD derivative however, does show an increased rate of thiol oxidation, especially for cysteine. Interestingly, the cysteine oxidation rate is more than five times larger than that of glutathione, suggesting that cysteine, binds more readily than glutathione in the CD cavity. Voltammograms of 2'-Fc-CD in the presence and absence of cysteine are shown in Figure 3.20, and a plot of electrocatalytic current at 400 mV against concentration according to equation 5 is shown in Figure 3.21.

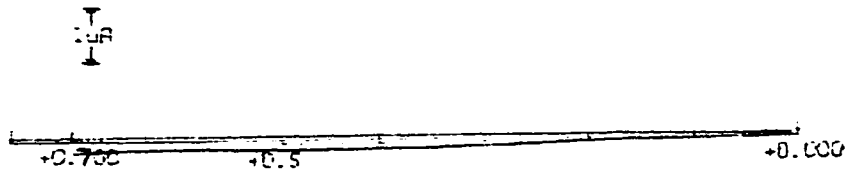

Figure 3.20(a)- Linear voltammetry scan (2 mV/sec) of 0.30 mM 2-Fc-β-CD in deaerated 0.10 M phosphate buffer, pH 7.0. GCE working; Ag/AgCl reference electrodes used.

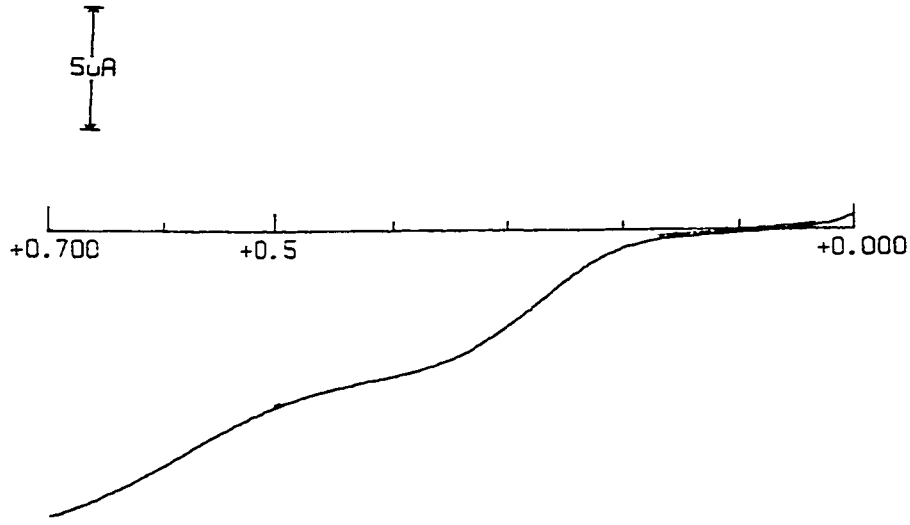

Figure 3.20(b)- Linear voltammetry scan (2 mV/sec) of 0.30 mM 2-Fc-β-CD and 8.2 mM cysteine in pH 7 phosphate buffer. GCE working; Ag/AgCl reference electrodes used.

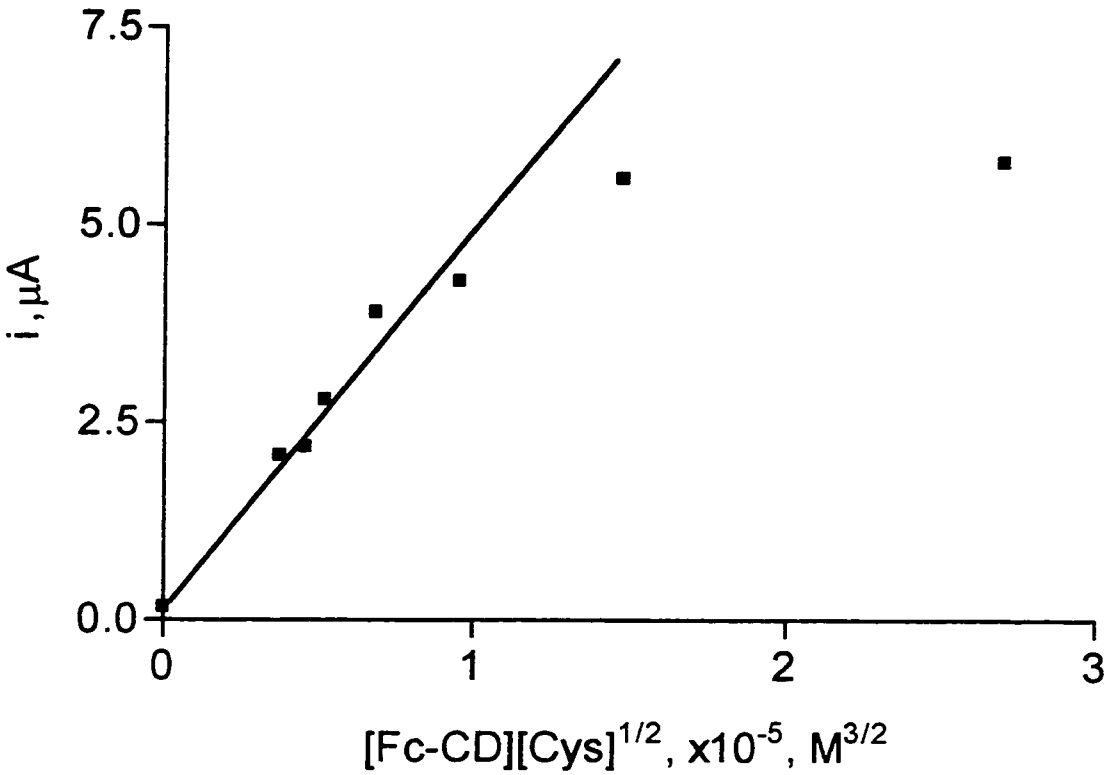

Figure 3.21- Plot of voltammetric experimental data of 2-Fc-β-CD as electrocatalyst for Cys oxidation in pH 7.0 phosphate buffer. Scan rate at 2 mV/sec, current measured at 400 mV, GCE as working and Ag/AgCl as reference electrodes. First 6 points used to determine cysteine oxidation rate by linear regression.

A further series of experiments were done using the 2-Fc-β-CD synzyme and cysteine at pH 8.0, to determine whether thiol deprotonation ($pK_a = 8.2$) yields a change in reactivity. The results are shown in Table 3.9.

Table 3.9 - Cysteine oxidation by 2-Fc-β-CD in 0.10 M phosphate buffer, pH 8.0

Catalyst	k_{obs}, $M^{-1}s^{-1}$
FMAM	30
FMAM/10 mMβ-CD	27
2-Fc-β-CD	4120

From these results it can be seen that there is a significant rate enhancement due to the thiol group on the cysteine becoming deprotonated. Although the cysteine oxidation rate by free FMAM is three-fold lower at pH 8.0 than at pH 7.0 (Table 3.8), the value obtained for 2-Fc-β-CD is three-fold larger at pH 8.0. The small decrease in cysteine oxidation rate by FMAM observed in the presence of 10 mM β-CD (from 30 to 27 $M^{-1}s^{-1}$) indicates binding of cysteine to free CD.

3.4 Behavior of Secondary Ferrocene-β-Cyclodextrin Derivative as a Synthetic Enzyme

Calibration curves of electrocatalytic current against glutathione and cysteine concentration at fixed 2-Fc-β-CD concentration were obtained using glassy carbon and carbon paste electrodes, and are shown in Figures 3.22 to 3.24. The two electrodes have different areas (approximately 0.071 and 0.13 cm^2 for GCE and CPE respectively) and the absolute magnitudes of the currents in the figures reflect this difference, as well as positive adsorptive interactions of the CD derivatives with the electrode materials.

The three calibration curves show an initial increase in current with concentration, as expected, but the current then decreases to a constant level at higher concentrations, suggesting inhibition by the disulfide products. The upper limit of the linear range occurs at about 6 mM for cysteine, and 4 mM for glutathione. Due to the shapes of these curves, which demonstrate more complicated behavior than expected for simple saturation kinetics, Michaelis-Menten parameters were not determined.

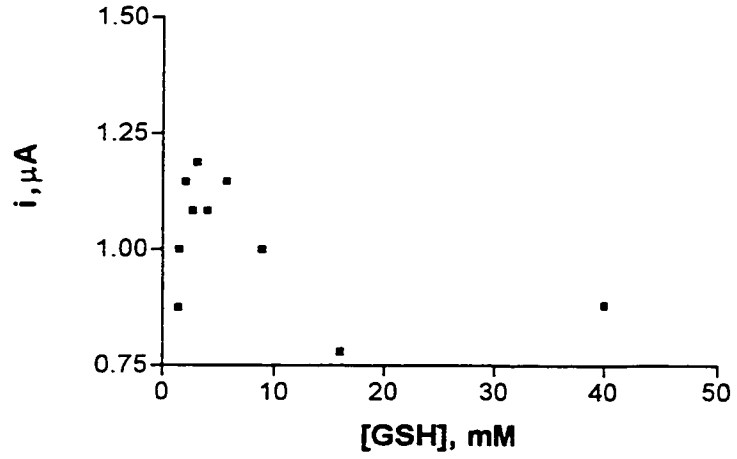

Figure 3.22 - Plot of 0.80 mM 2-Fc-β-CD as electrocatalyst for varying GSH concentration. GCE as working, Ag/AgCl as reference electrodes.

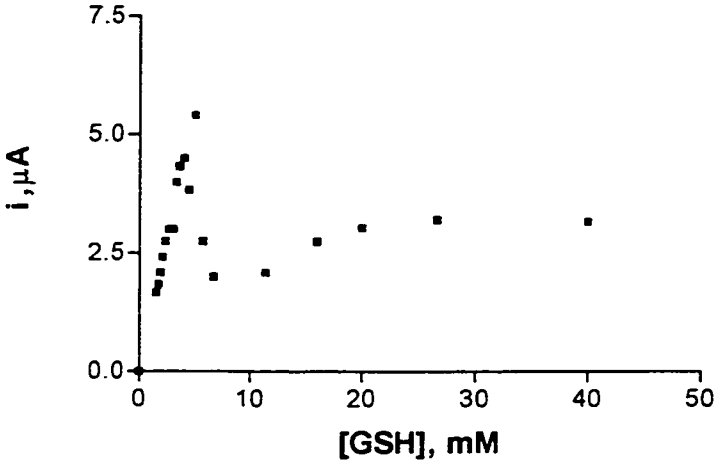

Figure 3.23 - Plot of 0.80 mM 2-Fc-β-CD as electrocatalyst for varying concentration of GSH. Carbon paste working, Ag/AgCl as reference electrodes.

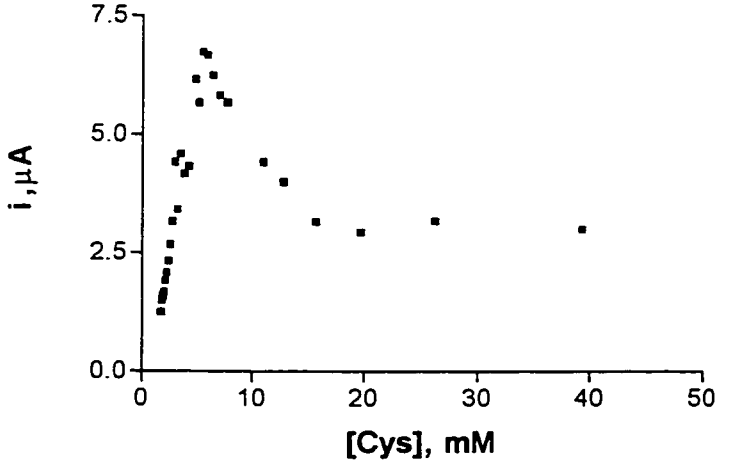

Figure 3.24 - Plot of 0.80 mM 2-Fc-β-CD and varying concentration of cysteine. GCE as working, Ag/AgCl as reference electrodes.

Confirmation of product inhibition was obtained by dilution experiments to determine thiol oxidation rates under psuedo-first order conditions in the presence and absence of added product (oxidized glutathione or cystine). The results of these experiments are shown in Table 3.10. A five-fold molar excess of GSSG can be seen to decrease k_{obs} by a factor of ten, while an even greater effect is seen for cystine.

Table 3.10-Thiol oxidation rates in the presence and absence of disulfide products, obtained by dilution experiments. Initial concentrations were 0.50 mM catalyst, 5.5 mM glutathione, 4.8 mM cysteine, 2.4 mM GSSG, and 0.17 mM cystine.

Catalyst	Substrate	Inhibitor	k_{obs}, $M^{-1}s^{-1}$
2-Fc-β-CD	Glutathione		8.4
2-Fc-β-CD	Glutathione	Glutathione-ox	6.0
2-Fc-β-CD	Cysteine		104
2-Fc-β-CD	Cysteine	Cystine	72

These results are consistent with results obtained by dilution experiments under pseudo-first order condtions (eg. see Section 3.3). In all of these experiments, a negative deviation from the straight line in the i_{obs} vs $[S]^{1.2}[C]$ plots were observed at the highest concentrations, and this is consistent with product inhibition.

In the calibration curves (Figs. 3.22 to 3.24), product inhibition occurs at an apparently higher substrate concentration due to the fact that the reaction occurs near the electrode surface, and no disulfide product is present in the bulk of the solution.

These results indicate that the 2-Fc-β-CD synzyme is a potentially useful recognition

agent for thiol-selective sensors up to about 5 mM thiol concentrations. Further studies of inhibition species that might interfere with its catalytic cycle are needed before applications in sensors can be considered.

Chapter 4

Conclusions and Suggestions for Future Research

From the various experiments performed, and discussed in the previous chapters a number of conclusions can be formed.

First, from all the various quinone groups tested, with and without free β-CD, only the DHBA group showed promise towards catalytic activity for thiol oxidation. Conversely, both ferrocene derivatives gave promising catalytic activity for enhanced thiol oxidation, when free β-CD was present. Thus, we had candidates for synthesis of a quinone based synzyme, and a ferrocene based synzyme.

Synthesis of the four types of potential artificial enzymes, yielded unique species based on RP-HPLC analysis, and preliminary ES-MS. UV-Vis scans showed a shift in the main peak, but spectra were still similar to starting quinone or ferrocene, so that concentrations of the new species could be estimated based on molar absorptivities of the starting catalytic groups. Separation and purification of the unique fractions from RP-HPLC runs provided enough product for kinetic analyses.

Each synzyme was examined for thiol oxidation under pseudo-first order conditions in order to determine k_{obs} values, the rates of thiol oxidation by the quinone or ferricinium group. The results of the experiments on the quinone based systems showed that the DHBA-CD synzyme is a poor catalyst for thiol oxidation, as there was a drop in thiol oxidation rates as compared to the free catalyst/β-CD systems.

The most promising candidate for the synzyme for thiol oxidation was the ferrocene-β-cyclodextrin system, where substitution of the catalytic group occurred on the secondary

hydroxyl side of the β-CD. Furthermore, a 50-fold enhancement was obtained at pH 8.0 for cysteine oxidation, in comparision with a similar free ferrocene. Calibration curves for cysteine and glutathione showed a drop in oxidation currents at higher thiol concentration as product inhibition occured. Further tests under pseudo-first order conditions showed much lower k_{obs} values in the presence of the disulfide product, confirming product inhibition.

Attempts to characterize the substituted cyclodextrins by ES-MS were not completely successful, as molecular ion peaks could not be found. However, the fragmentation or charging pattern obtained compared well to that of a substituted β-CD, hydroxypropyl-β-CD. UV-Visible spectroscopy and carbohydrate assays by the phenol-sulfuric acid method, indicated the presence of both the catalytic groups and carbohydrate in the products. Further work using alternative MS methods as well as ^{1}H or ^{13}C NMR could provide useful structural data.

Further work is required to characterize the derived species and certainly, a more detailed pH study needs to be performed on the 2-Fc-β-CD synzyme. As well, the effect of different thiols on thiol oxidation rates could be part of a more detailed mechanistic study. The ferrocene substituents could be varied to determine the effect of substituents on the ferrocene on the ability of this group to act as a catalytic site.

Appendix A - Experimental results used for determining rate constants for free systems

Table 1 - Hydroquinone/GSH in pH 7.0 phosphate buffer.

Hydroquinone, mM	GSH, mM	x-axis, $\times 10^{-5}$, $M^{3/2}$	i_{obs}, µA, at 300 mV
0.5631	----------	0	1.92
0.5631	5.62	4.221	7.00
0.4233	4.217	2.749	5.67
0.3378	3.374	1.962	3.92
0.2815	2.812	1.493	3.25
0.2252	2.256	1.070	2.83
0.1877	1.880	0.814	1.92
		slope, m =	1.80
		y intercept, b =	0.59
		r^2 =	0.989
		k_{obs} =	23.50

Table 2 - Hydroquinone/GSH/5 mM β-CD in pH 7.0 phosphate buffer

Hydroquinone, mM	GSH, mM	x-axis, $\times 10^{-5}$, $M^{3/2}$	i_{obs}, µA, at 300 mV
0.744	4.972	5.246	7.83
0.558	3.729	3.411	5.33
0.447	2.983	2.441	4.67
0.372	2.486	1.857	3.75
0.279	1.865	1.206	2.75
0.223	1.492	0.823	2.04
0.186	1.243	0.657	1.75
		slope, m =	1.30
		y intercept,b =	1.10
		r^2 =	0.994
		k_{obs} =	12.24

Table 3 - Hydroquinone/GSH in pH 7.0 phosphate buffer.

Hydroquinone, mM	GSH, mM	x-axis, $\times 10^{-5}$, $M^{3/2}$	i_{obs}, µA, at 300 mV
0.5631	----------	0	1.92
0.5631	5.62	4.221	7.00
0.4233	4.217	2.749	5.67
0.3378	3.374	1.962	3.92
0.2815	2.812	1.493	3.25
0.2252	2.256	1.070	2.83
0.1877	1.880	0.814	1.92
		slope, m =	1.80
		y intercept, b =	0.59
		r^2 =	0.989
		k_{obs} =	23.50

Table 4 - Hydroquinone/GSH/10 mM β-CD in pH 7.0 phosphate buffer

Hydroquinone, mM	GSH, mM	x-axis, $\times 10^{-5}$, $M^{3/2}$	i_{obs}, µA, at 300 mV
0.710	6.80	5.855	6.67
0.533	5.10	3.803	5.00
0.426	4.08	2.721	4.08
0.355	3.40	2.070	3.33
0.266	2.55	1.345	2.63
0.213	2.04	0.962	2.00
0.178	1.70	0.732	1.65
		slope, m =	1.21
		y intercept,b =	0.84
		r^2 =	0.995
		k_{obs} =	10.45

Table 5 - DHBA/GSH in pH 7.0 phosphate buffer.

DHBA, mM	GSH, mM	x-axis, $\times 10^{-5}$, $M^{3/2}$	i_{obs}, µA, at 300 mV
0.554	5.538	4.126	6.83
0.416	4.154	2.680	5.00
0.333	3.323	1.917	4.08
0.277	2.769	1.459	2.83
0.208	2.077	0.948	2.33
0.166	1.661	0.678	1.92
0.139	1.385	0.516	1.58
		slope, m =	1.60
		y intercept, b =	0.78
		r^2 =	0.992
		k_{obs} =	18.30

Table 6 - DHBA/GSH/10 mM β-CD in pH 7.0 phosphate buffer

DHBA, mM	GSH, mM	x-axis, $\times 10^{-5}$, $M^{3/2}$	i_{obs}, µA, at 300 mV
0.554	5.538	4.126	7.50
0.416	4.154	2.680	4.67
0.333	3.323	1.917	4.00
0.277	2.769	1.459	3.17
0.208	2.077	0.948	2.46
0.166	1.661	0.678	1.96
0.139	1.385	0.516	1.54
		slope, m =	1.69
		y intercept, b =	0.76
		r^2 =	0.997
		k_{obs} =	20.0

Table 7 - DHBA/GSH in pH 4.0 acetate buffer.

DHBA, mM	GSH, mM	x-axis, $\times 10^{-5}$, $M^{3/2}$	i_{obs}, µA, at 300 mV
0.582	5.538	4.328	7.37
0.436	4.154	2.811	6.63
0.349	3.323	2.012	5.58
0.291	2.769	1.530	4.42
0.218	2.077	0.994	3.37
0.175	1.661	0.711	3.00
01.45	1.385	0.541	2.16
		slope, m =	2.16
		y intercept, b =	1.20
		r^2 =	0.991
		k_{obs} =	33.86

Table 8 - DHBA/GSH/10 mM β-CD in pH 4.0 acetate buffer

DHBA, mM	GSH, mM	x-axis, $\times 10^{-5}$, $M^{3/2}$	i_{obs}, µA, at 300 mV
0.582	5.538	4.328	7.71
0.436	4.154	2.811	6.21
0.349	3.323	2.012	5.16
0.291	2.769	1.530	3.90
0.218	2.077	0.994	3.60
0.175	1.661	0.711	2.63
01.45	1.385	0.541	2.16
		slope, m =	1.32
		y intercept, b =	1.87
		r^2 =	0.974
		k_{obs} =	12.26

Table 9 - DHBA/GSH in pH 2.5 phosphate buffer.

DHBA, mM	GSH, mM	x-axis, $\times 10^{-5}$, $M^{3/2}$	i_{obs}, µA, at 700 mV
0.550	5.538	4.091	6.21
0.412	4.154	2.658	5.00
0.329	3.323	1.902	3.75
0.275	2.769	1.447	3.33
0.206	2.077	0.939	2.58
0.165	1.661	0.672	2.12
0.138	1.385	0.512	1.56
		slope, m =	1.50
		y intercept, b =	1.02
		r^2 =	0.992
		k_{obs} =	16.33

Table 10 - DHBA/GSH/10 mM β-CD in pH 2.5 phosphate buffer

DHBA, mM	GSH, mM	x-axis, $\times 10^{-5}$, $M^{3/2}$	i_{obs}, µA, at 300 mV
0.550	5.538	4.091	6.00
0.412	4.154	2.658	4.67
0.329	3.323	1.902	3.83
0.275	2.769	1.447	3.08
0.236	2.373	1.148	2.75
0.189	1.898	0.821	2.25
0.157	1.582	0.625	1.92
		slope, m =	1.36
		y intercept, b =	1.14
		r^2 =	0.997
		k_{obs} =	13.42

Table 11 - DHBA/Cysteine in pH 4.0 acetate buffer.

DHBA, mM	Cys, mM	x-axis, $\times 10^{-5}$, $M^{3/2}$	i_{obs}, µA, at 600 mV
0.573	5.780	4.353	
0.430	4.335	3.242	9.58
0.343	3.468	2.023	7.50
0.286	2.890	1.539	6.33
0.215	2.168	0.999	4.92
0.172	1.734	0.715	4.08
0.143	1.445	0.544	3.08
		slope, m =	2.86
		y intercept, b =	1.86
		r^2 =	0.991
		k_{obs} =	59.36

Table 12 - DHBA/Cysteine/10 mM β-CD in pH 4.0 acetate buffer

DHBA, mM	Cys, mM	x-axis, $\times 10^{-5}$, $M^{3/2}$	i_{obs}, µA, at 300 mV
0.573	5.780	4.353	12.29
0.430	4.335	3.242	9.17
0.343	3.468	2.023	7.33
0.286	2.890	1.539	5.83
0.215	2.168	0.999	4.75
0.172	1.734	0.715	3.83
0.143	1.445	0.544	3.17
		slope, m =	2.69
		y intercept, b =	1.85
		r^2 =	0.996
		k_{obs} =	52.91

Table 13 - Trolox/GSH in pH 7 phosphate buffer.

Trolox, mM	GSH, mM	x-axis, $\times 10^{-5}$, $M^{3/2}$	i_{obs}, µA, at 600 mV
0.611	5.623	4.584	1.75
0.459	4.217	2.977	1.29
0.367	3.374	2.131	0.88
0.306	2.812	1.621	0.83
0.229	2.109	1.053	0.65
0.183	1.687	0.753	0.54
0.153	1.406	0.573	0.37
		slope, m =	0.32
		y intercept, b =	0.31
		r^2 =	0.999
		k_{obs} =	0.73

Table 14 -Trolox/GSH/10 mM β-CD in pH 7.0 phosphate buffer

Trolox, mM	GSH, mM	x-axis, $\times 10^{-5}$, $M^{3/2}$	i_{obs}, µA, at 600 mV
0.611	5.623	4.584	1.58
0.459	4.217	2.977	1.17
0.367	3.374	2.131	0.92
0.306	2.812	1.621	0.69
0.229	2.109	1.053	0.58
0.183	1.687	0.753	0.44
0.153	1.406	0.573	nd
		slope, m =	0.32
		y intercept, b =	0.21
		r^2 =	0.995
		k_{obs} =	0.748

Table 15 - DHBA/GSH in pH 3.6 acetate buffer.

DHBA, mM	GSH, mM	x-axis, $\times 10^{-5}$, $M^{3/2}$	i_{obs}, µA, at 600 mV
0.586	5.567	4.374	8.96
0.440	4.175	2.841	6.74
0.352	3.340	2.033	5.17
0.293	2.784	1.547	4.50
0.220	2.088	1.004	3.67
0.176	1.670	0.718	3.04
0.147	1.392	0.547	2.12
		slope, m =	1.69
		y intercept, b =	1.87
		r^2 =	0.998
		k_{obs} =	20.73

Table 16 - DHBA/GSH/10 mM β-CD in pH 3.6 acetate buffer

DHBA, mM	GSH, mM	x-axis, $\times 10^{-5}$, $M^{3/2}$	i_{obs}, µA, at 600 mV
0.586	5.567	4.374	8.75
0.440	4.175	2.841	6.42
0.352	3.340	2.033	5.33
0.293	2.784	1.547	3.92
0.220	2.088	1.004	3.75
0.176	1.670	0.718	2.54
0.147	1.392	0.547	2.33
		slope, m =	1.78
		y intercept, b =	1.47
		r^2 =	0.981
		k_{obs} =	23.00

Table 17 - DHBA/GSH in pH 5.55 acetate buffer.

DHBA, mM	GSH, mM	x-axis, $\times 10^{-5}$, $M^{3/2}$	i_{obs}, µA, at 600 mV
0.545	5.616	4.086	6.21
0.409	4.212	2.654	5.26
0.327	3.370	1.899	4.67
0.273	2.808	1.445	3.50
0.205	2.106	0.939	2.83
0.164	1.685	0.672	2.63
0.136	1.404	0.511	2.04
		slope, m =	1.45
		y intercept, b =	1.51
		r^2 =	0.985
		k_{obs} =	16.60

Table 18 - DHBA/GSH/10 mM β-CD in pH 5.55 acetate buffer

DHBA, mM	GSH, mM	x-axis, $\times 10^{-5}$, $M^{3/2}$	i_{obs}, µA, at 600 mV
0.545	5.616	4.086	5.89
0.409	4.212	2.654	4.74
0.327	3.370	1.899	3.67
0.273	2.808	1.445	3.21
0.205	2.106	0.939	2.42
0.164	1.685	0.672	2.13
0.136	1.404	0.511	1.83
		slope, m =	1.19
		y intercept, b =	1.33
		r^2 =	0.999
		k_{obs} =	13.00

Table 19 - DHBA/GSH in pH 4.22 acetate buffer.

DHBA, mM	GSH, mM	x-axis, $\times 10^{-5}$, $M^{3/2}$	i_{obs}, µA, at 600 mV
0.577	5.639	4.334	7.92
0.433	4.229	2.815	5.63
0.346	3.383	2.014	4.67
0.289	2.819	1.532	4.00
0.247	2.417	1.216	3.38
0.186	1.813	0.790	2.80
0.149	1.450	0.566	2.30
		slope, m =	1.46
		y intercept, b =	1.62
		r^2 =	0.998
		k_{obs} =	15.05

Table 20 - DHBA/GSH/10 mM β-CD in pH 4.22 acetate buffer

DHBA, mM	GSH, mM	x-axis, $\times 10^{-5}$, $M^{3/2}$	i_{obs}, µA, at 600 mV
0.577	5.639	4.334	6.88
0.433	4.229	2.815	5.42
0.346	3.383	2.014	4.33
0.289	2.819	1.532	3.83
0.247	2.417	1.216	3.17
0.186	1.813	0.790	2.67
0.149	1.450	0.566	2.25
		slope, m =	1.39
		y intercept, b =	1.53
		r^2 =	0.997
		k_{obs} =	14.02

Table 21 - DHBA/GSH in pH 4.0 acetate buffer.

DHBA, mM	GSH, mM	x-axis, $\times 10^{-5}$, $M^{3/2}$	i_{obs}, µA, at 600 mV
0.623	5.691	4.696	8.75
0.467	4.268	3.050	6.50
0.374	3.415	2.183	5.25
0.311	2.845	1.660	4.50
0.233	2.134	1.078	3.58
0.187	1.707	0.772	3.50
0.156	1.423	0.587	nd
		slope, m =	1.42
		y intercept, b =	2.12
		r^2 =	0.999
		k_{obs} =	14.22

Table 22 - DHBA/GSH/10 mM β-CD in pH 4.0 acetate buffer

DHBA, mM	GSH, mM	x-axis, $\times 10^{-5}$, $M^{3/2}$	i_{obs}, µA, at 600 mV
0.623	5.691	4.696	8.33
0.467	4.268	3.050	6.67
0.374	3.415	2.183	5.08
0.311	2.845	1.660	4.50
0.233	2.134	1.078	3.33
0.187	1.707	0.772	2.75
0.156	1.423	0.587	2.29
		slope, m =	1.74
		y intercept, b =	1.40
		r^2 =	0.997
		k_{obs} =	20.98

Table 23 - DHBA/GSH in pH 3.90 acetate buffer.

DHBA, mM	GSH, mM	x-axis, $\times 10^{-5}$, $M^{3/2}$	i_{obs}, µA, at 600 mV
0.623	5.678	4.691	8.54
0.467	4.258	3.047	6.17
0.374	3.407	2.180	5.42
0.311	2.839	1.659	4.42
0.233	2.129	1.077	3.42
0.187	1.703	0.771	2.83
0.156	1.419	0.586	2.00
		slope, m =	1.82
		y intercept, b =	1.44
		r^2 =	0.999
		k_{obs} =	23.52

Table 24 - DHBA/GSH/10 mM β-CD in pH 3.90 acetate buffer

DHBA, mM	GSH, mM	x-axis, $\times 10^{-5}$, $M^{3/2}$	i_{obs}, µA, at 600 mV
0.623	5.678	4.691	7.92
0.467	4.258	3.047	6.33
0.374	3.407	2.180	5.17
0.311	2.839	1.659	3.58
0.233	2.129	1.077	3.17
0.187	1.703	0.771	2.67
0.156	1.419	0.586	2.17
		slope, m =	1.69
		y intercept, b =	1.32
		r^2 =	0.997
		k_{obs} =	20.97

Table 25 - DHBA/GSH in pH 3.79 acetate buffer.

DHBA, mM	GSH, mM	x-axis, $\times 10^{-5}$, $M^{3/2}$	i_{obs}, µA, at 600 mV
0.632	5.613	4.732	9.16
0.474	4.210	3.074	7.00
0.379	3.368	2.200	5.67
0.316	2.806	1.673	4.83
0.237	2.105	1.087	3.67
0.189	1.684	0.778	2.79
0.158	1.403	0.592	2.29
		slope, m =	1.88
		y intercept, b =	1.42
		r^2 =	0.993
		k_{obs} =	26.20

Table 26 - DHBA/GSH/10 mM β-CD in pH 3.79 acetate buffer

DHBA, mM	GSH, mM	x-axis, $\times 10^{-5}$, $M^{3/2}$	i_{obs}, µA, at 600 mV
0.632	5.613	4.732	9.38
0.474	4.210	3.074	6.67
0.379	3.368	2.200	6.00
0.316	2.806	1.673	4.83
0.237	2.105	1.087	3.67
0.189	1.684	0.778	3.00
0.158	1.403	0.592	2.21
		slope, m =	2.25
		y intercept, b =	1.09
		r^2 =	0.995
		k_{obs} =	35.13

Table 27 - DHBA/GSH in pH 4.0 acetate buffer.

DHBA, mM	GSH, mM	x-axis, $\times 10^{-5}$, $M^{3/2}$	i_{obs}, µA, at 600 mV
0.645	5.704	4.873	8.75
0.484	4.278	3.165	6.33
0.387	3.422	2.264	5.58
0.323	2.852	1.723	4.42
0.242	2.139	1.119	3.442
0.194	1.711	0.801	2.79
0.161	1.426	0.609	2.29
		slope, m =	1.93
		y intercept, b =	1.19
		r^2 =	0.998
		k_{obs} =	26.20

Table 28 - DHBA/GSH/10 mM β-CD in pH 4.0 acetate buffer

DHBA, mM	GSH, mM	x-axis, $\times 10^{-5}$, $M^{3/2}$	i_{obs}, µA, at 300 mV
0.645	5.704	4.873	8.33
0.484	4.278	3.165	6.33
0.387	3.422	2.264	4.92
0.230	2.444	1.139	3.75
0.184	1.955	0.815	3.04
0.154	1.630	0.620	2.50
0.140	1.482	0.538	2.33
		slope, m =	1.32
		y intercept, b =	1.95
		r^2 =	0.995
		k_{obs} =	12.26

Table 29 - DHBA/GSH in pH 3.71 acetate buffer.

DHBA, mM	GSH, mM	x-axis, $\times 10^{-5}$, $M^{3/2}$	i_{obs}, µA, at 600 mV
0.559	5.763	4.243	7.29
0.419	4.322	2.756	5.67
0.335	3.458	1.972	4.50
0.280	2.881	1.500	3.75
0.210	2.161	0.974	2.83
0.168	1.729	0.697	2.42
0.140	1.441	0.530	1.92
		slope, m =	1.65
		y intercept, b =	1.19
		r^2 =	0.998
		k_{obs} =	20.97

Table 30 - DHBA/GSH/10 mM β-CD in pH 3.71 acetate buffer

DHBA, mM	GSH, mM	x-axis, $\times 10^{-5}$, $M^{3/2}$	i_{obs}, µA, at 600 mV
0.559	5.763	4.243	6.88
0.419	4.322	2.756	5.33
0.335	3.458	1.972	4.42
0.280	2.881	1.500	3.75
0.210	2.161	0.974	2.83
0.168	1.729	0.697	2.17
0.140	1.441	0.530	1.88
		slope, m =	1.79
		y intercept, b =	0.98
		r^2 =	0.996
		k_{obs} =	23.52

Table 31 - Napthaquinone/GSH in pH 3.84 acetate buffer.

NQ, mM	GSH, mM	x-axis, $\times 10^{-5}$, $M^{3/2}$	i_{obs}, μA, at 400 mV
0.573	5.740	4.338	1.48
0.430	4.305	2.818	1.06
0.343	3.444	2.016	0.83
0.286	2.870	1.534	0.67
0.215	2.152	0.996	0.47
0.172	1.722	0.713	0.38
0.143	1.435	0.543	0.33
		slope, m =	0.33
		y intercept, b =	0.15
		r^2 =	0.999
		k_{obs} =	0.79

Table 32 - NQ/GSH/10 mM β-CD in pH 3.84 acetate buffer

NQ, mM	GSH, mM	x-axis, $\times 10^{-5}$, $M^{3/2}$	i_{obs}, μA, at 400 mV
0.573	5.740	4.338	1.33, 1.42
0.430	4.305	2.818	0.65, 0.90
0.343	3.444	2.016	0.75, 0.73
0.286	2.870	1.534	0.66, 0.42
0.215	2.152	0.996	0.45, 0.48
0.172	1.722	0.713	0.19, 0.33
0.143	1.435	0.543	0.16, 0.31
		slope, m =	0.26, 0.28
		y intercept, b =	0.23, 0.16
		r^2 =	0.997, 0.994
		k_{obs} =	0.48, 0.59

Table 33 -NQ/GSH in pH 6.99 phosphate buffer.

NQ, mM	GSH, mM	x-axis, $\times 10^{-5}$, $M^{3/2}$	i_{obs}, µA, at 300 mV
0.569	5.710	4.297	0.52
0.427	4.283	2.792	0.54
0.341	3.426	1.997	nd
0.284	2.855	1.520	0.36
0.213	2.141	0.987	0.12
0.171	1.713	0.706	0.10
0.142	1.428	0.534	0.07
		slope, m =	0.22
		y intercept, b =	-0.03
		r^2 =	0.982
		k_{obs} =	0.33

Table 34 -NQ/GSH/10 mM β-CD in pH 6.99 phosphate buffer

NQ, mM	GSH, mM	x-axis, $\times 10^{-5}$, $M^{3/2}$	i_{obs}, µA, at 300 mV
0.569	5.710	4.297	0.25
0.427	4.283	2.792	0.23
0.341	3.426	1.997	0.14
0.284	2.855	1.520	0.11
0.213	2.141	0.987	0.05
0.171	1.713	0.706	0.04
0.142	1.428	0.534	nd
		slope, m =	0.09
		y intercept, b =	-0.03
		r^2 =	0.995
		k_{obs} =	0.06

Table 35 -HQ/GSH in pH 3.8 acetate buffer.

HQ, mM	GSH, mM	x-axis, $\times 10^{-5}$, $M^{3/2}$	i_{obs}, µA, at 500 mV
0.826	5.662	6.218	9.79
0.620	4.246	4.039	7.50
0.496	3.397	2.890	6.00
0.413	2.831	2.199	5.00
0.310	2.123	1.428	3.50
0.248	1.698	1.022	2.67
0.207	1.415	0.777	2.04
		slope, m =	1.87
		y intercept, b =	0.73
		r^2 =	0.997
		k_{obs} =	25.38

Table 36 - HQ/GSH/10 mM β-CD in pH 3.8 acetate buffer

HQ, mM	GSH, mM	x-axis, $\times 10^{-5}$, $M^{3/2}$	i_{obs}, µA, at 500 mV
0.826	5.662	6.218	8.33
0.620	4.246	4.039	6.11
0.496	3.397	2.890	4.53
0.413	2.831	2.199	4.00
0.310	2.123	1.428	2.79
0.248	1.698	1.022	2.17
0.207	1.415	0.777	1.88
		slope, m =	1.29
		y intercept, b =	0.92
		r^2 =	0.997
		k_{obs} =	12.08

Table 37 -HQ/GSH in pH 6.99 phosphate buffer.

HQ, mM	GSH, mM	x-axis, $\times 10^{-5}$, $M^{3/2}$	i_{obs}, µA, at 300 mV
0.881	5.759	6.685	10.42
0.661	4.319	3.474	7.83
0.529	3.456	3.108	5.83
0.441	2.880	2.364	5.00
0.378	2.468	1.875	3.75
0.302	1.975	1.342	3.42
0.252	1.646	1.021	2.83
		slope, m =	1.33
		y intercept, b =	1.54
		r^2 =	0.997
		k_{obs} =	12.92

Table 38 -HQ/GSH/10 mM β-CD in pH 6.99 phosphate buffer

HQ, mM	GSH, mM	x-axis, $\times 10^{-5}$, $M^{3/2}$	i_{obs}, µA, at 300 mV
0.881	5.759	6.685	8.54
0.661	4.319	3.474	6.17
0.529	3.456	3.108	4.50
0.441	2.880	2.364	4.08
0.378	2.468	1.875	3.33
0.302	1.975	1.342	2.92
0.252	1.646	1.021	2.04
		slope, m =	1.61
		y intercept, b =	0.47
		r^2 =	0.992
		k_{obs} =	18.72

Table 39 - BQ/GSH in pH 3.84 acetate buffer.

BQ, mM	GSH, mM	x-axis, $\times 10^{-5}$, $M^{3/2}$	i_{obs}, µA, at 400 mV
0.648	5.561	4.829	3.58
0.486	4.171	3.137	2.67
0.389	3.336	2.244	2.17
0.323	2.780	1.707	1.71
0.243	2.085	1.109	1.27
0.194	1.668	0.794	0.85
0.167	1.390	0.604	0.79
		slope, m =	0.74
		y intercept, b =	0.42
		r^2 =	0.996
		k_{obs} =	3.97

Table 40 - BQ/GSH/10 mM β-CD in pH 3.84 acetate buffer

BQ, mM	GSH, mM	x-axis, $\times 10^{-5}$, $M^{3/2}$	i_{obs}, µA, at 400 mV
0.648	5.561	4.829	3.33
0.486	4.171	3.137	2.34
0.389	3.336	2.244	1.92
0.323	2.780	1.707	1.63
0.243	2.085	1.109	1.04
0.194	1.668	0.794	0.92
0.167	1.390	0.604	0.67
		slope, m =	0.76
		y intercept, b =	0.25
		r^2 =	0.993
		k_{obs} =	4.30

Table 41 -BQ/GSH in pH 6.91 phosphate buffer.

BQ, mM	GSH, mM	x-axis, $\times 10^{-5}$, $M^{3/2}$	i_{obs}, µA, at 400 mV
0.601	6.049	4.677	2.74
0.451	4.537	3.038	2.08
0.361	3.629	2.174	1.50
0.301	3.025	1.654	0.75
0.226	2.268	1.074	0.96
0.180	1.815	0.769	0.45
0.150	1.512	0.584	0.63
		slope, m =	0.58
		y intercept, b =	0.30
		r^2 =	0.998
		k_{obs} =	2.43

Table 42 - BQ/GSH/10 mM β-CD in pH 6.91 phosphate buffer

BQ, mM	GSH, mM	x-axis, $\times 10^{-5}$, $M^{3/2}$	i_{obs}, µA, at 400 mV
0.601	6.049	4.677	2.33
0.451	4.537	3.038	1.29
0.361	3.629	2.174	1.17
0.301	3.025	1.654	1.08
0.226	2.268	1.074	0.75
0.180	1.815	0.769	0.29
0.150	1.512	0.584	0.52
		slope, m =	0.41
		y intercept, b =	0.28
		r^2 =	0.977
		k_{obs} =	1.22

Table 43 -HQ/GSH in pH 6.99 phosphate buffer.

HQ, mM	GSH, mM	x-axis, $\times 10^{-5}$, $M^{3/2}$	i_{obs}, μA, at 400 mV
0.944	5.785	7.184	8.75
0.708	4.339	4.666	8.17
0.566	3.471	3.339	5.83
0.472	2.893	2.540	5.50
0.354	2.169	1.650	4.08
0.283	1.736	1.181	2.83
0.236	1.446	0.898	2.83
		slope, m =	1.27
		y intercept, b =	1.89
		r^2 =	0.975
		k_{obs} =	11.65

Table 44 - HQ/GSH/10 mM β-CD in pH 6.99 phosphate buffer

HQ, mM	GSH, mM	x-axis, $\times 10^{-5}$, $M^{3.2}$	i_{obs}, μA, at 400 mV
0.944	5.785	7.184	8.33
0.708	4.339	4.666	6.42
0.566	3.471	3.339	5.08
0.472	2.893	2.540	3.83
0.354	2.169	1.650	3.08
0.283	1.736	1.181	2.50
0.236	1.446	0.898	1.96
		slope, m =	1.16
		y intercept, b =	1.04
		r^2 =	0.997
		k_{obs} =	9.85

Appendix B - Experimental results for free ferrocene-based systems

Table 1 - FCO/GSH in pH 7.0 phosphate buffer.

FCO, mM	GSH, mM	x-axis, $\times 10^{-5}$, $M^{3/2}$	i_{obs}, µA, at 700 mV
0.580	5.515	4.337	nd
0.438	4.136	2.817	0.96
0.350	3.309	2.016	0.65
0.292	2.758	1.533	0.52
0.219	2.068	0.996	0.37
0.175	1.655	0.713	0.33
0.146	1.379	0.542	0.24
		slope, m =	0.26
		y intercept, b =	0.11
		r^2 =	0.996
		k_{obs} =	2.27

Table 2 -FCO/GSH/10 mM β-CD in pH 7.0 phosphate buffer

FCO, mM	GSH, mM	x-axis, $\times 10^{-5}$, $M^{3/2}$	i_{obs}, µA, at 700 mV
0.580	5.515	4.337	3.17
0.438	4.136	2.817	2.67
0.350	3.309	2.016	1.96
0.292	2.758	1.533	1.38
0.219	2.068	0.996	1.02
0.175	1.655	0.713	0.83
0.146	1.379	0.542	0.75
		slope, m =	0.85
		y intercept,b =	0.20
		r^2 =	0.994
		k_{obs} =	24.26

Table 3 - FCN/GSH in pH 7.0 phosphate buffer.

FCN, mM	GSH, mM	x-axis, $\times 10^{-5}$, $M^{3/2}$	i_{obs}, μA, at 500 mV
0.522	5.408	3.839	5.50
0.392	4.056	2.491	3.83
0.313	3.245	1.785	3.08
0.261	2.704	1.358	2.33
0.196	2.028	0.882	1.92
0.157	1.622	0.631	1.58
0.131	1.352	0.479	1.12
		slope, m =	1.29
		y intercept, b =	0.67
		r^2 =	0.993
		k_{obs} =	12.08

Table 4 -FCN/GSH/10 mM β-CD in pH 7.0 phosphate buffer

FCN, mM	GSH, mM	x-axis, $\times 10^{-5}$, $M^{3/2}$	i_{obs}, μA, at 500 mV
0.522	5.408	3.839	4.33
0.392	4.056	2.491	3.33
0.313	3.245	1.785	2.33
0.261	2.704	1.358	2.08
0.196	2.028	0.882	1.33
0.157	1.622	0.631	1.21
0.131	1.352	0.479	1.00
		slope, m =	1.14
		y intercept,b =	0.43
		r^2 =	0.994
		k_{obs} =	9.43

Table 5 - FCN/Cysteine in pH 7.0 phosphate buffer.

FCN, mM	Cys, mM	x-axis, $\times 10^{-5}$, $M^{3/2}$	i_{obs}, μA, at 500 mV
0.518	5.748	3.924	8.12
0.388	4.311	2.549	5.21
0.311	3.449	1.824	5.00
0.259	2.874	1.387	3.25
0.194	2.156	0.901	2.83
0.155	1.725	0.645	2.50
0.129	1.437	0.491	1.63
		slope, m =	1.76
		y intercept, b =	1.02
		r^2 =	0.993
		k_{obs} =	22.48

Table 6 -FCN/Cysteine/10 mM β-CD in pH 7.0 phosphate buffer

FCN, mM	Cys, mM	x-axis, $\times 10^{-5}$, $M^{3/2}$	i_{obs}, μA, at 500 mV
0.518	5.748	3.924	3.13
0.388	4.311	2.549	2.63
0.311	3.449	1.824	2.58
0.259	2.874	1.387	1.92
0.194	2.156	0.901	1.67
0.155	1.725	0.645	1.08
0.129	1.437	0.491	1.04
		slope, m =	1.14
		y intercept,b =	0.46
		r^2 =	0.981
		k_{obs} =	9.27

Table 7 - FMAM/GSH in pH 7.0 phosphate buffer.

FMAM, mM	GSH, mM	x-axis, $\times 10^{-5}$, $M^{3/2}$	i_{obs}, μA, at 500 mV
0.556	5.349	4.063	9.38
0.417	4.012	2.639	5.67
0.333	3.210	1.889	4.00
0.278	2.675	1.437	3.58
0.208	2.006	0.933	2.42
0.167	1.605	0.668	2.08
0.139	1.337	0.508	1.67
		slope, m =	1.82
		y intercept, b =	0.79
		r^2 =	0.994
		k_{obs} =	111.23

Table 8 -FMAM/GSH/10 mM β-CD in pH 7.0 phosphate buffer

FMAM, mM	GSH, mM	x-axis, $\times 10^{-5}$, $M^{3/2}$	i_{obs}, μA, at 500 mV
0.556	5.349	4.063	7.92
0.417	4.012	2.639	6.46
0.333	3.210	1.889	5.16
0.278	2.675	1.437	4.33
0.208	2.006	0.933	2.83
0.167	1.605	0.668	2.46
0.139	1.337	0.508	1.92
		slope, m =	2.15
		y intercept,b =	0.97
		r^2 =	0.995
		k_{obs} =	155.22

Table 9 - FCO/GSH in pH 3.8 acetate buffer.

FCO, mM	GSH, mM	x-axis, $\times 10^{-5}$, $M^{3/2}$	i_{obs}, μA, at 600 mV
0.580	5.515	4.337	3.75
0.438	4.136	2.817	3.33
0.350	3.309	2.016	0.83
0.292	2.758	1.533	0.75
0.219	2.068	0.996	0.52
0.175	1.655	0.713	0.43
0.146	1.379	0.542	0.42
		slope, m =	0.31
		y intercept, b =	0.23
		r^2 =	0.987
		k_{obs} =	3.23

Table 10 -FCO/GSH/10 mM β-CD in pH 3.8 acetate buffer

FCO, mM	GSH, mM	x-axis, $\times 10^{-5}$, $M^{3/2}$	i_{obs}, μA, at 600 mV
0.580	5.515	4.337	1.67
0.438	4.136	2.817	1.25
0.350	3.309	2.016	1.02
0.292	2.758	1.533	0.85
0.219	2.068	0.996	0.46
0.175	1.655	0.713	0.38
0.146	1.379	0.542	0.31
		slope, m =	0.51
		y intercept,b =	0.01
		r^2 =	0.989
		k_{obs} =	8.70

Table 11 - FMAM/GSH in pH 3.8 acetate buffer.

FMAM, mM	GSH, mM	x-axis, $\times 10^{-5}$, $M^{3/2}$	i_{obs}, μA, at 500 mV
0.556	5.509	4.124	5.21
0.417	4.132	2.679	4.33
0.333	3.305	1.917	3.08
0.278	2.754	1.458	2.50
0.208	2.066	0.947	1.75
0.167	1.653	0.678	1.17
0.139	1.377	0.515	1.08
		slope, m =	1.21
		y intercept, b =	0.61
		r^2 =	0.983
		k_{obs} =	49.16

Table 12 -FMAM/GSH/10 mM β-CD in pH 3.8 acetate buffer

FMAM, mM	GSH, mM	x-axis, $\times 10^{-5}$, $M^{3/2}$	i_{obs}, μA, at 500 mV
0.556	5.509	4.124	5.83
0.417	4.132	2.679	4.21
0.333	3.305	1.917	3.00
0.278	2.754	1.458	2.63
0.208	2.066	0.947	1.63
0.167	1.653	0.678	1.17
0.139	1.377	0.515	0.92
		slope, m =	1.37
		y intercept,b =	0.36
		r^2 =	0.995
		k_{obs} =	63.03

Appendix C - Experimental data used to calculate rates for synzymes

Table 1 -1-DHBA-CD/GSH in pH 7 phosphate buffer.

1-DHBA-CD, mM	GSH, mM	x-axis, $\times 10^{-5}$, $M^{3/2}$	i_{obs}, µA, at 400 mV
0.919	9.610	9.009	4.83
0.613	6.407	4.904	3.16
0.460	4.805	3.185	2.63
0.368	3.844	2.279	1.92
0.306	3.203	1.734	1.75
0.263	2.746	1.376	1.38
0.230	2.403	1.126	1.40
		slope, m =	0.51
		y intercept, b =	0.79
		r^2 =	0.986
		k_{obs} =	4.61

Table 2 -1-DHBA-CD/GSH in pH 3.84 acetate buffer

1-DHBA-CD, mM	GSH, mM	x-axis, $\times 10^{-5}$, $M^{3/2}$	i_{obs}, µA, at 600 mV
0.919	----------	0	0.73
0.919	9.610	9.009	3.64
0.613	6.407	4.904	5.83
0.460	4.805	3.185	4.73
0.368	3.844	2.279	3.91
0.306	3.203	1.734	3.27
0.263	2.746	1.376	2.72
0.230	2.403	1.126	2.41
		slope, m =	1.30
		y intercept,b =	0.85
		r^2 =	0.996
		k_{obs} =	29.96

Table 3 -1-DHBA-CD/Cysteine in pH 7 phosphate buffer.

1-DHBA-CD, mM	Cys, mM	x-axis, $\times 10^{-5}$, $M^{3/2}$	i_{obs}, µA, at 400 mV
1.75	21.10	25.42	23.33
1.167	14.07	13.84	16.42
0.875	10.55	8.987	12.92
0.700	8.44	6.431	9.67
0.583	7.033	4.892	7.83
0.500	6.029	3.882	6.50
0.438	5.275	3.178	6.00
		slope, m =	1.25
		y intercept, b =	1.76
		r^2 =	0.998
		k_{obs} =	27.70

Table 4 -2-DHBA-CD/GSH in pH 7 phosphate buffer.

2-DHBA-CD, mM	GSH, mM	x-axis, $\times 10^{-5}$, $M^{3/2}$	i_{obs}, µA, at 300 mV
1.50	14.80	18.20	1.21
1.00	9.87	9.93	0.84
0.75	7.40	6.45	0.83
0.60	5.92	4.62	0.50
0.50	4.93	3.51	0.43
0.429	4.23	2.79	0.34
0.375	3.70	2.28	0.34
		slope, m =	0.12
		y intercept, b =	0.02
		r^2 =	0.972
		k_{obs} =	0.26

Table 5 -2-DHBA-CD/Cysteine in pH 7 phosphate buffer.

2-DHBA-CD, mM	Cys, mM	x-axis, $\times 10^{-5}$, $M^{3/2}$	i_{obs}, µA, at 300 mV
1.50	12.90	17.00	4.17
1.00	8.66	9.27	2.75
0.75	6.45	6.02	1.92
0.60	5.16	4.31	1.67
0.50	4.30	3.28	1.33
0.43	3.69	2.61	1.17
0.38	3.23	2.13	0.83
		slope, m =	0.25
		y intercept, b =	0.46
		r^2 =	0.989
		k_{obs} =	1.11

Table 6 -1-Fc-CD/GSH in pH 7 phosphate buffer.

1-Fc-CD, mM	GSH, mM	x-axis, $\times 10^{-5}$, $M^{3/2}$	i_{obs}, μA, at 300 mV
0.595	----------	0	0.31
0.595	5.97	4.60	5.33
0.397	3.98	2.50	3.58
0.298	2.99	1.63	2.17
0.238	2.39	1.16	1.83
0.198	1.99	0.883	1.46
0.170	1.71	0.703	1.25
0.149	1.49	0.575	0.88
		slope, m =	1.32
		y intercept, b =	0.23
		r^2 =	0.992
		k_{obs} =	142.91

Table 7 -1-Fc-CD/Cysteine in pH 7 phosphate buffer.

1-Fc-CD, mM	Cys, mM	x-axis, $\times 10^{-5}$, $M^{3/2}$	i_{obs}, μA, at 400 mV
0.595	6.19	4.68	4.83
0.397	4.13	2.55	3.33
0.298	3.10	1.66	2.50
0.238	2.48	1.19	1.71
0.198	2.06	0.90	1.63
0.170	1.77	0.72	1.23
0.149	1.55	0.59	1.17
		slope, m =	1.13
		y intercept, b =	0.50
		r^2 =	0992
		k_{obs} =	104.73

Table 8 -2-Fc-CD/Cysteine in pH 7 phosphate buffer.

2-Fc-CD, mM	Cys, mM	x-axis, $\times 10^{-5}$, $M^{3/2}$	i_{obs}, µA, at 400 mV
0.297	----------	0	0.17
0.297	8.248	2.70	5.83
0.198	5.499	1.47	5.63
0.149	4.124	0.954	4.33
0.119	3.299	0.683	3.92
0.991	2.749	0.520	2.83
0.849	2.887	0.456	2.17
0.713	2.526	0.374	2.08
		slope, m =	4.23
		y intercept, b =	0.54
		r^2 =	0.951
		k_{obs} =	1467

Table 9 -2-Fc-CD/Cysteine in pH 7 phosphate buffer.

2-Fc-CD, mM	Cys, mM	x-axis, $\times 10^{-5}$, $M^{3/2}$	i_{obs}, µA, at 400 mV
0.193	2.03	0.870	2.17
.129	1.35	0.474	1.38
0.965	1.02	0.308	1.13
0.772	0.812	0.220	0.74
0.643	0.677	0.167	0.42
0.551	0.580	0.133	0.32
0.483	0.508	0.109	0.25
		slope, m =	5.02, 3.27
		y intercept, b =	-0.41, -0.07
		r^2 =	0.967
		k_{obs} =	1471 (avg)

Table 10 -2-Fc-CD/GSH in pH 7 phosphate buffer.

2-Fc-CD, mM	GSH, mM	x-axis, $\times 10^{-5}$, $M^{3/2}$	i_{obs}, μA, at 400 mV
0.297	6.052	2.313	3.83
0.198	4.035	1.259	2.58
0.149	3.026	0.818	1.67
0.119	2.421	0.585	1.46
0.099	2.017	0.445	1.21
0.085	1.729	0.353	0.98
0.075	1.513	0.289	0.73
0.066	1.345	0.242	nd
		slope, m =	1.78
		y intercept, b =	0.33
		r^2 =	0.990
		k_{obs} =	259.87

Appendix D- pH effect on oxidation of cysteine by ferrocenes

Table 1 -2-Fc-CD/Cysteine in pH 8 phosphate buffer.

2-Fc-CD, mM	Cys, mM	x-axis, $\times 10^{-5}$, $M^{3/2}$	i_{obs}, µA, at 500 mV
0.088	----------	0	0
0.088	2.40	0.43	2.42
0.0635	1.70	0.26	1.83
0.0497	1.36	0.18	1.25
0.0409	1.11	0.14	1.00
0.0347	0.94	0.11	0.71
0.0301	0.82	0.086	0.63
		slope, m =	7.09
		y intercept, b =	-0.02
		r^2 =	0.998
		k_{obs} =	4123

Table 2 -FMAM/Cysteine in pH 8 phosphate buffer.

FMAM, mM	Cys, mM	x-axis, $\times 10^{-5}$, $M^{3/2}$	i_{obs}, μA, at 400 mV
2.52	----------	0	6.32
2.52	27.90	42.10	46.67
1.68	18.60	22.91	26.67
1.26	14.00	14.91	20.00
1.01	11.20	10.69	15.00
0.84	9.30	8.10	12.50
0.72	8.00	6.44	9.17
		slope, m =	1.03
		y intercept, b =	3.66
		r^2 =	0.992
		k_{obs} =	30.81

Table 3 -FMAM/Cysteine/10 mM β-CD in pH 8 phosphate buffer.

FMAM, mM	Cys, mM	x-axis, $\times 10^{-5}$, $M^{3/2}$	i_{obs}, μA, at 400 mV
2.52	27.90	42.10	36.67
1.68	18.60	22.91	24.17
1.26	14.00	14.91	18.33
1.01	11.20	10.69	14.17
0.84	9.30	8.10	11.67
0.72	8.00	6.44	9.17
		slope, m =	0.89
		y intercept, b =	4.26
		r^2 =	0.994
		k_{obs} =	26.59

Appendix E -Product inhibition study

Table 1 -2-Fc-CD/Cysteine in pH 7 phosphate buffer.

2-Fc-CD, mM	Cys, mM	x-axis, $\times 10^{-5}$, $M^{3/2}$	i_{obs}, µA, at 400 mV
1.11	----------	0	0
0.555	4.810	3.849	3.00
0.370	3.206	2.095	2.58
0.278	2.405	1.361	2.50
0.222	1.924	0.974	1.79
0.185	1.603	0.741	1.17
0.159	1.374	0.588	1.08
		slope, m =	1.13
		y intercept, b =	0.56
		r^2 =	0.936
		k_{obs} =	104.73

Table 2 -2-Fc-CD/Cysteine/Cystine in pH 7 phosphate buffer.

Cysteine, mM	Cystine, mM	2-Fc-CD, mM	i_{obs}, µA, at 400 mV
4.80	0.166	0.555	2.79
3.206	0.111	0.370	2.21
2.405	0.830	0.276	1.58
1.924	0.664	0.222	1.04
1.603	0.554	0.185	1.00
1.374	0.474	0.159	nd
		slope, m =	0.94
		y intercept, b =	0.24
		r^2 =	0.989
		k_{obs} =	72.47

Table 3 -2-Fc-CD/GSH in pH 7 phosphate buffer.

2-Fc-CD, mM	GSH, mM	x-axis, $\times 10^{-5}$, $M^{3/2}$	i_{obs}, µA, at 400 mV
0.555	5.57	4.142	1.08
0.370	3.71	2.254	0.54
0.278	2.79	1.464	0.46
0.222	2.23	1.048	0.27
0.185	1.86	0.797	0.23
0.159	1.59	0.633	0.19
0.139	1.39	0.518	nd
		slope, m =	0.32, 0.23
		y intercept, b =	-0.02, 0.06
		r^2 =	0.979, 0.967
		k_{obs} =	8.40, 4.34

Table 4 -2-Fc-CD/GSH/Glu-ox in pH 7 phosphate buffer.

GSH, mM	Glu-ox, mM	2-Fc-CD, mM	i_{obs}, µA, at 400 mV
5.57	2.403	0.555	1.08
3.71	1.602	0.370	0.63
2.785	1.202	0.276	0.40
2.228	0.961	0.222	0.29
1.857	0.801	0.185	0.23
1.591	0.687	0.159	0.18
		slope, m =	0.27
		y intercept, b =	0.01
		r^2 =	0.999
		k_{obs} =	5.98

Appendix F - Raw Data for Calibration Plots

Table 1 - 0.15 mM 2-Fc-CD in pH 7 phosphate buffer with varying substrate concentration

Cysteine, mM	i_{obs}, μA at 500 mV	i_{obs}, μA at 300 mV	i_{obs}, μA at 400 mV
0	0	0	0
39.30	3.00	0.50	1.50
26.20	3.14		
19.70	2.84	0.95	1.68
15.70	3.16	0.92	1.83
12.80	4.00	1.08	2.25
11.00	3.42	1.08	2.00
9.69	2.66		1.75
8.63	3.08	1.25	2.08
7.77	5.67	2.58	4.00
7.07	5.83	2.75	4.25
6.49	6.25	3.16	4.75
5.99	6.67	3.50	5.33
5.56	6.75	4.58	6.17
5.19	5.67	3.33	4.67
4.87	6.17	4.16	5.67
4.34	4.33	3.33	4.50
3.90	4.17	3.50	4.33
3.55	4.58	3.25	4.25
3.25	4.42	3.17	3.67
3.00	3.42	3.33	
2.79	3.17	3.17	3.33
2.60	2.33	3.25	2.67
2.44	2.67	3.25	2.83

Cysteine, mM	i_{obs}, µA at 500 mV	i_{obs}, µA at 300 mV	i_{obs}, µA at 400 mV
2.30	2.08	3.17	2.33
2.17	1.92	2.92	2.16
2.05	1.67	2.75	1.92
1.95	1.58	2.33	1.75
1.85	1.50	2.17	1.58
1.77	1.25	1.67	1.42

Table 2 - Raw Data for 0.15 mM 2-Fc-CD and glutathione substrate

	i_{obs}, μA for :		
GSH, mM	GCE electrode	Au electrode	Cn electrode
----------	0	0	0
40.00	1.33	0.375	3.167
26.67		0.333	3.208
20.00		0.337	3.042
16.00	1.25	0.326	2.75
11.43		0.316	2.083
8.89	1.00	0.326	2.833
8.00	1.21	0.326	2.917
6.67		0.337	2.00
5.71	1.15	0.326	2.75
5.00		0.326	5.417
4.44		0.337	3.833
4.00	1.08	0.326	4.50
3.63		0.316	4.33
3.33		0.326	4.00
3.08	1.19	0.316	3.00
2.67	1.08	0.358	3.00
2.38		0.316	2.75
2.11	1.15	0.326	2.417
1.91		0.326	2.083
1.74		0.386	1.833
1.53	1.00	0.326	1.667
1.49	0.88	nd	nd